UNIVERSITÀ DEGLI STUDI DI PADOVA

Dipartimento di Fisica e Astronomia "Galileo Galilei"

Master's Degree in Astrophysics and Cosmology

Final Dissertation

Investigating the Cosmological Gravitational Wave Background Anisotropies

Thesis Supervisor
Prof. Nicola Bartolo

Thesis Co-supervisor
Prof. Sabino Matarrese

Candidate
Shrouk Sayed Abdulsadiq Abdulshafy

Academic Year 2022/2023

Abstract

Studying the Stochastic Gravitational Wave Background (SGWB) anisotropies, can offer new tools to discriminate between different sources of GWs. While PTA's detection has recently confirmed the presence of the SGWB, the origin of this background is still debatable. In this thesis, we provide a wide review on the production of the SGWB from some cosmological sources, on characterizing the anisotropies of this backrgound, and on the sensitivity forecast of several detectors to the SGWB and its anisotropies. These anisotropies can be inherited at the time of the SGWB production and during its propagation through our perturbed universe. The Boltzmann approach has been used to study the propagation effects on the SGWB through scalar and tensor perturbations. Throughout that approach, the initial anisotropies turns out to have an order-one dependence on the frequency, which can be seen in the example of Axion-Inflaton, while those due to propagation are independent of the frequency at linear order. We also discussed the case of anisotropies for Phase Transitions and expressed it in terms of the photon density. The anisotropies are also affected by the presence of various decoupled particle species through their effect on the Sachs-Wolfe (SW) and Integrated Sachs-Wolfe (ISW) effects, we show that this effect is mainly a suppression of the anisotropies at larger cosmic scales in the angular power spectrum of the SGWB. As for the initial conditions, they have usually been considered to be adiabatic. We explore the recently proposed possibility of non-adiabaticity of the initial conditions, which in fact enhances the angular power-spectrum w.r.t the adiabatic case by a factor of 10. The cross-correlation between the Cosmological GWB (CGWB) and CMB can give us information about the primordial perturbations and the initial conditions. The total contribution $C_\ell^{\mathrm{CMB}\times\mathrm{CGWB}}$ turns out to be dominated by the SW x SW and SW x ISW contributions. Finally, we explore the sensitivity of some detectors to the SGWB and its anisotropies to have an idea of the values that could be relevant to us. For the SGWB itself, we show LISA's sensitivity to three different scenarios of first-order PTs, its sensitivity to different multipoles, and its sensitivity to detect the kinematic dipole and quadrupole. For the anisotropies, SNR analysis for the CMB x CGWB cross-correlation shows that BBO can have a higher SNR than LISA for the same signal amplitude. Using Fisher analysis, we explore different detectors' sensitivity and precision to detect the anisotropies. For the case of LISA and LISA-Taiji (LT), LT has powerful sensitivity to more ℓ modes than LISA does, and for adiabatic perturbations LT can access weaker signals. BBO, on the other hand, can probe the cosmological anisotropies with more precision. Lastly, ET alone does not have powerful sensitivity to odd ℓ modes, but a combination ET+CE significantly improves that, making it sensitive to all modes between $\ell = 1$ and $\ell = 6$.

Contents

Chapter 1

Introduction to Cosmology

Cosmology is the study of the universe, or cosmos, regarded as a whole. It is the scientific discipline that studies the origin, structure, evolution, and overall nature of the universe as a whole. It seeks to understand the fundamental properties and processes that govern the cosmos, including the distribution of galaxies, the formation of stars and planets, the cosmic microwave background radiation, dark matter, dark energy, and the large-scale structure of space and time. By employing observations, mathematical models, and theoretical frameworks, cosmology aims to unravel the mysteries of the universe's past, present, and future, providing insights into its underlying laws and guiding principles.

In this chapter, we review the basic concepts of Cosmology, we start by giving an idea on the observed universe, the concept of homogeneity and isotropy, the expanding universe and Cosmic Microwave Background Radiation (CMB). Then we turn to the background and the Standard cosmology, we define the Friedmann-Robertson-Walker metric and give a brief summary of Einstein and Friedmann equations. After that, we head to one of the two main topics we are going to discuss; Inflation and Phase Transitions. We talk about the theory of Inflation, how it was introduced as a solution to the shortcomings of the big bang model and introduce the scalar field named Inflaton and its dynamics. We give an introduction to phase transitions and the resulting topological defects. Inflation and Phase Transitions are two possible sources of the cosmological gravitational wave background (CGWB) and its anisotropies. So, it is important to give an introduction about these two mechanisms before proceeding with studying the production of gravitational waves (GWs) and its anisotropies. We end this introductory chapter by a brief talk about the measurement of the Stochastic Gravitational Wave Background (SGWB) by the Pulsar Timing Array (PTA) collaboration.

1.1 The Observed Universe

1.1.1 Homogeneity and Isotropy

Saying that the universe is isotropic means that there are no preferred directions in the universe; it looks the same no matter which way you point your telescope. Saying that the universe is homogeneous means that there are no preferred locations in the universe; it looks the same no matter where you set up your telescope. But bear in mind that, the universe is isotropic and homogeneous on large scales. And by "large scales" we mean scales of roughly 100 Mpc or more. The isotropy of the universe is not immediately obvious. In fact, on small scales, the universe is very obviously anisotropic. And on significantly larger scales, the universe is still anisotropic. It isn't until you get to considerably larger scales that the universe can be considered as isotropic. Similarily, on small scales, the universe is obviously inhomogeneous, or lumpy, in addition to being anisotropic. And on significantly larger scales, the universe is still inhomogeneous. It's only when you contemplate a

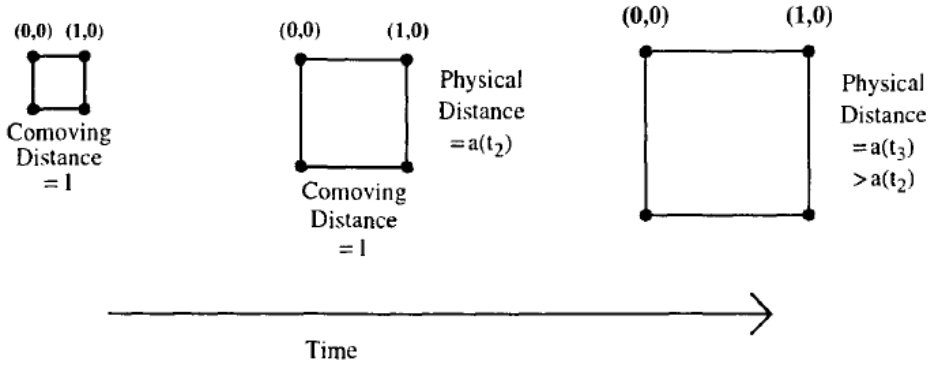

Figure 1.1: Expansion of the universe. The comoving distance between points on a hypothetical grid remains constant as the universe expands. The physical distance is proportional to the comoving distance times the scale factor, so it gets larger as time evolves. Taken from [46].

sphere $\gg$ 100 Mpc in diameter that you feel the homogeneity.

Note that homogeneity does not imply isotropy. Note also that isotropy around a single point does not imply homogeneity. In general, then, saying that something is homogeneous is quite different. from saying it is isotropic. However, modern cosmologists have adopted the cosmological principle, which states "There is nothing special about our location in the universe." But in fact, the cosmological principle holds true only on large scales [94].

1.1.2 The Expanding Universe

We have good evidence that the universe is expanding. This means that early in its history the distance between us and distant galaxies was smaller than it is today. It is convenient to describe this effect by introducing the scale factor a, whose present value is set to one. At earlier times a was smaller than it is today. We can picture space as a grid as in Fig. 1.1 which expands uniformly as time evolves [46]. Points on the grid maintain their coordinates, so the comoving distance between two points — which just measures the difference between coordinates — remains constant. However, the physical distance is proportional to the scale factor, and the physical distance does evolve with time.

If the Universe is homogeneous and isotropic, the distance between any two comoving points is proportional to a universal scale factor $a(t)$, where t is the cosmic time. A comoving point is the one moving with the expansion of the Universe. To understand the history of the universe, we must determine the evolution of the scale factor a with cosmic time t. Note that the dependence of a on t varies as the universe evolves. At early times, $a \propto t^{1/2}$ while at later times the dependence switches to $a \propto t^{2/3}$. How the scale factor varies with time is determined by the energy density in the universe. The relation between the scale factor, temperature and cosmic time is shown in Fig. 1.2. To quantify the change in the scale factor and its relation to the energy, it is first useful to define the Hubble rate,

$$H(t) \equiv \frac{da/dt}{a} \equiv \frac{\dot{a}}{a}\,, \tag{1.1}$$

which measures how rapidly the scale factor changes, i.e. the rate of expansion of the Universe. For example, if the universe is flat and matter-dominated, so that $a \propto t^{2/3}$, then $H = (2/3)t^{-1}$.

Present measures of the Hubble rate are parameterized by h defined via [46],

$$\begin{aligned} H_0 &= 100h \text{ km sec}^{-1} \text{ Mpc}^{-1} \\ &= \frac{h}{0.98 \times 10^{10} years} = 2.133 \times 10^{-33} h \text{ eV}/\hbar\,, \end{aligned} \tag{1.2}$$

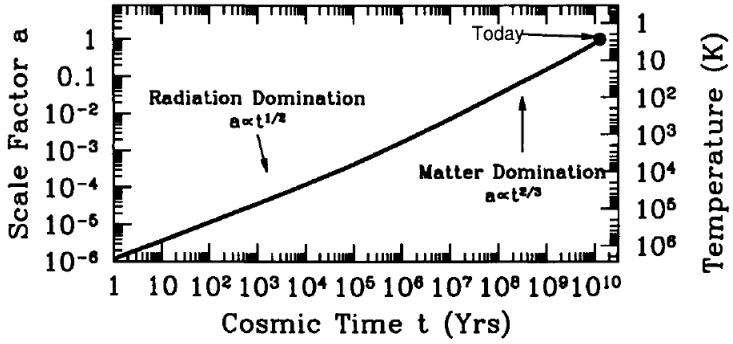

Figure 1.2: Evolution of the scale factor of the universe with cosmic time. When the universe was very young, radiation was the dominant component, and the scale factor increased as $t^{1/2}$. At later times, when matter came to dominate, this dependence switched to $t^{2/3}$. The right axis shows the corresponding temperature, today around 2.7 K. Taken from [46].

where h has nothing to do with Planck's constant $\hbar$. It is a dimensionless parameter, often used to parameterize H_0 in cosmological equations. It typically ranges between 0.6 and 0.8, with the best-fitting values based on various cosmological observations.

The distance of a given comoving point, measured from our location, can be written $r(t) = xa(t)$. The constant x is called the comoving distance and is equal to the physical distance at the present epoch, since the scale factor today is 1. The relative velocity of a pair of nearby comoving observers, separated by distance $dr \ll H^{-1}$, is $v = Hdr \ll 1$. With our chosen unit $c = 1$, this is equal to the redshift $\frac{d\lambda}{\lambda}$ of a photon passing between the observers. It is also equal to the fractional increase da/a in the scale factor, and the wavelength λ of a photon as seen by a sequence of comoving observers stretches with the scale factor.

At the present epoch, the redshift z of light from a cosmological source is defined by [79],

$$1 + z \equiv \frac{\lambda_{obs}}{\lambda_{emit}} , \tag{1.3}$$

where λ_{obs} is the observed wavelength and λ_{emit} is the wavelength at the point of emission.

For $z \ll 1$, the redshift is given by Hubble's law as $z = Hdr$, which would allow an accurate determination of the present value H_0 if the distances of galaxies were known accurately.
Whether or not z is small, the redshift z of the light emitted at time t_1 is given by,

$$1 + z = \frac{a(t_0)}{a(t_1)} . \tag{1.4}$$

We usually specify both times and distances in terms of redshift. When redshift is used to refer to a time, it simply means the time at which the scale factor was a fraction $1/(1 + z)$ of its present value. When used to refer to a distance, it means the distance that light can have travelled since that time. It is important to understand that because the Universe expands as the light propagates, the redshift distance is not equal to the redshift time multiplied by the speed of light.

The universe is also characterized by its geometry. There are three possibilities: flat, open, or closed universes. We can imagine them by considering two freely traveling particles which start their journeys moving parallel to each other. For each possibility there's a different scenario:

1. In the case of a **flat** universe, the particles remain parallel as long as they travel freely.
2. In the case of **closed** universe, gradually the initially parallel particles converge. In this case the universe is said to have positive curvature.
3. In the case of **open** universe, the initially parallel paths diverge.

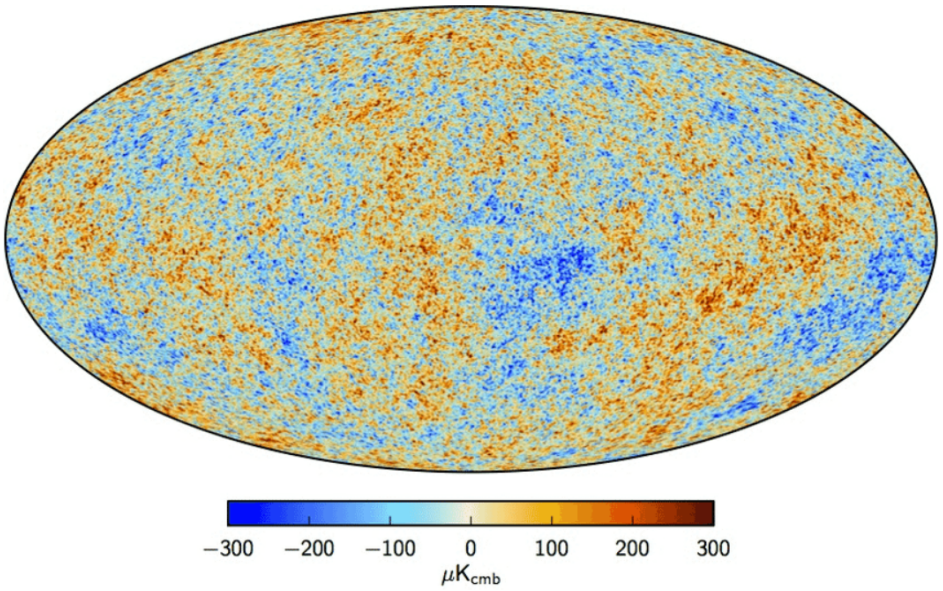

Figure 1.3: The map of CMB temperature fluctuations $\Delta T/T$ over the whole sky, as measured by the Planck satellite. The foreground emission from the Milky Way galaxy and the dipole component due to the motion of the galaxy relative to the CMB have been removed. The colours from blue to red indicate the magnitude of underdensity to overdensity. *Photo Credit: ESA and Planck Collaboration.*

These possibilities are also related to the energy density as we will see in section 1.2.3.

1.1.3 Cosmic Microwave Background Radiation

Cosmic Microwave Background is a faint, nearly uniform glow of microwave radiation that fills the universe. The CMB is a crucial piece of evidence for the Big Bang theory, which is the prevailing cosmological model explaining the origin and evolution of the universe. The CMB is incredibly uniform, with tiny fluctuations or temperature variations. These fluctuations correspond to the seeds of structure formation in the universe, leading to the formation of galaxies and galaxy clusters. The CMB radiation is in the microwave portion of the electromagnetic spectrum, with a temperature of approximately 2.7 Kelvin. It is extremely cold by human standards but is still detectable with sensitive instruments. The temperature of the CMB radiation across the sky is remarkably uniform: $\Delta T/T \sim 10^{-5}$ on angular scales ranging from 10 arc seconds to 180° (after the dipole anisotropy has been removed) [72]. The map of CMB temperature fluctuations $\Delta T/T$ over the whole sky, as measured by the Planck satellite is shown in Fig. 1.3.

The photons in the cosmic microwave background last scattered off electrons at redshift $z \sim 1100$; since then they have traveled freely through space. They are therefore the most powerful probes of the early universe. A crucial fact about this history, though, is that the collisions with electrons before last scattering ensured that the photons were in equilibrium. That is, they should have a blackbody spectrum.

The specific intensity of a stream of photons with a blackbody spectrum is,

$$I_\nu = \frac{4\pi\hbar\nu^3/c^2}{\exp\{2\pi\hbar\nu/k_BT\} - 1}\,, \tag{1.5}$$

where I_ν is the specific intensity, ν is the photon frequency, k_B is Boltzmann constant and T is the temperature in kelvin.

1.2 Background and Standard Cosmology

Our current understanding of the evolution of the Universe is based upon the Friedmann-Lemaître-Robertson-Walker (FLRW) cosmological model, or the hot big bang model as it is usually called. The model is so successful that it has become known as the standard cosmology.

1.2.1 FLRW Spacetime

We now proceed following our previous discussion that our observable universe is homogeneous and isotropic on large scales, and also that our spacetime is maximally symmetric space satisfying the Cosmological Principle. The best evidence for the isotropy of the observed universe is the uniformity of the temperature of the cosmic microwave background radiation: intrinsic temperature anisotropies is smaller than about one part in 10^5 as we mentioned earlier.

The FLRW metric, can be written as,

$$ds^2 = -dt^2 + a^2(t)\Big[\frac{dr^2}{1-kr^2} + r^2 d\theta^2 + r^2 sin^2\theta d\phi^2\Big] \ , \tag{1.6}$$

where $(t;\ r;\ \theta;\ \phi)$ are comoving coordinates, $a(t)$ is the cosmic scale factor and k can be chosen to be $+1$, -1, or 0 by rescaling the coordinates for spaces of constant positive, negative, or zero spatial curvature, respectively. We can also write the FLRW metric as,

$$ds^2 = -dt^2 + a^2(t) g_{ij} dx^i d^j \ , \tag{1.7}$$

where we have,

$$\begin{aligned} g_{11} &= \frac{1}{1-kr^2} \\ g_{22} &= r^2 \\ g_{33} &= r^2 sin^2\theta \ . \end{aligned} \tag{1.8}$$

Recalling from the GR course, one can then calculate the Christoffel symbols from,

$$\Gamma^{\mu}_{\nu\lambda} = \frac{1}{2} g^{\mu\rho}\Big(\frac{\partial g_{\rho\nu}}{\partial x^{\lambda}} + \frac{\partial g_{\rho\lambda}}{\partial x^{\nu}} - \frac{\partial g_{\nu\lambda}}{\partial x^{\rho}}\Big) \ , \tag{1.9}$$

The relevant components of the Riemann tensor can also be calculated from,

$$R^{\lambda}_{\sigma\mu\nu} = \partial_{\mu}\Gamma^{\lambda}_{\sigma\nu} - \partial_{\nu}\Gamma^{\lambda}_{\sigma\mu} + \Gamma^{\lambda}_{\mu\rho}\Gamma^{\rho}_{\nu\sigma} - \Gamma^{\lambda}_{\nu\rho}\Gamma^{\rho}_{\mu\sigma} \ , \tag{1.10}$$

And calculate the Ricci Tensor $R_{\mu\nu}$ and the Ricci Scalar R down to the Einstein tensor from,

$$G_{\mu\nu} = R_{\mu\nu} - \frac{1}{2} g_{\mu\nu} R \ . \tag{1.11}$$

1.2.2 Einstein Equations

The evolution of the background metric can be obtained starting from the following action,

$$S = \int d^4x \sqrt{-g}\Big(\frac{1}{16\pi G} R + \mathcal{L}_m(g_{\mu\nu}, \phi_m)\Big) \ , \tag{1.12}$$

where g denotes the determinant of the metric and R the Ricci scalar.
The first term of the action (1.12) corresponds to the Einstein-Hilbert action. Thus containing all the information about the geometry of the spacetime. The second term $\mathcal{L}_m(g_{\mu\nu}, \phi_m)$, instead, accounts for

all the energetic content of the Universe, let's call it "the rest of the world", which acts as a source for the gravitational field $g_{\mu\nu}$. In this sense ϕ_m is the field associated to any of the particles of the system.

Varying the action with respect to the metric $g_{\mu\nu}$ we obtain Einstein's equations:

$$G_{\mu\nu} \equiv R_{\mu\nu} - \frac{1}{2} g_{\mu\nu} R = 8\pi G T_{\mu\nu} \ , \tag{1.13}$$

where $R_{\mu\nu}$ and $G_{\mu\nu}$ are the Ricci and Einstein tensors, respectively.
We have defined the stress-energy tensor for the rest of the world (matter, radiation, and so on) as:

$$T_{\mu\nu} = -\frac{2}{\sqrt{-g}} \frac{\delta(\sqrt{-g}\mathcal{L}_m)}{\delta g^{\mu\nu}} \ , \tag{1.14}$$

for a perfect fluid, isotropic and homogeneous,

$$T^{\mu}_{\nu} = (\rho + P) u^{\mu} u_{\nu} + P \delta^{\mu}_{\nu} = \mathrm{diag}(-\rho, P, P, P) \ , \tag{1.15}$$

with u_μ the 4-velocity of the fluid. In its rest frame, where $u_\mu = (1, 0, 0, 0)$, and it is normalized as $u^\mu u_\mu = -1$, it follows immediately $T^0_0 = -\rho$ and $T^i_j = P\delta^i_j$, where ρ is the background energy density and P is the background isotropic pressure. Usually, a linear relationship between P and ρ of the type,

$$P = w\rho \ , \tag{1.16}$$

is considered. Where w is known as the equation of state parameter. From the conservation laws associated with the energy-momentum tensor,

$$\nabla_\mu T^{\mu\nu} = 0 \ , \tag{1.17}$$

one gets,

$$\dot{\rho} + 3H(\rho + P) = 0 \tag{1.18}$$

$$\begin{aligned} &\Rightarrow \ \dot{\rho} + 3H(\rho + w\rho) = 0 \\ &\Rightarrow \ \dot{\rho} + 3H\rho(1 + w) = 0 \\ &\Rightarrow \ \dot{\rho} + 3\frac{\dot{a}}{a}\rho(1 + w) = 0 \\ &\Rightarrow \ \frac{d\rho}{\rho} + 3\frac{da}{a}(1 + w) = 0 \ , \end{aligned} \tag{1.19}$$

and by integrating (1.19) we get,

$$\rho a^{3(1+w)} = \text{constant} \ . \tag{1.20}$$

This relation relates the scale factor to the energy density, confirming what we said earlier about them being related.

1.2.3 Friedmann Equations

Rewriting Einstein equation in the form,

$$R_{\mu\nu} = 8\pi G_{\mathrm{N}} \Big(T_{\mu\nu} - \frac{1}{2} g_{\mu\nu} T^{\lambda}_{\lambda} \Big) \ . \tag{1.21}$$

Because of isotropy, there are only two independent equations, namely the 00-component and any one of the non-zero ij-components. Then,

$$-3\frac{\ddot{a}}{a} = 4\pi G_{\mathrm{N}}(\rho + 3P) \ , \tag{1.22}$$

$$\frac{\ddot{a}}{a} + 2\frac{\dot{a}^2}{a^2} + 2\frac{k}{a^2} = 4\pi G_{\mathrm{N}}(\rho - P) \ , \tag{1.23}$$

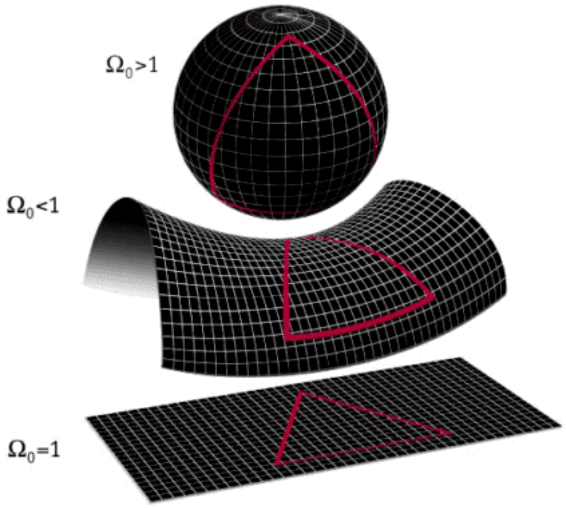

Figure 1.4: Depiction of possible geometries of our universe. *Photo Credit: Physics Forums.*

using the first equation to eliminate $\ddot{a}/a$ from the second, one obtains the set of equations for the Hubble rate,

$$H^2 + \frac{k}{a^2} = \frac{8\pi G_{\rm N}}{3}\rho \,, \tag{1.24}$$

and for the acceleration,

$$\frac{\ddot{a}}{a} = -\frac{4\pi G_{\rm N}}{3}(\rho + 3P) \,, \tag{1.25}$$

together, this set of equation is known as the Friedman equations.

The expansion rate of the universe is determined by the Hubble rate H which is not a constant and generically scales like t^{-1}. The Friedmann equation can be recast as,

$$\Omega - 1 = \frac{\rho}{3H^2/8\pi G_{\rm N}} = \frac{k}{a^2 H^2} \,, \tag{1.26}$$

where we have defined the parameter Ω as the ratio between the energy density ρ and the critical energy density ρ_c,

$$\Omega = \frac{\rho}{\rho_c}, \qquad \rho_c = \frac{3H^2}{8\pi G_{\rm N}} \,. \tag{1.27}$$

Since $a^2H^2 > 0$, there is a correspondence between the sign of k and the sign of $(\Omega - 1)$,

$$\begin{aligned} k = +1 \quad &\Rightarrow \quad \Omega > 1 \quad \text{CLOSED} \\ k = 0 \quad &\Rightarrow \quad \Omega = 1 \quad \text{FLAT} \\ k = -1 \quad &\Rightarrow \quad \Omega < 1 \quad \text{OPEN} \end{aligned} \tag{1.28}$$

there, the relation we promised. Such possible geometries of the universe and their relation to the current energy density paramater is shown in Fig. 1.4.

1.3 Inflation

The theory of inflation was first proposed by Alan Guth in 1981 [59] as a way to solve the shortcomings of the Big Bang model. It is described as a rapid and exponential expansion of the

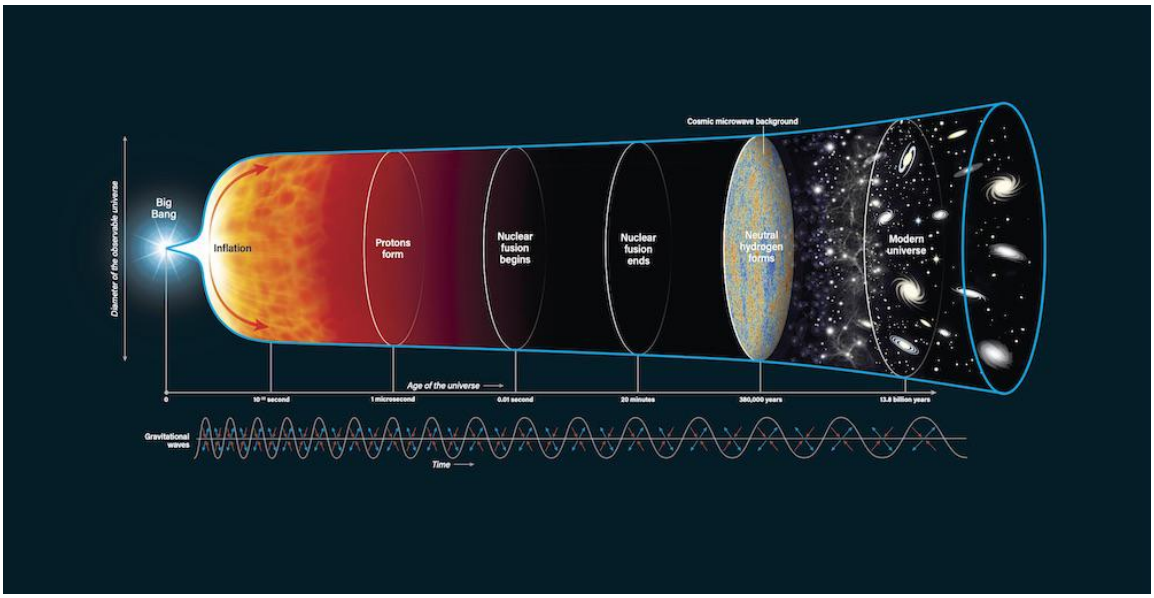

Figure 1.5: History of the Universe – gravitational waves are hypothesized to arise from cosmic inflation. *Photo Credit: Roen Kelly, after BICEP2 Collaboration.*

early universe during its very first moments, driven by the vacuum energy density of a scalar field which we call inflaton. As we mentioned before, one of the early universe possible mechanisms for the production of GWs is the cosmic inflation. The history of the universe and the accompanying GWs are shown in Fig. 1.5.

1.3.1 Shortcomings of the Standard Cosmology

We list here some of the shortcomings of the Standard Cosmology that were the motivation for proposing Inflation. But before we go through the different problems, we have to define a necessary concept; *Number of e-foldings*.

Number of e-foldings

It is necessary to define a way in order to quantify the amount of inflation, since both the horizon and the flatness problem require not only a period of inflation, but actually a large enough amount of expansion. This is done by defining the number of e-foldings:

$$N = \int_{t_i}^{t_f} H(t)dt = \ln(\frac{a_f}{a_i}) \ , \tag{1.29}$$

which is essentially related to the ratio of the scale factors at the beginning (t_i) and at the end (t_f) of inflation.

One can calculate the minimum number of e-foldings needed to address the limitations of the Hot Big Bang model. To successfully solve both the horizon and flatness problems, inflation begin from arbitrary initial conditions and evolve them such that they end up today in what we experimentally measure. Following such an approach, the required number of e-foldings is found to be at least $N \simeq 60 - 70$ [33].

Horizon Problem

At a given time t, what are actually the regions in the universe that could have been possibly

causally connected with us? The answer to this we call the *Particle Horizon*; it is the farthest distance from which we, or any other observer, can receive a signal. Assuming that a photon could have been emitted at $t = 0$, the particle horizon is defined as [33]:

$$R_H(t) = a(t) \int_0^t \frac{dt'}{a(t')} \, . \tag{1.30}$$

To evaluate this expression, it is necessary to find the solution for $a(t)$ in an expanding Universe. For standard RW cosmologies, we have,

$$a(t) \propto t^{\alpha} \, , \tag{1.31}$$

where $\alpha = 2/[3(1+\omega)]$. This proportionality holds in spatially flat universe, or at least we can say that it is a good approximation at early times as k is negligible.

So, one finds:

$$a(t) = a_* \left(\frac{t}{t_*}\right)^{\frac{2}{3(1+w)}} \, , \tag{1.32}$$

where t_* is an arbitrary reference time and $a_* = a(t_*)$. Substituting (1.32) inside (1.30) and integrate, we get:

$$R_H(t) = \frac{3(1+w)t}{1+3w} \, , \tag{1.33}$$

and it follows that R_H is finite if and only if $w > -1/3$, i.e. $\ddot{a} < 0$. This suggests that the Standard Hot Big Bang model, which describes an always decelerating expansion, cannot explain the causal connection between points farther than the particle horizon distance. This contradicts the experimental evidence of an homogeneous CMB, since points separated by an angle of more than few degrees could not have been able to be in causal connection at the epoch of last scattering. So, how come they share the same properties?

Actually the situation is even worse. The particle horizon is the distance from which an observer can receive a signal emitted any time after the Big Bang. But to have an homogeneous CMB a constant exchange of information between points is needed, so that they can share the same temperature. Such a causal connection is described by the *Hubble Radius*:

$$R_c = \frac{1}{H(t)} \, , \tag{1.34}$$

and corresponds to the maximum distance between points that can exchange information over a Hubble time $\tau_{_H} = H^{-1}$. What is interesting about Hubble radius is that the evolution of its Comoving counterpart $r_c = (aH)^{-1}$ depends on the dynamics of the Universe. In fact:

$$\dot{r}_c = -\frac{\ddot{a}}{\dot{a}^2} \, . \tag{1.35}$$

It is then possible to define the comoving Hubble sphere, which contains all the points in causal contact, at a given instant, with the observer located at the centre. We see from equation (1.35) that, in the case of a decelerating Universe $\ddot{a} < 0$, such a sphere expands over time, such that the observer comes in causal contact with new, never seen before, points. It follows that we, as observers, are now in causal contact with points that could not have been able to communicate before the last scattering epoch, and thus we can explain the homogeneity of the CMB only by means of finely-tuned initial conditions. This is what is called the horizon problem.

Flatness Problem

Another problem, similar to the horizon one, involves the measured spatial curvature of the space-time. We know that observationally the Universe is very close to be flat. This is due to the

fact that today the density parameters of the various components add up almost exactly to a total $\Omega_0 \sim 1$, which corresponds to $k = 0$ inside the first Friedmann equation (1.26). The latter can be rewritten as,

$$\Omega(t) - 1 = \frac{k}{(aH)^2} = kr_c^2 \,, \tag{1.36}$$

where in the second equality we have applied the definition of the comoving Hubble radius.
It is then possible to define the density parameter associated with the spatial curvature $\Omega_k(t) \equiv 1 - \Omega(t) = -kr_c^2$. From this definition, it follows that Ω_k vanishes in the spatially flat case and it is positive (negative) for a spatially open (close) spacetime. The latest measurements from the Planck collaboration [38] constrain the value today to be $\Omega_{k0} = 0.001 \pm 0.002$. This value is compatible with a spatially flat Universe and it is way too small to be reasonable after the standard Hot Big Bang evolution.

We can understand why by looking back to the first Friedmann equation (1.24) and analyzing the two terms after H^2: the first term is, as already stressed, related to the spatial curvature and goes like a^{-2}, the second accounts for the energy contribution of the fluid components, whose energy density decreases at best as a^{-3} in the case of matter. We can then conclude that, approaching early times, the curvature term, along with Ω_k, starts to become more and more negligible inside the Friedmann equation. The so-called flatness problem lies in the fact that the measured value for Ω_{k0}, frequently expressed as $|\Omega_0 - 1| < 10^{-3}$, would require an initial condition, computed at Planck time t_P, of $|\Omega(t_P) - 1| \simeq |\Omega_0 - 1|10^{-60}$, which is of course a finely-tuned assumption.

The same conclusion can be deduced by taking the time derivative of the density parameter Ω_k:

$$\frac{d}{dt}\Omega_k = -k\frac{d}{dt}r_c^2 = 2kr_c\frac{\ddot{a}}{\dot{a}^2} \,, \tag{1.37}$$

this result tells us how the spatial curvature density parameter evolves when going back in time. It is straightforward to verify that, for a decelerating Universe ($\ddot{a} < 0$), Ω_k approaches zero at early times, both in the case of positive or negative curvature. This leads to the same conclusion given before about the necessity for a fine-tuning at early times.

1.3.2 Inflation in a nutshell

The precise definition of inflation is simply any epoch during which the scale factor of the Universe is accelerating:

$$\text{INFLATION} \iff \ddot{a} > 0 \,, \tag{1.38}$$

Inflation sometimes is described just as a rapid expansion, though it is not very clear with respect to what the expansion is supposed to be rapid.

There is an equivalent alternative expression of the condition for inflation that gives it a more physical interpretation:

$$\text{INFLATION} \iff \frac{d}{dt}\frac{H^{-1}}{a} < 0 \,, \tag{1.39}$$

because H^{-1}/a is the comoving Hubble radius, the condition for inflation is that the comoving Hubble radius, which is the most important characteristic scale of the expanding Universe, is decreasing with time. Viewed in coordinates fixed with the expansion, the observable Universe actually becomes smaller during inflation because the characteristic scale occupies a smaller and smaller coordinate size as inflation proceeds.

Assuming that we work within general relativity, the condition for inflation can be rewritten as

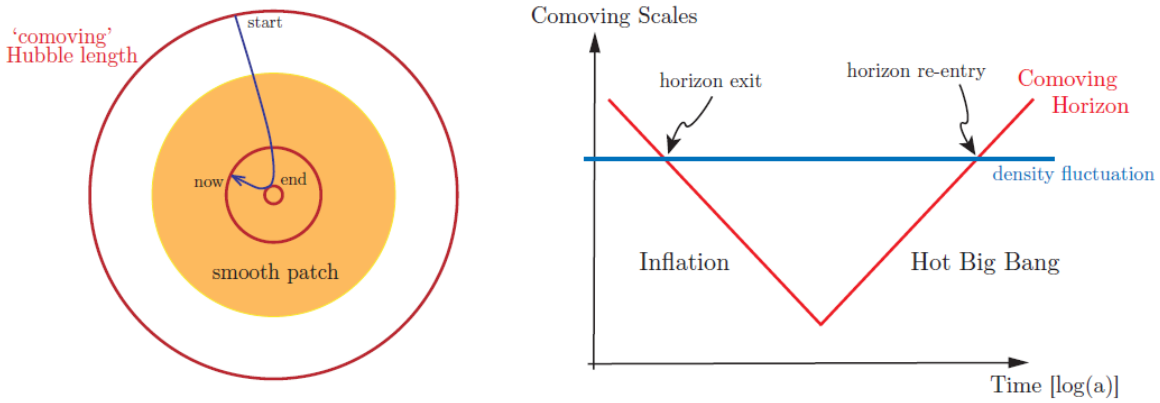

Figure 1.6: *Left*: Evolution of the comoving Hubble radius, $(aH)^{-1}$, in the inflationary universe. The comoving Hubble sphere shrinks during inflation and expands after inflation. Inflation is therefore a mechanism to 'zoom-in' on a smooth sub-horizon patch. *Right*: Solution of the horizon problem. All scales that are relevant to cosmological observations today were larger than the Hubble radius until $a \sim 10^{-5}$. However, at sufficiently early times, these scales were smaller than the Hubble radius and therefore causally connected. Similarly, the scales of cosmological interest came back within the Hubble radius at relatively recent times. Taken from [24].

a requirement on the material driving the expansion. Dircetly from the acceleration equation (1.25), we find,

$$\text{INFLATION} \iff \rho + 3P < 0 \,, \tag{1.40}$$

which is equivalent to saying that we must have $w < -1/3$. Because we always assume ρ be positive, it is necessary for P to be negative to satisfy this condition, which is independent of the curvature of the Universe. The three equivalent conditions for inflation therefore are:

- Decreasing comoving horizon
- Accelerated expansion
- Negative pressure

Horizon Problem Revisited

Looking again at equation (1.35), it seems natural to try to solve this inconsistency by admitting an early time of accelerated expansion, during which the Hubble radius decreases and points in causal connection get pushed far apart. A decreasing comoving horizon means that large scales entering the present universe were inside the horizon before inflation (see Fig. 1.6) [24]. Causal physics before inflation therefore established spatial homogeneity. With a period of inflation, the uniformity of the CMB is not a mystery.

It is then sufficient to request the comoving Hubble radius today to be less than what it was before inflation:

$$r_c(t_0) < r_c(t_i) \tag{1.41}$$
$$\Rightarrow \quad \dot{r}_c < 0 \,, \tag{1.42}$$

which is consistent with $\ddot{a} > 0$, according to Eq. (1.35). And we obtain a past causal connection with all the points from which we can receive signals today (see Fig. 1.7). Condition (1.41) can be made more explicit by combining the definition of comoving Hubble radius and equation (1.32) for the evolution of the scale factor. The latter assumes different values for different equation of states

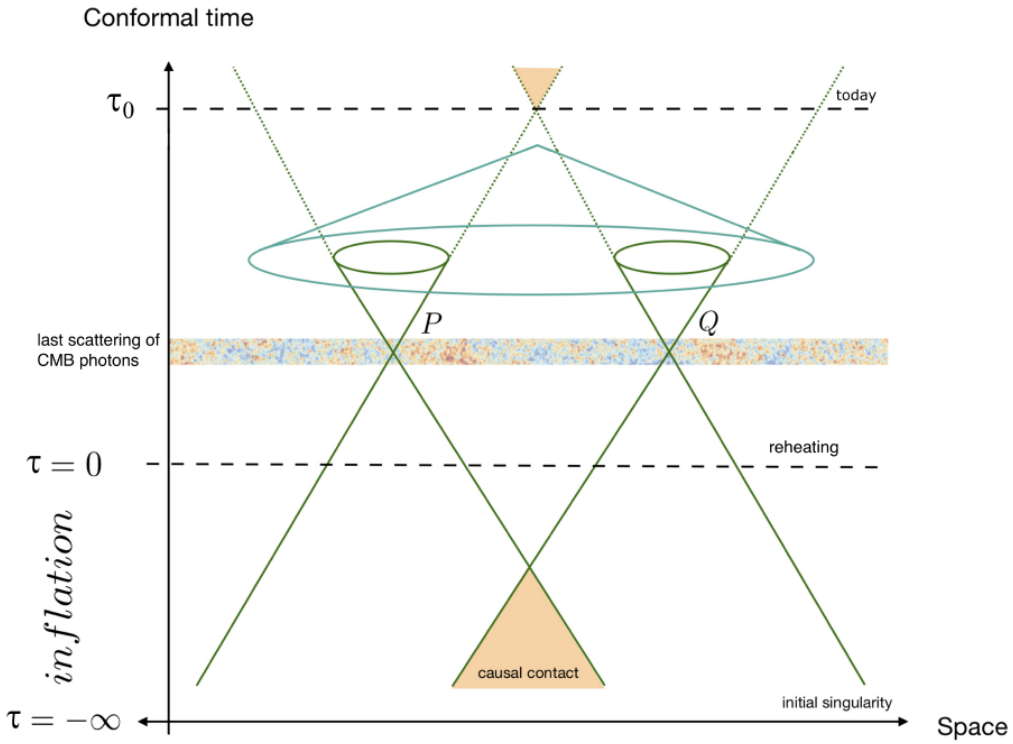

Figure 1.7: How inflation solves the horizon problem. Taken from [51].

w, determined by the dominating fluid component during a certain period of expansion. Accounting, after the end of inflation, for a radiation dominated period followed by a matter dominated one, the condition (1.41) brings to the qualitative result:

$$N \gtrsim 60 \, . \tag{1.43}$$

Flatness Problem Revisited

Once again, the solution is to admit a period of inflation sufficiently long to satisfy, in analogy with (1.41), the inequality:

$$\frac{1 - \Omega_i^{-1}}{1 - \Omega_0^{-1}} \geq 1 \, , \tag{1.44}$$

which corresponds to asking that the density parameter today (Ω_0) must be closer to unity than the density parameter at the beginning of inflation (Ω_i). The main mechanism is that, Ω, starts at the beginning of inflation from a generic value which deviates considerably from 1. But because of the accelerated expansion, it quickly decrease and it is pushed toward 1 at the end of inflation. If the inflation lasts sufficient number of e-foldings, this means that Ω at the end of inflation will be pushed so close to 1 that even if after inflation Ω starts growing again, it will still be very close to 1, see Fig. 1.8.

Furthermore, from the first Friedmann equation (1.24), it is possible to derive that the combination $(\Omega^{-1} - 1)\rho a^2 = const$ is actually conserved over time. Using this result inside (1.44), remembering (1.32) and splitting again the history of the Universe into the three periods of inflation ($w \simeq -1$), radiation domination ($w = 1/3$), and matter domination ($w = 0$), it is possible to recover the same amount of required inflation as the one computed by solving the horizon problem, which is approximately $N \gtrsim 60$.

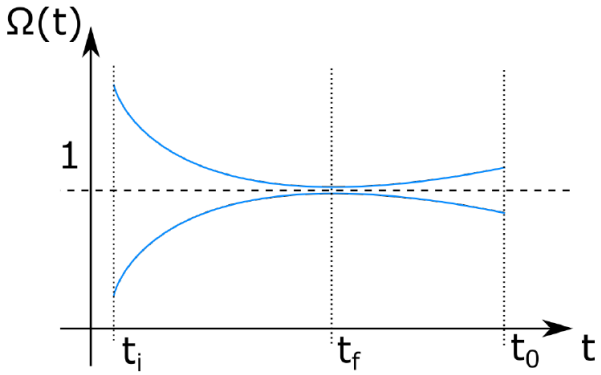

Figure 1.8: How inflation solves the flatness problem. Taken from [51].

1.3.3 Scalar Field Dynamics

But how to achieve such a period of early accelerated expansion?
The most straightforward method to achieve a phase of cosmic inflation involves the existence of a scalar field during the universe's earliest moments. This scalar field, which we refer to as the inflaton field $\varphi(t,\vec{x})$, plays the main role in driving the accelerated expansion of the universe at that time. This field's energy density is responsible for powering the inflationary epoch, during which the universe rapidly expands. The starting point to study the single scalar field inflation is then the following action:

$$S = \int d^4x\sqrt{-g}\Big(\frac{1}{16\pi G}R - \frac{1}{2}g^{\mu\nu}\nabla_{\mu\varphi}\nabla_{\mu\varphi} - V(\varphi)\Big)\ , \tag{1.45}$$

which basically corresponds to the action (1.12) where subdominant fields, other than the inflaton, have been neglected in $\mathcal{L}_m$. Apart from the Einstein-Hilbert sector, action (1.45) contains the most standard scalar field Lagrangian, with a canonical kinetic term and a self-interaction potential. In principle, it is possible to construct different inflationary models by choosing various profiles for the potential, but later we will see that there are some underlying requirements which have to be fulfilled. An example is given in Fig. 1.9.

Varying the action (1.45) with respect to φ results in the Klein-Gordon equation for the inflaton:

$$\ddot{\varphi} + 3H\dot{\varphi} - \frac{\nabla^2\varphi}{a^2} = -\frac{\partial V}{\partial\varphi}\ . \tag{1.46}$$

Applying (1.14) to the inflaton part of the action (1.45), it is possible to compute the inflaton stress-energy tensor:

$$T_{\mu\nu} = \partial_\mu\varphi\partial_\nu\varphi - g_{\mu\nu}\Big(\frac{1}{2}g^{\alpha\beta}\partial_\alpha\varphi\partial_\beta\varphi + V(\varphi)\Big)\ . \tag{1.47}$$

In order to proceed, it is necessary to split the inflaton into its background value plus a small fluctuation around it [72]:

$$\varphi(t,\vec{x}) = \varphi_0(t) + \delta\varphi(t,\vec{x})\ . \tag{1.48}$$

The background value $\varphi_0(t)$ is allowed to be only a function of time due to the symmetries of the background FLRW spacetime, and it represents the classical background evolution (trajectory) of the inflaton field, with $\delta\varphi \ll \varphi_0$ being the quantum fluctuation of $\varphi(t,\vec{x})$ around the classical trajectory. By definition, $\langle\delta\varphi(t,\vec{x})\rangle = 0$, so that $\langle\varphi(t,\vec{x})\rangle = \varphi_0(t)$ is the inflaton vacuum expectation value. At first, we will focus only on the background evolution, leaving the treatment of the fluctuations for later, when we will see how they can be regarded as the origin of the structures we observe today.

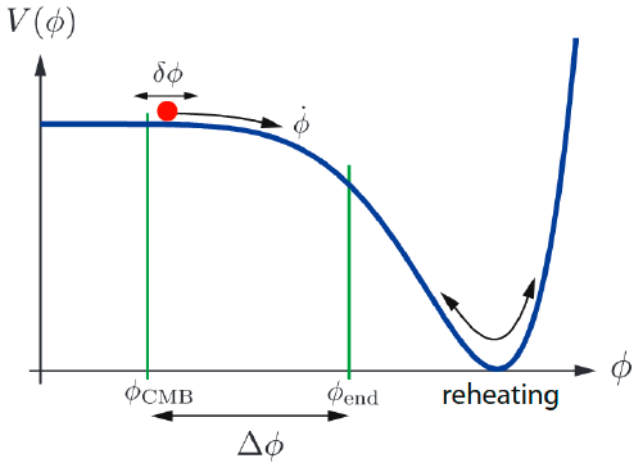

Figure 1.9: Example of a slow-roll potential. During inflation, the inflaton ϕ rolls down along the plateau of the potential. Taken from [24].

Equation (1.47), evaluated for the background inflaton, can be written in components as follows:

$$T^0{}_0 = -\rho_\varphi = -\Big(\frac{1}{2}\dot{\varphi}^2 + V(\varphi)\Big)\,, \tag{1.49}$$

$$T^i{}_j = p_\varphi \delta^i{}_j = \Big(\frac{1}{2}\dot{\varphi}^2 - V(\varphi)\Big)\delta^i{}_j\,, \tag{1.50}$$

where, from now on in this section, we indicate the background inflaton just with φ. The first Friedmann equation (1.24) now reads:

$$H^2 = \frac{8\pi G}{3}\Big(\frac{1}{2}\dot{\varphi}^2 + V(\varphi)\Big)\,, \tag{1.51}$$

where we have neglected the spatial curvature. This is possible because during inflation, the curvature density parameter is pushed to zero.

We can finally verify how the inflaton stress-energy tensor can behave as the driving force of an inflationary period. Remembering the condition (1.40) and substituting (1.49) and (1.50), we get:

$$w_\varphi = \frac{p_\varphi}{\rho_\varphi} = \frac{\frac{1}{2}\dot{\varphi}^2 - V(\varphi)}{\frac{1}{2}\dot{\varphi}^2 + V(\varphi)} < -\frac{1}{3}\,, \tag{1.52}$$

which is the constraint that the equation of state of the inflaton must satisfy in order to achieve $\ddot{a} > 0$, i.e., accelerated expansion. In particular, making the assumption $V(\varphi) \gg \dot{\varphi}^2$, it follows $w_\varphi \simeq -1$, with the inflaton behaving almost like a cosmological constant. This is called slow-roll inflation, from the fact that the inflaton has little kinetic energy and slowly rolls down its potential. We stress that it can't be $w_\varphi = -1$ (de Sitter spacetime case) exactly because in such a case there would not be a way to end the period of accelerated expansion. In the slow-roll regime, considering the background value of the inflaton field, equations (1.46) and (1.51) can be approximated to:

$$3H\dot{\varphi} \simeq -V'(\varphi)\,, \tag{1.53}$$

$$H^2 \simeq \frac{8\pi G}{3}V(\varphi)\,, \tag{1.54}$$

where we have also assumed, reasonably, $\ddot{\varphi} \ll 3H\dot{\varphi}$ in the first equation. This condition ensures that the slow-roll requirement $\dot{\varphi}^2 \ll V(\varphi)$ is fulfilled for a long enough period.

We can now introduce some useful parameters in order to better quantify the condition of slowly rolling we have just introduced. The first slow-roll parameter is defined in the following way:

$$\epsilon \equiv -\frac{\dot{H}}{H^2}\,. \tag{1.55}$$

Furthermore, we can write:

$$0 < \ddot{a} = \dot{a}H + a\dot{H} = aH^2(1-\epsilon) \ . \tag{1.56}$$

From which it immediately follows the condition $\epsilon < 1$, necessary to obtain an accelerated expansion. However, inflation requires a more stringent constraint. Rearranging (1.55), in fact, with the help of (1.54), results in $\epsilon \propto \frac{\dot{\varphi}^2}{V(\varphi)} \ll 1$. Exploiting also (1.53), it is possible to obtain a constraint on the first-order derivative of the potential:

$$\epsilon = \frac{1}{16\pi G}\left(\frac{V'}{V}\right)^2 \ll 1 \ , \tag{1.57}$$

meaning that the inflaton potential has to be sufficiently flat. A second parameter may also be introduced, exploiting the assumption made on the inflaton acceleration $\ddot{\varphi} \ll 3H\dot{\varphi}$:

$$\eta \equiv -\frac{\ddot{\varphi}}{H\dot{\varphi}} \ll 1 \ , \tag{1.58}$$

from which it follows a condition on the second derivative of the potential:

$$\eta_V \equiv \eta + \epsilon = \frac{1}{8\pi G}\frac{V''}{V} \ , \tag{1.59}$$

with $|\eta_V| \ll 1$. A whole hierarchy of slow-roll parameters may follow, of higher orders than the two just introduced, constraining higher order derivatives of the potential.

Therefore, the situation can be summed up as follows: during inflation, the Universe undergoes an accelerating expansion, driven by the energy density (mostly potential) of a single scalar field, which slowly rolls along its potential. This goes on until the slow-roll conditions are satisfied (essentially until $\epsilon \sim 1$). At this point, inflation ends, and the inflaton energy density gets converted into all the particles needed to start the Hot Big Bang phase, via a process called reheating [72]. This situation is described in Fig. 1.9., where a typical potential profile is represented. In particular, it can be observed that inflation occurs while the potential is sufficiently flat, so that the inflaton can slowly roll on the plateau. Eventually, this flatness is spoiled, and inflation ends: the inflaton starts oscillating around the true minimum of the potential and decays into other particles.

1.3.4 Primordial Fluctuations from Inflation

Now that we have seen the basic idea behind the background evolution in a single scalar field inflationary model, we can turn to a fundamental topic for the scope of this thesis, which is the treatment of quantum fluctuations during inflation. In other words, we now consider the full $\varphi(t,\vec{x})$ as a quantum field and see what is the evolution of the fluctuation $\delta\varphi(t,\vec{x})$ we have previously neglected. Because of this fluctuation, there will be local differences $\delta t(\vec{x})$ in the time when the inflation ends. This means that the local expansion history varies from one point to another, in other words, on large scales φ will assume the same value φ_0 everywhere, making every point in the universe experience the same history, but at slightly different times, and leads to the production of local inhomogeneities in the energy density $\delta\rho(\vec{x})$, which then evolve into the CMB temperature inhomogeneities $\delta T(\vec{x})$ we measure today. The aim of this section and the following one is to show how these perturbations generate from the primordial inflaton fluctuations $\delta\varphi(t,\vec{x})$.

We start by writing the perturbed part (linear in $\delta\varphi$) of the Klein-Gordon equation (1.46):

$$\ddot{\delta\varphi} + 3H\dot{\delta\varphi} - \frac{\nabla^2\delta\varphi}{a^2} = -V''(\varphi_0)\delta\varphi \ , \tag{1.60}$$

It is now convenient to perform the following rescaling:

$$\delta\varphi(t.\vec{x}) = \frac{\delta\tilde{\varphi}(t,\vec{x})}{a(t)} \ . \tag{1.61}$$

Using this and passing to conformal time τ, equation (1.60) becomes:

$$\delta\tilde{\varphi}'' - \frac{a''}{a}\delta\tilde{\varphi} - \nabla^2\delta\tilde{\varphi} = -\frac{\partial^2 V}{\delta\varphi^2}(\varphi_0)\delta\tilde{\varphi} \,, \tag{1.62}$$

where the $'$ symbol denotes derivatives with respect to τ. In order to solve this equation, it is useful to write it in Fourier space:

$$u''_{\vec{k}}(\tau) + \left[k^2 - \frac{a''}{a} + \frac{\partial^2 V}{\delta\varphi^2}(\varphi_0)\right] u_{\vec{k}}(\tau) = 0 \,, \tag{1.63}$$

Where $u_{\vec{k}}$ is defined as the Fourier transform of $\delta\tilde{\varphi}$:

$$\delta\tilde{\varphi}(\tau, \vec{x}) = \frac{1}{(2\pi)^3}\int d^3\vec{k} e^{i\vec{k}\vec{x}} u_{\vec{k}}(\tau) \,. \tag{1.64}$$

We first consider the massless scalar field case, where $m^2\varphi = \frac{\partial^2 V(\varphi_0)}{\partial\varphi^2} = 0$. Equation (1.63) can be rewritten as:

$$u''_{\vec{k}} + \omega_k^2 u_{\vec{k}} = 0 \,. \tag{1.65}$$

So that each Fourier mode satisfies the harmonic oscillator equation of motion with frequency $\omega_k^2 = k^2 - \frac{a''}{a}$. Canonical quantization can thus be performed in analogy to the quantum harmonic oscillator [24]. We promote the perturbation $\delta\tilde{\varphi}(\tau, \vec{x})$ to a quantum operator $\delta\hat{\varphi}(\tau, \vec{x})$, such that the mode expansion can be written as:

$$\delta\hat{\varphi}(\tau, \vec{x}) = \frac{1}{(2\pi)^3}\int d^3\vec{k}\left[u_k(\tau)\hat{a}_{\vec{k}} e^{i\vec{k}\vec{x}} + u_k^*(\tau)\hat{a}^\dagger_{-\vec{k}} e^{-i\vec{k}\vec{x}}\right] \,, \tag{1.66}$$

where $\hat{a}_{\vec{k}}$, $\hat{a}^\dagger_{\vec{k}}$ are, respectively, the annihilation and creation operators, i.e., $\hat{a}_{\vec{k}}|0\rangle = 0$ and $\langle 0|\hat{a}^\dagger_{\vec{k}} = 0$, where $|0\rangle$ is the vacuum state. The vector notation in $u_{\vec{k}}$ and $u^*_{\vec{k}}$ has been dropped since the frequency $\omega_k^2(\tau) = k^2 - \frac{a''}{a}$ depends only on the absolute value k, and the same happens for the mode's evolution [24]. Canonical quantization conditions read:

$$[\hat{a}_{\vec{k}}, \hat{a}_{\vec{k'}}] = [\hat{a}^\dagger_{\vec{k}}, \hat{a}^\dagger_{\vec{k'}}] = 0 \,, \tag{1.67}$$

$$[\hat{a}_{\vec{k}}, \hat{a}^\dagger_{\vec{k'}}] = (2\pi)^3\delta^{(3)}(\vec{k} + \vec{k'}) \,. \tag{1.68}$$

And are ensured by the following normalization for the modes:

$$u'_k(\tau)u_k^*(\tau) - u_k(\tau)u_k^{*\prime}(\tau) = -i \,. \tag{1.69}$$

To fix the vacuum state $|0\rangle$, we exploit the information that at sufficiently early time ($\tau \to -\infty$) all modes of interest are still inside the horizon ($k^2 \gg \frac{a''}{a}$).

In the sub-horizon regime ($k \gg aH \leftrightarrow k^2 \gg \frac{a''}{a}$):
In this case $\omega_k^2 = k^2$, and so,

$$u''_{\vec{k}} + k^2 u_{\vec{k}} = 0 \,. \tag{1.70}$$

The solution at early times corresponds to a plane wave in a flat spacetime:

$$\lim_{\tau\to-\infty} u_k(\tau) = \frac{1}{\sqrt{2k}} e^{-ik\tau} \,. \tag{1.71}$$

This initial condition for the mode functions defines what is called the Bunch-Davis vacuum. Similar to the rescaling we did before, we have,

$$\begin{aligned} \delta\varphi_k = \frac{u_k}{a} &= \frac{1}{a\sqrt{2k}} e^{-ik\tau} \,, \\ \Rightarrow \; |\delta\varphi_k| &= \frac{1}{a\sqrt{2k}} \,. \end{aligned} \tag{1.72}$$

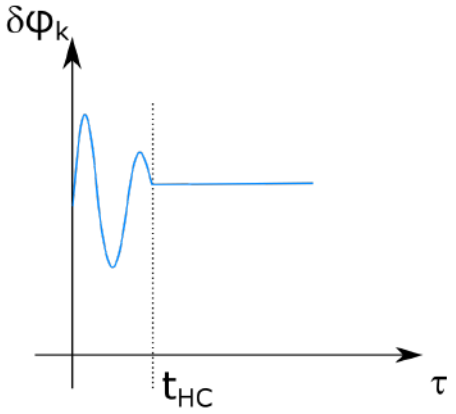

Figure 1.10: Fluctuations getting frozen on super-horizon scales. Taken from [51].

This solution tells us that, during inflation, modes inside the horizon oscillate while their amplitudes decrease as the inverse of the scale factor a. This behavior goes on, for a given k, until the mode crosses the horizon when $k^2 \sim \frac{a''}{a}$.

In the super-horizon regime ($k \ll aH \leftrightarrow k^2 \ll \frac{a''}{a}$):
In this case $\omega_k^2 = -\frac{a''}{a}$, and so,

$$u_{\vec{k}}'' - \frac{a''}{a} u_{\vec{k}} = 0 \, . \tag{1.73}$$

This kind of equations are solved by,

$$u_k(\tau) = B(k)a(\tau) + A(k)a^{-2}(\tau) \, , \tag{1.74}$$

where A, B are integration constants. Therefore,

$$\delta\varphi_k = B(k) + A(k)a^{-3}(\tau) \simeq B(k) = \text{constant} \, , \tag{1.75}$$

where we have neglected the decaying term which gets washed away by inflation. This solution means that fluctuations don't die out on super-horizon scales, instead they get frozen (see Fig. 1.10). We can find the amplitude in this regime making a matching between the two regimes at horizon crossing, since from that moment on it will get constant. At horizon-crossing $k = aH$, thus,

$$|B(k)|a = \frac{1}{\sqrt{2k}}\Big|_{k=aH} \, , \tag{1.76}$$

therefore,

$$|\delta\varphi_k| = |B(k)| = \frac{1}{a\sqrt{2k}}\Big|_{k=aH} = \frac{H}{\sqrt{2k^3}} \, . \tag{1.77}$$

We have already said that inflation needs some dynamics, and the Universe cannot end up in a de Sitter spacetime, since otherwise, it would go on inflating forever. We thus want to solve equation (1.65) in a so-called quasi de-Sitter spacetime, where, using the slow-roll parameter already introduced, $\epsilon = -\frac{\dot{H}}{H^2} \ll 1$. In this approximation, it is possible to rewrite (1.65) in the form of a Bessel equation [15]:

$$u_k''(\tau) + \left[k^2 - \frac{\nu^2 - \frac{1}{4}}{\tau^2}\right] u_k(\tau) = 0 \, , \tag{1.78}$$

where $\nu^2 = \frac{9}{4}+3\epsilon$. Solutions of this equation can be found going into the sub-horizon or super-horizon limit. In the first case, it is similar to the solution already given in Eq. (3.40). Without going too much into details, solving Eq. (1.78) in the super-horizon regime leads to the following result [15]:

$$|\delta\varphi_k| \simeq \frac{H}{\sqrt{2k^3}}\left(\frac{k}{aH}\right)^{\frac{3}{2}-\nu} , \tag{1.79}$$

with $\frac{3}{2}-\nu = -\epsilon$, this thin-scale dependence of order ϵ would be absent in the case of a pure de-Sitter spacetime. What the result (1.79) tells us is that, after crossing the horizon, an oscillating k-mode (with vanishing expectation value) freezes out with an almost constant amplitude, thus generating a classical perturbation of the field φ. In the more general case of a massive field, the same result (1.79) holds, this time with $\frac{3}{2}-\nu = \eta_V - \epsilon$ [15], where $\eta_V = \frac{m_\varphi^2}{3H^2}$. The slow-roll condition $|\eta_V| \ll 1$ then requires φ to be very light (with respect to the Hubble parameter).

1.3.5 Primordial Power Spectrum

To facilitate the comparison between theoretical predictions and observational data, it becomes necessary to define the observable properties associated with these fluctuations. Quantum fluctuations, while inherently non-deterministic, can be characterized using a quantum random field denoted as $\delta\varphi(\vec{x},t)$. This field describes the amplitude of fluctuations at each point in spacetime.

It's important to note that these fluctuations exhibit correlations across different points in spacetime. In fact, even if the ensemble average is zero by definition (it is in fact the vacuum expectation value), one can calculate the two-point correlation function. This function quantifies the statistical relationships between fluctuations at different spacetime locations, providing valuable insights into the behavior of these quantum fluctuations. The two point correlation function is,

$$\xi = \langle\delta(\vec{x}+\vec{r},t)\delta(\vec{x},t)\rangle , \tag{1.80}$$

which in a homogeneous and isotropic universe is a function of $|\vec{r}|$. If we take the two point correlation function of the Fourier transform of a generic stochastic field,

$$\delta(\vec{x},t) = \frac{1}{(2\pi)^3}\int d^3k e^{i\vec{k}\cdot\vec{x}}\delta_k(t) , \tag{1.81}$$

the result is,

$$\langle\delta(\vec{k},t)\delta(\vec{k}',t)\rangle = (2\pi)^3 P(|\vec{k}|)\delta^3(\vec{k}+\vec{k}') , \tag{1.82}$$

where P is the power spectrum . It depends only on the modulus of $\vec{k}$ due to isotropy, the presence of the delta function comes due to homogeneity. Furthermore, the power spectrum P is the Fourier transform of ξ, using Eq. (1.82),

$$\begin{aligned}\xi(\vec{r}) = \langle\delta(\vec{x}+\vec{r},t)\delta(\vec{x},t)\rangle &= \frac{1}{(2\pi)^6}\int d^3k \int d^3k\, e^{i\vec{k}\vec{x}+i\vec{k}'(\vec{x}+\vec{r})}\langle\delta(\vec{k}_1,t)\,\delta(\vec{k}_2,t)\\ &= \frac{1}{(2\pi)^3}\int d^3k' e^{i\vec{k}'\vec{r}}P(|\vec{k}_1|) .\end{aligned} \tag{1.83}$$

The variance, i.e. the two-point correlation function at zero separation, is then,

$$\begin{aligned}\langle\delta^2(\vec{x},t)\rangle = \xi(0) &= \frac{1}{(2\pi)^3}\int d^3k P(|\vec{k}|) = \frac{1}{2\pi^2}\int_0^\infty dk k^2 P(k)\\ &= \frac{1}{2\pi^2}\int_0^\infty \frac{dk}{k}k^3P(k) = \int_0^\infty \frac{dk}{k}\Delta(k) ,\end{aligned} \tag{1.84}$$

where we defined the adimensional power spectrum as $\Delta(k) = k^3/(2\pi^2)P(|k|)$, which is the contribution to the variance per logarithmic integral.

For the inflaton field quantum fluctuations, remembering that, $|\delta\varphi_k| = |u_k|/a$,

$$\langle \delta\varphi_{\vec{k}_1}, \delta\varphi^*_{\vec{k}_2} \rangle = (2\pi)^3 |\delta\varphi_{\vec{k}_1}|^2 \delta^3(\vec{k}_1 - \vec{k}_2) \,, \tag{1.85}$$

therefore,

$$P(k) = |\delta\varphi_k|^2 = \frac{|u_k|^2}{a^2} \qquad \rightarrow \qquad \Delta(k) = \frac{k^3}{2\pi^2}\frac{|u_k|^2}{a^2} \,. \tag{1.86}$$

On super-horizon scales, from Eq. (1.79), we get,

$$P_\varphi(k) = \frac{H^2}{2k^3}\left(\frac{k}{aH}\right)^{3-2\nu} , \qquad \Delta_\varphi(k) = \left(\frac{H}{2\pi}\right)^2 \left(\frac{k}{aH}\right)^{3-2\nu} , \tag{1.87}$$

where in the most general case $3 - 2v = 2\eta_V - 6\epsilon$. We can then define the spectral index $n(k)$ as,

$$n(k) - 1 = \frac{d \ln \Delta(k)}{d \ln k} \,, \tag{1.88}$$

which describes the shape of the power spectrum.

Let's discuss two cases:

- $n \equiv 1 \leftrightarrow$ Harrison-Zel'dovich spectrum: it means that the amplitude of $\delta\varphi$ does not depend on the cosmological scale.
- $n = constant \leftrightarrow \Delta(k)$ can be written w.r.t. a "pivot scale" k_0 as,

$$\Delta(k) = \Delta(k_0)\left(\frac{k}{k_0}\right)^{n-1} , \tag{1.89}$$

n and $\Delta(k_0)$ are indeed the two main observables one can constrain observing the CMB.

To assess how well inflationary models align with cosmological observations, an additional step is required. This is because when we observe phenomena like the anisotropies and polarization in the CMB, we are not directly detecting quantum fluctuations of the inflaton field. Instead, our observations pertain to fluctuations in the energy density of matter, which includes entities like CMB photons, as well as perturbations in the metric of spacetime, present, e.g., at the last scattering surface. Let us consider ζ, which is called curvature perturbation on uniform energy density hypersurfaces. It has three properties:

1. ζ is a gauge invariant quantity defined as,

$$\zeta = -\hat{\Phi} - H\frac{\delta\rho}{\dot{\rho}} \,. \tag{1.90}$$

In the $\hat{\Phi} = 0$ gauge, therefore, we have,

$$\zeta = -H\frac{\delta\rho}{\dot{\rho}} \,. \tag{1.91}$$

2. This is a very general definition, since in the case of inflation the density is the density of the scalar field, but it also applies during all the evolution of the universe:

$$\zeta \rightarrow \frac{\delta\rho_\varphi}{\dot{\rho}_\varphi}, \quad \frac{\delta\rho_m}{\dot{\rho}_m}, \quad \frac{\delta\rho_\gamma}{\dot{\rho}_\gamma}, \quad \frac{\delta\rho_\Lambda}{\dot{\rho}_\Lambda} \,. \tag{1.92}$$

3. On super horizon scales it is constant in time (in single field models of inflation)

$$\zeta\Big|_{t_H^{(1)}(k)} = \zeta\Big|_{t_H^{(2)}(k)} \,. \tag{1.93}$$

In that sense, we are able to compare the amplitude of primordial density perturbations with known quantities, as CMB temperature fluctuations.

Let us imagine looking at two different scales λ, λ', where the latter re-enters during matter dominated epoch and the former during radiation domination. Let us then call $t_H^{(1)}(k)$ the time at which λ crosses out the horizon and $t_H^{(2)}(k)$ the time in which it re-enters. The same will apply to $\lambda' \to k'$. Thanks to Eq. (1.93), we can compare density perturbation at the time of inflation with respect to radiation epoch,

$$\begin{aligned} \zeta\Big|_{t_H^{(1)}(k)} &= \zeta\Big|_{t_H^{(2)}(k)} \,, \\ -H\frac{\delta\varphi}{\dot{\varphi}}\Big|_{t_H^{(1)}(k)} &= \frac{1}{4}\,\frac{\delta\rho_\gamma}{\rho_\gamma}\Big|_{t_H^{(2)}(k)} \,, \end{aligned} \tag{1.94}$$

since during radiation domination the density is given by $\rho = \rho_\gamma \propto T^4 \to \delta\rho/\dot{\rho} = 4\delta T/T$ and $\dot{\rho_\gamma} \simeq -4H\rho_\gamma$. In other words, there is a direct link between temperature fluctuation and primordial inflaton fluctuations,

$$\zeta_\varphi \sim \frac{\delta T}{T} \sim 10^{-5} \,. \tag{1.95}$$

1.4 Phase Transitions

Phase transitions in cosmology refer to abrupt changes in the fundamental properties of the universe as it evolves over time. These transitions are similar to the familiar phase transitions in condensed matter physics, such as the transition from a liquid to a gas or from a solid to a liquid. In cosmology, phase transitions can have profound effects on the universe's structure, dynamics, and evolution. They can lead to the generation of cosmic defects like cosmic strings, domain walls, and monopoles, which can leave imprints on the large-scale structure of the universe. The effects of phase transitions can potentially be observed through their imprints on the CMB radiation, the distribution of galaxies, and the formation of large-scale structures. Detecting these signatures can provide valuable insights into the universe's early history and fundamental physics.

They can also be related to the production of gravitational waves. The cosmic defects we mentioned earlier are topological features that arise when a field undergoes a phase transition and settles into a new vacuum state. Cosmic strings, in particular, are one of the most significant sources of gravitational waves in the context of phase transitions. They are one-dimensional topological defects that can form during a phase transition. These strings have extremely high energy densities and can stretch across vast cosmic distances. As they move through the expanding universe, they can generate gravitational waves through various mechanisms, such as kinks and cusps along the strings. The gravitational waves produced by cosmic strings have a characteristic spectrum, which depends on the cosmic string network's properties. This spectrum includes contributions at different frequencies, and it can extend from very low frequencies to potentially observable frequencies in the gravitational wave spectrum.

Detecting the gravitational waves from cosmic strings and other cosmic defects is a challenging but exciting possibility for gravitational wave observatories like LIGO and Virgo. These gravitational waves could leave distinctive signatures in the CMB radiation and the large-scale structure of the universe. They could also be detected directly through precise measurements of gravitational wave detectors.

It is also worth mentioning that Inflation is thought to have been driven by a scalar field that underwent a phase transition. While inflation itself is not typically associated with the generation of gravitational waves, some inflationary models can generate primordial gravitational waves.

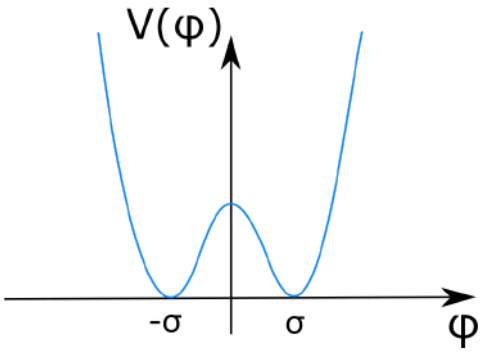

Figure 1.11: An example of a potential that implements SSB. Taken from [51].

1.4.1 Spontaneous Symmetry Breaking (SSB)

We are referring to relics produced in the early universe as a consequence of the spontaneous symmetry breaking (SSB) of some (gauge) symmetry: breaking of grand unified theory (GUT) at $T_{GUT} \sim 10^{14} - 10^{16}$ GeV into a lower gauge symmetry that includes a U(1) group leads to the production of point-like (0-dimension) magnetic monopoles, cosmic strings (1-dimension) can be produced by the SSB of a U(1) gauge group, domain walls (2-dimension) arise when a discrete symmetry is spontaneously broken, and textures (3-dimension) arise from SSB of, e.g., SU(2) gauge theories.

We will explain below how such a mechanism can be realized dynamically in a cosmological context through phase transitions at high temperatures in the early universe. Also, the SSB is key to understand some of the inflationary models proposed in the "early days of inflation" in the context of particle physics. On the other hand some aspects related to phase transitions and cosmic topological defects are of present interest. For example, both phase transitions and cosmic defects can be a source of primordial gravitational waves, and indeed they are the target of present and future direct interferometers (together with the stochastic background of gravitational waves produced during inflation).

We illustrate this mechanism using a simple model. Consider a real scalar field described by the Lagrangian density [72],

$$\mathcal{L} = \frac{1}{2}\partial_\mu\varphi\partial^\mu\varphi - V(\varphi) \,, \tag{1.96}$$

$$V(\varphi) = -\frac{1}{2}m^2\varphi^2 + \frac{1}{4}\lambda\varphi^4 \,. \tag{1.97}$$

The potential $V(\varphi)$ is shown in Fig 1.11. Note that the Lagrangian is invariant under the discrete symmetry transformation $\varphi \leftrightarrow -\varphi$. The minima of the potential (determined by the conditions $V' \equiv \partial V/\partial\varphi = 0$ and $V'' \equiv \partial^2 V/\partial\varphi^2 > 0$), denoted by $\sigma_\pm$ and are called the "True Vacua", and the value of the potential and its second derivative at the minima, are given by,

$$\begin{aligned} \sigma_\pm &= \pm\sqrt{\frac{m^2}{\lambda}} \,, \\ V(\sigma_\pm) &= -\frac{m^4}{4\lambda} \,, \\ V''(\sigma_\pm) &= 2m^2 \,. \end{aligned} \tag{1.98}$$

Since $V(+(m^2/\lambda)^{1/2}) = V(-(m^2/\lambda)^{1/2})$, both $\sigma_\pm = \pm(m^2/\lambda)^{1/2}$ are equivalent minima of the potential. On the other hand, although $V'(0) = 0$, $\langle\varphi\rangle = 0$ is an unstable extremum of the potential because $V''(0) < 0$, and it is called the "False Vacuum". Since the quantum theory must be constructed about a stable extremum of the classical potential, the ground state of the system is either

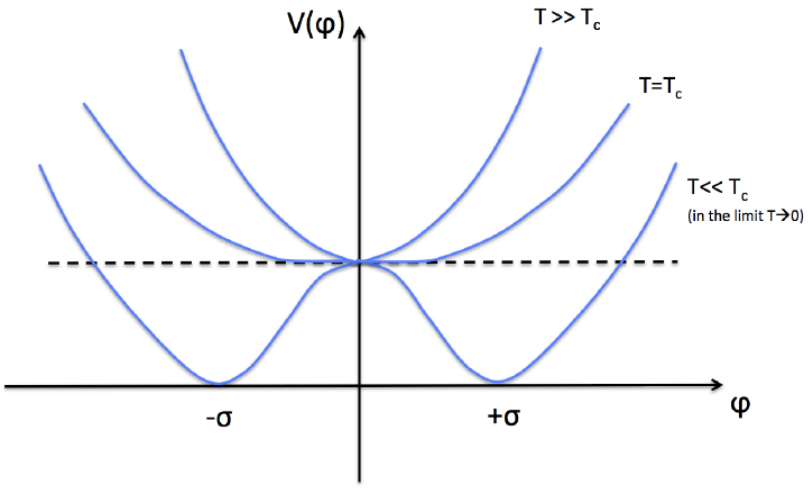

Figure 1.12: The temperature dependence of $V(\varphi)$ for a first-order phase transition. Taken from [51].

$\langle\varphi\rangle = +(m^2/\lambda)^{1/2}$ or $\langle\varphi\rangle = -(m^2/\lambda)^{1/2}$, and the reflection symmetry $\varphi \leftrightarrow -\varphi$ present in the Lagrangian is broken by the choice of a vacuum state. A symmetry of the Lagrangian not respected by the vacuum is said to be spontaneously broken. The mass of the physical boson of the theory is determined by the curvature of the potential about the true ground state: $M^2 = V''(\sigma_\pm) = 2m^2 = 2\lambda\sigma_\pm^2$.

The stress tensor for a scalar field φ is given by,

$$T_{\mu\nu} = \partial_\mu\varphi\partial_\nu\varphi - \mathcal{L}g_{\mu\nu} \ . \tag{1.99}$$

Taking φ to be constant, $\varphi = \langle\varphi\rangle$, we find that $T^{\mu\nu} = V(\langle\varphi\rangle)g^{\mu\nu}$, so that the energy density of the vacuum is,

$$\langle T^0{}_0\rangle \equiv \rho_{_V} = -\frac{m^4}{4\lambda} \ . \tag{1.100}$$

The contribution of the vacuum energy to the energy density of the Universe today can at most be comparable to the critical density $\rho_c = 1.88 \times 10^{-29} h^2 g\ cm^{-3} \simeq 10^{-46}$ GeV. A larger vacuum energy would lead to a present expansion rate greater than that observed. Since the vacuum energy must be so incredibly small relative to any other fundamental energy scale, it is tempting to require $\rho_{_V} = 0$. This can be accomplished by adding the constant $+m^4/4\lambda = \lambda\langle\varphi\rangle^4$ to the Lagrangian. This constant term will not affect the equations of motion or the quantum theory; its sole effect is to make the present vacuum energy vanish. By adding this constant, we can write the potential in the form,

$$V(\varphi) = \frac{\lambda}{4}(\varphi^2 - \sigma^2)^2, \qquad \sigma^2 = \sigma_\pm^2 \ . \tag{1.101}$$

The phase transition from the symmetric phase to the broken phase in this model is second order. In general, a symmetry-breaking phase transition can be first or second order. The temperature dependence of $V(\varphi)$ for a first-order phase transition is shown in Fig. 1.12, where T_c is known as "critical temperature" and it is our reference scale. For $T \gg T_c$ the potential is quadratic, with only one minimum at $\varphi = 0$. For $T = T_c$, the two minima become degenerate, and below T_c, the $\varphi \neq 0$ minimum becomes the global minimum. If for $T \leq T_c$ the extremum at $\varphi = 0$ remains a local minimum, there must be a barrier between the minima at $\varphi = 0$ and $\varphi \neq 0$. Therefore, the change in φ in going from one phase to the other must be discontinuous, indicating a first-order phase transition.

Moreover, the transition cannot take place classically, but must proceed either through quantum or thermal tunnelling. Finally, when $T \ll T_c$ the barrier disappears and the transition may proceed classically.

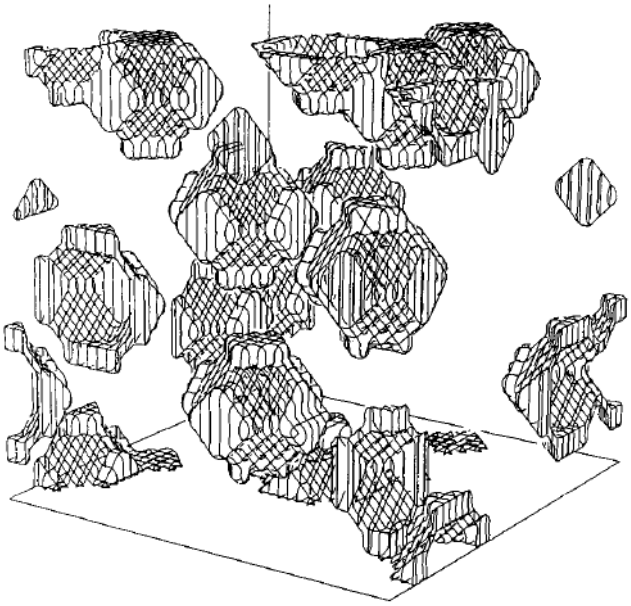

Figure 1.13: From [72] a domain wall network formed in a numerical simulation of a cosmological phase transition where a Z_2 symmetry is spontaneously broken. The contour lines indicate the domain walls that separate the regions of different vacua.

1.4.2 Domain Walls

Domain walls are hypothetical two-dimensional surfaces or boundaries that separate different regions of the universe with distinct vacuum states or field configurations. These vacuum states are associated with different energy levels or properties of a scalar field. Domain walls are a type of cosmic defect that can form during phase transitions in the early universe.

The energy density within a domain wall is typically higher than that in the surrounding regions. This elevated energy density is due to the energy associated with the scalar field transitioning from one vacuum state to another across the wall. Imagine that symmetry-breaking transitions were not "perfect", and that false vacuum remnants were left behind, frozen in the form of topological defects: domain walls, strings, and monopoles.

While domain walls can form during phase transitions, they are not observed in the universe today. This is known as the domain wall problem. If domain walls had persisted until the present day, they would have had significant effects on the large-scale structure of the universe, creating sharp boundaries between regions with different properties. In many cosmological models, domain walls are assumed to have decayed or annihilated long before the formation of galaxies and galaxy clusters. This assumption is based on the idea of a scaling solution, where the number density of domain walls decreases over time as the universe expands.

Recall that the Lagrangian for a real scalar field that undergoes SSB can be written as,

$$\mathcal{L} = \frac{1}{2}(\partial_\mu \varphi)^2 - \frac{1}{4}\lambda(\varphi^2 - \sigma^2)^2 \, . \tag{1.102}$$

The Z_2 reflection symmetry of the Lagrangian, i.e., invariance under $\varphi \leftrightarrow -\varphi$, is spontaneously broken when φ takes on the vacuum expectation value $\langle\varphi\rangle = +\sigma$ or $\langle\varphi\rangle = -\sigma$. So far we have assumed that all of space is in the same ground state, but this need not be the case! Imagine that space is divided into two regions. In one region of space $\langle\varphi\rangle = +\sigma$, and in the other region of space $\langle\varphi\rangle = -\sigma$. Since the scalar field must make the transition from $\varphi = -\sigma$ to $\varphi = +\sigma$ smoothly, there must be a region where $\varphi = 0$, i.e., a region of false vacuum. This transition region between the two

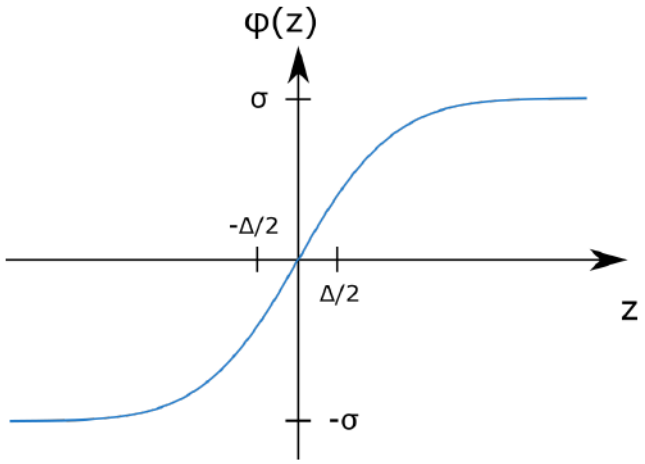

Figure 1.14: The solution $\varphi_w(z)$ for an infinite wall in the $x-y$ plane. Taken from [51].

vacua is called a domain wall. As we shall see, domain walls can arise whenever a Z_2 (or any discrete) symmetry is broken.

Imagine something similar to Fig. 1.13 but consider an infinite wall in the x-y plane at $z = 0$. At $z = -\infty$, $\varphi = -\sigma$, and at $z = +\infty$, $\varphi = +\sigma$. The equation of motion for φ is,

$$-\frac{\partial^2\varphi}{\partial z^2} + \lambda\varphi(\varphi^2 - \sigma^2) = 0 \; . \tag{1.103}$$

The solution to the equation of motion, subject to the boundary conditions above, is,

$$\varphi_w(z) = \sigma \tanh(z/\Delta) \; , \tag{1.104}$$

where the "thickness" of the wall is characterized by,

$$\Delta = (\lambda/2)^{-1/2}\sigma^{-1} \; . \tag{1.105}$$

This solution is illustrated in Fig. 1.14.
The finite, but non-zero, thickness of the wall is easy to understand. The terms contributing to the surface energy density include a gradient term, proportional to,

$$\Delta \times (\nabla\varphi)^2 \sim \sigma^2/\Delta \; , \tag{1.106}$$

and a potential energy term, proportional to,

$$\Delta \times V(\varphi) \sim \Delta\lambda\sigma^4 \; . \tag{1.107}$$

The gradient term is minimized by making the wall as thick as possible, while the potential term is minimized by making the wall as thin as possible. The balance between these terms results in a wall of thickness,

$$\Delta \sim \lambda^{-1/2}\sigma^{-1} \; . \tag{1.108}$$

1.4.3 Cosmic Strings

Cosmic strings are hypothetical one-dimensional topological defects in the fabric of spacetime, predicted by some theories in the field of cosmology and high-energy physics. Cosmic strings are thought to form when the universe undergoes phase transitions. During these transitions, the symmetry of the universe changes, leading to the formation of topological defects. Cosmic strings are

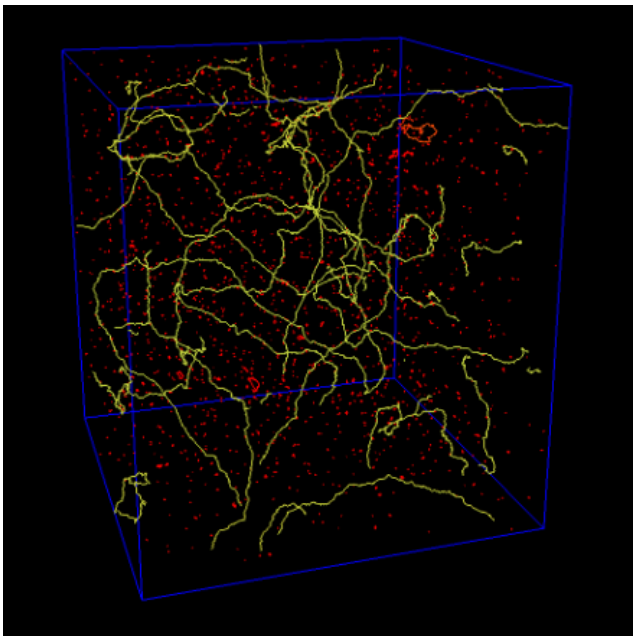

Figure 1.15: Cosmic Strings. *Photo Credit: The Stephen Hawking CTC.*

one such defect. They are extremely thin and dense. They are essentially one-dimensional (see Fig. for a graphical representation) objects with a concentration of energy along their length. The core of a cosmic string is characterized by high energy density. Cosmic strings can cause gravitational lensing, bending light from distant objects as it passes near the string. This can lead to observable effects such as the creation of multiple images of a single distant object. They can also generate density perturbations in the early universe, which can affect the distribution of galaxies and large-scale structure formation. The motion of cosmic strings through the universe can generate gravitational waves. These gravitational waves could potentially be detected by gravitational wave observatories.

1.5 Pulsar Timing Array's Detection of the SGWB

Pulsar Timing Array (PTA) is a collaborative project that aims to detect and study low-frequency gravitational waves by precisely monitoring the arrival times of pulses from a network of millisecond pulsars, which are rapidly rotating neutron stars that emit beams of electromagnetic radiation from their magnetic poles. PTAs are designed to detect gravitational waves in the nanohertz (nHz) frequency range, which is significantly lower than the frequency range observable by ground-based detectors like LIGO and Virgo. PTA involve international collaborations of astronomers and institutions. Examples of PTA initiatives include the North American Nanohertz Observatory for Gravitational Waves (NANOGrav), the European Pulsar Timing Array (EPTA), the Parkes Pulsar Timing Array (PPTA), the Chinese Pulsar Timing Array (CPTA), and the Indian Pulsar Timing Array (InPTA).

The PTA collaborations, NANOGrav [5], EPTA/InPTA [9], PPTA [91], and CPTA [103], have presented evidence for an isotropic SGWB by measuring to $\sim (3-4)\sigma$ the expected Hellings-Downs angular correlation between pulsars' line of sight [61][68]. The GWB is a persistent signal that should increase in significance with number of pulsars and observing time span. This is confirmed by the analysis made by [5]. The detection of a cosmological GWB offers a new window into the physics beyond the standard model that characterize the early Universe [31].

Using the data given by the PTA collaboration, the authors of [50] have recently discussed the interpretation of the detected signal by PTA observations as a GWB of cosmological origin, including

supermassive black hole binaries (SMBHBs), inflation, cosmic strings, first-order phase transitions, large scalar fluctuations, and audible axions. For example, for the case of inflation, their fit to a Power Law spectrum leads to a tensor-to-scalar ratio (at the pivot scale $k_* = 0.05$ Mpc^{-1}) within the range $r_{0.05} \in [4.37 \times 10^{-14},\ 3.47 \times 10^{-9}]$ at 68% CL, which is much below current CMB constraints $r_{0.05} < 0.032$ [99]. A condition of a low-reheating temperature $T_{reh} \lesssim 10.6$ GeV at 68% CL also must be imposed to respect extra radiation ΔN_{eff} constraints [7][25][27][31][76][97]. Also the interpretation calls for an extremely blue tensor spectrum, with spectral index $n_T \simeq 2$ ($n_T \simeq 1.8 \pm 0.3$ [100]). While not impossible, an inflationary origin for the PTA signal looks implausible: within well-motivated inflationary models it is hard to achieve such a blue tilt, whereas models who do tend to predict sizeable non-Gaussianities, excluded by observations [100]. Their fit of the PTA signal also shows a Broken Power Law spectrum, which can be interpreted as a GWB originated in a first-order phase transition. In that case they obtained a central temperature of $T_* \simeq 20$ MeV ($\simeq 94$ MeV) for a strong (weak) PT, which suggests a first-order PT at the MeV scale that is in tension with lattice QCD [11] and BBN prediction [28]. For magneto hydrodynamic (MHD) turbulence (see Chapter 3), their best fit peak position corresponds [85] to a primordial magnetic field of strength $B_0 \simeq 23.3\ \mu$G and correlation length $l_B \simeq 0.25$ pc, which is close to the current constraints on primordial magnetic fields [34][35][67][86].

They also analyzed the other scenarios. To determine which of the models is favored, a model selection/comparison Bayesian analysis was performed. They found that Scalar Induced GWB with a Gaussian bump (gSIGWB) provides the best fit, with a very strong evidence in NANOGrav data and strong in EPTA data [50]. However, Refs. [5][10][48] show that SMBHBs can also fit well the data. Therefore, we still don't have a clear conclusion about the origin of the signal. And this is why we are trying to construct reliable tools to distinguish between the different origins.

Chapter 2

The Cosmological Perturbations

Cosmological perturbations are thought to have originated during the early moments of the universe, possibly during the inflationary epoch. Quantum fluctuations in the energy density and other fields during these early times are believed to have been stretched to cosmological scales during inflation. Understanding the nature of these initial fluctuations, such as their amplitude, spectrum, and statistical properties, is a fundamental aspect of the theory of cosmological perturbations. These initial conditions serve as the seeds for the structure that we observe in the universe today. The perturbations grow and evolve over cosmic time due to the influence of gravity. Regions that are slightly denser than average attract more matter over time, leading to the formation of structures like galaxies and galaxy clusters. The theory of cosmological perturbations helps describe how these fluctuations evolve and give rise to the large-scale structure we observe.

As we mentioned before, one of the most significant pieces of evidence for the theory of cosmological perturbations comes from the Cosmic Microwave Background CMB radiation. The CMB is a snapshot of the universe's early state, and it exhibits tiny temperature fluctuations. These fluctuations in the CMB are directly related to the primordial perturbations. The theory of cosmological perturbations is closely linked to the inflationary model of the universe. Inflationary theory provides a mechanism for generating the initial perturbations during the early universe's rapid expansion, and it predicts specific properties of these perturbations that match observations.

In this chapter, we study the cosmological perturbations at first order, we define the gauge issue and the gauge choice, and review the gauge transformations and gauge-invariant quantities. We also review the comoving curvature perturbation and the curvature perturbation on spatial slices of uniform energy density, and show that on super-hubble scales they're both equal.

2.1 Cosmological Perturbations at First Order

The components of a perturbed spatially flat Robertson–Walker metric can be written as (adopting the notations used in [81]),

$$g_{00} = -a^2(\eta)\left(1 + 2\sum_{r=1}^{+\infty}\frac{1}{r!}\,\psi^{(r)}\right)\,, \tag{2.1}$$

$$g_{0i} = a^2(\eta)\sum_{r=1}^{+\infty}\frac{1}{r!}\,\omega_i^{(r)}\,, \tag{2.2}$$

$$g_{ij} = a^2(\eta)\left\{\left[1 - 2\left(\sum_{r=1}^{+\infty}\frac{1}{r!}\,\phi^{(r)}\right)\right]\delta_{ij} + \sum_{r=1}^{+\infty}\frac{1}{r!}\,\chi_{ij}^{(r)}\right\}\,, \tag{2.3}$$

where $\hat{\chi}_i^{(r)i} = 0$, and η is the conformal time. The functions $\psi^{(r)}$, $\omega_i^{(r)}$, $\phi^{(r)}$, and $\chi_{ij}^{(r)}$ represent the r-th order perturbation of the metric. In the context of perturbations, it is a common practice to decompose them into distinct components known as scalar, vector, and tensor parts. This decomposition help us understand how different types of perturbations behave and interact:

- Scalar Perturbations (Scalar Parts): These are associated with a scalar potential, and they represent variations in the density and pressure of a physical quantity. Scalar perturbations are often referred to as longitudinal perturbations. They describe changes that can be expressed as a scalar field, which can have both spatial and temporal variations.
- Vector Perturbations (Vector Parts): These perturbations are related to transverse vector fields. They describe variations in a physical quantity that can be represented as a divergence-free (solenoidal) vector field. Vector perturbations typically involve changes in the directional flow or rotation of quantities.
- Tensor Perturbations (Tensor Parts): Tensor perturbations are associated with transverse trace-free tensors. They describe variations that can be represented as symmetric traceless tensors. In cosmology, tensor perturbations are often used to describe gravitational waves.

In our specific case, the shift field $\omega_i^{(r)}$ can be decomposed as,

$$\omega_i^{(r)} = \partial_i \omega^{(r)\parallel} + \omega_i^{(r)\perp} \,, \tag{2.4}$$

where $\omega_i^{(r)\perp}$ is a solenoidal vector, i.e., $\partial^i \omega_i^{(r)\perp} = 0$. Similarly, the traceless part of the spatial metric can be decomposed at any order as,

$$\chi_{ij}^{(r)} = \mathrm{D}_{ij}\chi^{(r)\parallel} + \partial_i \chi_j^{(r)\perp} + \partial_j \chi_i^{(r)\perp} + \chi_{ij}^{(r)\top} \,, \tag{2.5}$$

where $\chi^{(r)||}$ is a suitable function, $\chi_i^{(r)\perp}$ is a solenoidal vector field, and $\partial^i \chi_{ij}^{(r)\top} = 0$; subsequently,

$$\mathrm{D}_{ij} \equiv \partial_i \partial_j - \frac{1}{3}\delta_{ij}\nabla^2 \,. \tag{2.6}$$

To first-order only, the full perturbed line element has the following expression:

$$ds^2 = a^2(\eta)\Big[-(1+2\phi)d\eta^2 + 2\hat{\omega}_i d\eta dx^i + \big((1-2\psi)\delta_{ij} + \hat{\chi}_{ij}\big)dx^i dx^j \Big] \,. \tag{2.7}$$

We can write the perturbed stress-energy tensor as,

$$T_{\mu\nu} = T_{\mu\nu}^{(0)} + \delta T_{\mu\nu} = \rho u_\mu u_\nu + p h_{\mu\nu} + \Pi_{\mu\nu} \,, \tag{2.8}$$

where u_μ is the four-velocity of the fluid, while ρ and p are the energy density and isotropic pressure as defined before, and $h_{\mu\nu} = g_{\mu\nu} + u_\mu u_\nu$ is a projection tensor onto the hypersurfaces orthogonal to the four-velocity. The perturbative term $\Pi_{\mu\nu}$ accounts for the presence of anisotropic stresses and thus has a vanishing background value. Let's write the perturbed expression for each component. The energy density can be written as,

$$\rho(\eta, \vec{x}) = \rho^{(0)}(\eta) + \sum_{r=1}^{\infty} \delta\rho^{(r)}(\eta, \vec{x}) \,, \tag{2.9}$$

and similarily for the pressure $p(\vec{x}, \eta)$,

$$p(\eta, \vec{x}) = p^{(0)}(\eta) + \sum_{r=1}^{\infty} \delta p^{(r)}(\eta, \vec{x}) \,. \tag{2.10}$$

Writing $p = p(\rho, S)$, with S being the entropy, its perturbation can also be split in the following way:

$$\delta p = \left(\frac{\partial p}{\partial \rho}\right)_S \delta\rho + \left(\frac{\partial p}{\partial S}\right)_\rho \delta S \,. \tag{2.11}$$

Where the second term accounts for non-adiabatic ($\delta S \neq 0$) contributions, while the first defines the adiabatic speed of sound $c_s^2 = (\partial p/\partial \rho)_S$, computed at constant entropy S.

The anisotropic stress tensor $\Pi_{\mu\nu}$ has only non-vanishing spatial components $\hat{\Pi}_{ij}$, which can be further decomposed into scalar, vector and tensor parts as:

$$\hat{\Pi}_{ij} = D_{ij}\Pi + \partial_i \Pi_j + \partial_j \Pi_i + \Pi_{ij} \ . \tag{2.12}$$

It is considered to be traceless, $\hat{\Pi}^i_i = 0$, since its trace can be absorbed into the definition of the isotropic pressure p. In analogy to the spatial components of the metric, the tensor degrees of freedom Π_{ij} are defined as transverse $\partial_i \Pi_{ij} = 0$. We will consider only the linear part of perturbation (2.12), but in principle, it includes terms up to any order.

Substituting the perturbative expansions back into Eq. (2.8), and keeping terms up to first order, it is possible to recover an explicit expression for the linear perturbation of the stress-energy tensor.

On the other hand, the four-velocity of a comoving observer is,

$$u^\mu = \frac{1}{a}\left(\delta^\mu{}_0 + \sum_{r=1}^{\infty} v^{\mu(r)}(\eta, \vec{x})\right) \ , \tag{2.13}$$

since the unperturbed four-velocity is just $u^\mu_{(0)} = \delta^\mu_0/\sqrt{-g_{00}} = \delta^\mu_0/a$. As for the perturbations, it can be shown (from the normalization condition $u^2 = -1$) that at linear order,

$$v^0 = -\phi \ . \tag{2.14}$$

2.2 The Gauge Issue

The Newtonian view of space-time is adequate only for scales well inside the horizon. On larger scales, one has to worry about the choice of coordinates, and in the presence of perturbations there is no uniquely preferred choice.

Let us continue to denote the coordinates by the same symbols that we used for the Newtonian case, namely t and $\vec{x} \equiv (x_1, x_2, x_3)$. A choice of coordinates defines a threading of space-time into lines (corresponding to fixed $\vec{x}$) and a slicing into hypersurfaces (corresponding to fixed t) [79]. The lines of fixed $\vec{x}$ are chosen to be timelike, so that they are the worldlines of possible observers. Also, the slices are chosen to be spacelike. We can imagine that the Universe is populated by observers corresponding to the threading. On each of the slices one can ask whether geometry is Euclidean. If it is, the coordinates $\vec{x}$ can be chosen to be Cartesian, and the space defined by the slices is said to be flat. Otherwise it is said to have (intrinsic) curvature.

Consider first the limiting case of the unperturbed Universe. In that case there are indeed preferred coordinates, distinguished on several grounds. The threading corresponds to the motion of comoving observers, defined as those who see zero momentum density at their own position. The comoving observers are free-falling, and the expansion defined by them is isotropic. The slicing is orthogonal to the threading, and on each slice, the Universe is homogeneous. The time coordinate is chosen to correspond to proper time along cach worldline. In the critical-density case the slices are flat, and the space coordinates can be chosen to be Cartesian. This formidable array of properties makes the preferred coordinates so valuable that no others are ever considered, except that one sometimes uses spherical polar coordinates instead of Cartesian coordinates.

In the presence of perturbations, it is impossible to find coordinates satisfying all of these properties, and there is no uniquely preferred choice. The only universally accepted constraint is that

the coordinates must reduce to the standard ones in the limit where the perturbations vanish. A choice of coordinates satisfying this constraint is called a ***gauge***, and there is no unique preferred gauge, though there are a few simple choices. In particular, we can find gauges that satisfy some but not all of the conditions listed in the preceding paragraph. Well after horizon entry, all gauges ever suggested become the same, corresponding to the Newtonian description of space-time.

As will become clear, the only function of a gauge choice in cosmological perturbation theory is to define a slicing and threading of space-time. The slicing and threading in turn define the perturbations. For a perturbation $g(\vec{x}, t)$, the space-time coordinates can be regarded as those of unperturbed space-time because to include their perturbation would be a second-order effect. Once defined, the perturbations live in unperturbed space-time!
We can consider the gauge choices for scalar, vector, and tensor perturbations separately. It turns out that the evolution equations for the tensor perturbations are gauge independent, and we are taking the vector perturbations to vanish, which means that we actually are concerned only with the gauge choice for scalar perturbations.

Following the work of [23], we consider the homogeneous FRW spacetime and make the following change of the spatial coordinates,

$$\tilde{x}^i = x^i + \xi^i(\eta, \vec{x}) \ . \tag{2.15}$$

We assume that ξ^i is small, so that it can also be treated as a perturbation. Using:

$$dx^i = \frac{\partial x^i}{\partial \tilde{x}^\nu} d\tilde{x}^\nu = d\tilde{x}^i - \xi^{i\prime} d\eta - \partial_j \xi^i d\tilde{x}^j \ . \tag{2.16}$$

Therefore, we get,

$$ds^2 = a^2\big[-d\eta^2 - 2\xi_i' d\eta d\tilde{x}^i + (\delta_{ij} + \partial_i \xi_j + \partial_j \xi_i) d\tilde{x}^i d\tilde{x}^j \big] \ . \tag{2.17}$$

2.2.1 Gauge Transformations

Consider now the gauge transformation induced by a generic infinitesimal change of coordinates:

$$\tilde{x}^\mu = x^\mu - \xi^\mu(x) \ . \tag{2.18}$$

Where the presence of the minus sign is such that the results we find agree with the sign convention usually adopted in the literature. It is necessary to understand how a given quantity transforms as a consequence of (2.18). In order to do so, we exploit the transformation properties of tensors. We know, in fact, that any given tensor T transforms with the Jacobian (and its inverse) of the change of coordinates, namely:

$$\tilde{T}^\mu{}_\nu(\tilde{x}) = \frac{\partial \tilde{x}^\mu}{\partial x^\rho} \frac{\partial x^\sigma}{\partial \tilde{x}^\nu} T^\rho{}_\sigma(x) \ . \tag{2.19}$$

Where the generalization to a different combination of indices is straightforward. We want to compute the consequences on T of a gauge transformation along the direction ξ. We thus combine equations (2.18) and (2.19) to obtain the relation between the new and old tensors, both evaluated at the same coordinate point:

$$\tilde{T}^\mu{}_\nu = (\delta^\mu{}_\rho - \partial_\rho \xi^\mu)(\delta^\sigma{}_\nu + \partial_\nu \xi^\sigma) T^\rho{}_\sigma(x + \xi) = T^\mu{}_\nu - \partial_\rho \xi^\mu T^\rho{}_\nu + \partial_\nu \xi^\rho T^\mu{}_\rho + \xi^\rho \partial_\rho T^\mu{}_\nu \ , \tag{2.20}$$

where we have kept the linear order in ξ. A similar transformation law is valid for tensors of any order. All the first-order terms in (2.20) can be grouped together into what is known as the Lie derivative of the tensor T along the direction ξ:

$$\mathcal{L}_\xi T^\mu{}_\nu = \partial_\rho T^\mu{}_\nu \xi^\rho - T^\rho{}_\nu \partial_\rho \xi^\mu + T^\mu{}_\rho \partial_\nu \xi^\rho \ , \tag{2.21}$$

where all the terms are evaluated at the same coordinate point. This reflects the independence on the coordinate system of the Lie derivative. Furthermore, the fact that all terms in (2.21) are already

linear in the perturbations lets us consider only the unperturbed part of a tensor T_0 inside the Lie derivative when dealing with first-order CPT.

It is now possible to derive what is the behavior under a gauge transformation of all the metric and stress-energy tensor perturbations we have previously defined. In doing so, it is useful to scalar, vector and tensor decompose the infinitesimal displacement ξ_μ in the following way:

$$\xi^0 = \alpha \,, \tag{2.22}$$
$$\xi^i = \partial^i \beta + d^i \,, \tag{2.23}$$

with $\partial_i d_i = 0$, so that the 4 degrees of freedom are split up between two scalars and one divergenceless vector.

Applying the transformation law (2.20) on the perturbations of the linearly perturbed metric (2.7), we can find how they behave under the infinitesimal change of coordinates (2.18):

$$\tilde{g}_{\mu\nu} = g_{\mu\nu} + \mathcal{L}_\xi g^{(0)}_{\mu\nu} \,. \tag{2.24}$$

As an example, we show the explicit computation for the perturbation ϕ of the $g_{00} = -a^2(1+2\phi)$ component:

$$-a^2(1+2\tilde{\phi}) = -a^2(1+2\phi) - 2aa'\alpha - 2a^2\alpha' \,, \tag{2.25}$$

where we have applied equation (2.24) and used the decomposition (2.23) for the infinitesimal displacement ξ. Solving for $\tilde{\phi}$, we find the following gauge transformation law:

$$\tilde{\phi} = \phi + \mathcal{H}\alpha + \alpha' \,, \tag{2.26}$$

with $\mathcal{H} \equiv a'/a$ defined in analogy with the Hubble parameter but using instead the conformal time η. In a similar way, it is possible to obtain an analogous expression for each of the perturbations in the metric (2.7). We just write down the results of the computations:

$$\begin{aligned}
\tilde{\psi} &= \psi - \mathcal{H}\alpha - \frac{1}{3}\nabla^2\beta \,, \\
\tilde{\hat{\omega}}_i &= \hat{\omega}_i + \partial_i\alpha + \partial_i\beta' + d_i' \,, \\
\tilde{\hat{\chi}}_{ij} &= \hat{\chi}_{ij} + 2D_{ij}\beta + \partial_i d_j + \partial_j d_i \,.
\end{aligned} \tag{2.27}$$

Applying an scalar, vector and tensor decomposition, it is also possible to separate the scalar, vector, and tensor degrees of freedom defined in (2.4) and (2.5):

$$\begin{aligned}
\tilde{\omega} &= \omega - \alpha + \beta' \,, \\
\tilde{\omega}_i &= \omega_i + d_i' \,, \\
\tilde{\chi} &= \chi + 2\beta \,, \\
\tilde{\chi}_i &= \chi_i + d^i \,, \\
\tilde{\chi}_{ij} &= \chi_{ij} \,,
\end{aligned} \tag{2.28}$$

from which it is clear that (transverse and traceless) tensor components are gauge-invariant, at least at linear order in the perturbations.

Similarly, one can compute gauge transformations for the stress-energy tensor perturbations. The procedure is totally analogous to what we have done in the metric perturbations case. For the energy density, it gives:

$$\tilde{\delta\rho} = \delta\rho + \rho_0'\alpha \,. \tag{2.29}$$

Considering instead the 4-velocity, and separating the temporal and spatial components, the gauge transformations are:

$$\tilde{v}^0 = v^0 - \mathcal{H}\alpha - \alpha' \,, \tag{2.30}$$
$$\tilde{v}^i = \hat{v}^i + \partial^i\beta + d^{i\prime} \,. \tag{2.31}$$

The scalar, vector and tensor decomposition allows to write $\hat{v}^i = \partial^i v + v^i$, so that it follows:

$$\tilde{v} = v + \beta \,, \tag{2.32}$$

$$\tilde{v}^i = v^i + d^{i\prime} \,. \tag{2.33}$$

2.3 Curvature Perturbation

2.3.1 The Comoving Curvature Perturbation

The intrinsic spatial curvature on hypersurfaces on constant conformal time η and for a flat universe is given by [93],

$$^{(3)}R = \frac{4}{a^2}\nabla^2 \psi \,. \tag{2.34}$$

The quantity ψ is usually referred to as the *curvature perturbation*. We have seen, however, that the curvature potential ψ is not gauge invariant, but is defined only on a given slicing. Under a transformation on constant time hypersurfaces $\eta \to \eta + \xi^0$ (change of the slicing),

$$\psi \to \psi + \mathcal{H}\xi^0 \,. \tag{2.35}$$

We now consider the *comoving slicing*, which is defined to be the slicing orthogonal to the world lines of comoving observers. These observers are free-falling, and the expansion defined by them is isotropic. In practice, this means that there is no flux of energy measured by these observers, i.e., $T_{0i} = 0$. During inflation, this means that these observers measure $\delta\phi_{com} = 0$ since T_{0i} goes like $\partial_i \delta\phi(\vec{x}, \eta)\phi'(\eta)$. Since $\delta\phi \propto \delta\phi - \phi'\delta\xi^0$ for a transformation on constant time hypersurfaces, this means that,

$$\delta\phi \to \delta\phi_{\rm com} = \delta\phi - \phi'\,\xi^0 = 0 \Longrightarrow \xi^0 = \frac{\delta\phi}{\phi'} \,. \tag{2.36}$$

That is, $\xi^0 = \delta\phi/\phi'$ is the time-displacement needed to go from a generic slicing with a generic $\delta\phi$ to the comoving slicing where $\delta\phi_{com} = 0$. At the same time, the curvature perturbation ψ transforms into,

$$\psi \to \psi_{\rm com} = \psi + \mathcal{H}\,\xi^0 = \phi + \mathcal{H}\frac{\delta\phi}{\phi'} \,. \tag{2.37}$$

The quantity,

$$\mathcal{R} = \psi + \mathcal{H}\frac{\delta\phi}{\phi'} = \psi + H\frac{\delta\phi}{\phi} \,, \tag{2.38}$$

is the *comoving curvature perturbation*. This quantity is gauge-invariant by construction and is related to the gauge-dependent curvature perturbation ψ on a generic slicing to the inflaton perturbation $\delta\phi$ in that gauge. By construction, the meaning of $\mathcal{R}$ is that it represents the gravitational potential on comoving hypersurfaces where $\delta\phi = 0$.

2.3.2 The Curvature Perturbation on Spatial Slices of Uniform Energy Density

We now consider the *slicing of uniform energy density*, which is defined as the slicing where there is no perturbation in the energy density, $\delta\rho = 0$. Since $\delta\rho \propto \delta\rho - \rho'\xi^0$ for a transformation on constant time hypersurfaces, this means that,

$$\mathcal{R} = \psi|_{_{\delta\phi=0}} \,. \tag{2.39}$$

That is, $\xi^0 = \delta\rho/\rho'$ is the time-displacement needed to go from a generic slicing with a generic $\delta\rho$ to the slicing of uniform energy density where $\delta\rho_{unif} = 0$. At the same time, the curvature perturbation ψ transforms into,

$$\delta\rho \to \delta\rho_{\rm unif} = \delta\rho - \rho'\,\xi^0 = 0 \Longrightarrow \xi^0 = \frac{\delta\rho}{\rho'}\ . \tag{2.40}$$

The quantity,

$$\psi \to \psi_{\rm unif} = \psi + \mathcal{H}\,\xi^0 = \psi + \mathcal{H}\frac{\delta\rho}{\rho'}\ , \tag{2.41}$$

is the *curvature perturbation on slices of uniform energy density.* This quantity is gauge-invariant by construction and is related to the gauge-dependent curvature perturbation ψ on a generic slicing and to the energy density perturbation $\delta\rho$ in that gauge. By construction, the meaning of ζ is that it represents the gravitational potential on slices of uniform energy density.

$$\zeta = \psi + \mathcal{H}\frac{\delta\rho}{\rho'} = \psi + H\frac{\delta\rho}{\rho'}\ . \tag{2.42}$$

Notice that, using the energy conservation equation $\rho' + 3\mathcal{H}(\rho + P) = 0$, the curvature perturbation on slices of uniform energy density can also be written as:

$$\zeta = \psi|_{_{\delta\rho=0}}\ . \tag{2.43}$$

During inflation, $\rho + P = \dot{\phi}^2$. Furthermore, on super-Hubble scales from what we have learned that the inflaton fluctuation $\delta\phi$ is frozen in and $\delta\dot{\phi} =$ (slow-roll parameters)$\times H\delta\phi$ This implies that $\delta\rho = \dot{\phi}\delta\dot{\phi} + V'\delta\phi \simeq -3H\dot{\phi}\delta\phi$ leading to,

$$\zeta = \psi - \frac{\delta\rho}{3(\rho + P)}\ , \tag{2.44}$$

where V is the potential of the inflaton field.

$$\zeta \simeq \psi + \frac{3H\dot{\phi}}{3\dot{\phi}^2}\delta\phi = \psi + H\frac{\delta\phi}{\dot{\phi}} = \mathcal{R} \quad \text{(ON SUPER - HUBBLE SCALES)}\ . \tag{2.45}$$

The comoving curvature pertubation and the curvature perturbation on uniform energy density slices are equal on super-Hubble scales during inflation.

Chapter 3

The Cosmological Gravitational Wave Background

Gravitational waves are ripples in spacetime caused by the acceleration of massive objects, particularly those with strong gravitational fields. This includes events such as the collision or merger of black holes, neutron stars, or other massive astrophysical objects, as well as the asymmetric motion of massive objects, like rotating neutron stars. They are a fundamental prediction of Albert Einstein's theory of general relativity, which was published in 1915. Gravitational waves carry energy away from their source and travel at the speed of light, like electromagnetic waves, but they interact with matter and spacetime in a distinct way. They are transverse waves, meaning that their oscillations are perpendicular to their direction of propagation. They cause space to stretch and compress in a rhythmic fashion as they pass through, imagine the stretching and compressing of a rubber sheet, well, it is very similar.

The Laser Interferometer Gravitational-Wave Observatory (LIGO) and the Virgo interferometer are ground-based observatories designed to detect gravitational waves. They use laser interferometry to measure tiny changes in the lengths of two perpendicular arms caused by passing gravitational waves. LIGO and Virgo have made groundbreaking detections, including the first observation of gravitational waves from merging black holes. This first detection of gravitational waves on Sept. 2015 [1], has happily ended 50 years of experimental effort towards a direct detection of GWs.

Gravitational waves can be generated by a variety of astrophysical sources, including binary neutron star systems, binary black hole systems, supernovae, and even the early universe during different possible mechanisms like Inflation, Phase Transitions or Primordial Black Holes. Each type of source produces gravitational waves with different frequencies and amplitudes. In this chapter we focus on the cosmological (early universe) sources, particularly Inflation and Phase Transitions. These waves are described mathematically by the linearized form of Einstein's field equations, which is a set of partial differential equations. These equations describe how spacetime curvature changes due to the presence of mass and energy. The linearized equations reveal how gravitational waves propagate through spacetime as small oscillations or ripples.

In this chapter, we start by describing the Gravitational Waves in a linearized theory of gravity in both cases, the flat Minkowski background, and the curved background. We show how we can distinguish the GWs from the background. We then define the concept of the Stochastic Gravitational Wave Backrgound (SGWB) and its different contributions. We end the chapter by discussing the case of two of these contributions, Inflation and Phase Transitions.

3.1 Gravitational Waves in a Linearized Theory of Gravity

We already know that Einstein's field equations, which describe the behavior of gravity in terms of the metric tensor, are highly nonlinear. However, for small perturbations of a flat spacetime (i.e., weak gravitational fields), they can be linearized. This means that you can write down simplified equations that describe how these small perturbations propagate through spacetime. So, in order to describe the GWs in such a linearized theory of gravity, we start by the approach followed in [31], where we consider a small perturbation over a flat Minkowski background $\eta_{\mu\nu} \equiv diag(-1, +1, +1, +1)$,

$$g_{\mu\nu}(x) = \eta_{\mu\nu} + h_{\mu\nu}(x) \ , \qquad |h_{\mu\nu}(x)| \ll 1 \ , \tag{3.1}$$

where $h_{\mu\nu}$ is that small perturbation and it describes how the spacetime metric deviates from flat Minkowski spacetime. The condition $|h_{\mu\nu}| \ll 1$ holds only if we are considering weak gravitational fields as we just mentioned, and for a restricted set of coordinate systems where Eq. (3.1) holds. General Relativity is invariant under general coordinate transformations,

$$x^{\mu} \longrightarrow x'^{\mu}(x) \ , \tag{3.2}$$

and so the metric tensor can transform as,

$$g'_{\mu\nu}(x') = \frac{\partial x^{\alpha}}{\partial x'^{\mu}} \frac{\partial x^{\beta}}{\partial x'^{\nu}} g_{\alpha\beta}(x) \ . \tag{3.3}$$

So, under general infinitesimal coordinate transformations,

$$x'^{\mu} \longrightarrow x^{\mu} + \xi^{\mu} \ , \tag{3.4}$$

with $\xi^{\mu}(x)$ an arbitrary infinitesimal vector, to derive the transformation law for the perturbation field $h'_{\mu\nu}(x')$, we proceed as follows:

From (3.1) and (3.4) and using (3.3), since we're interested in the linearized theory ($|h_{\mu\nu}(x)| \ll 1$), we can use a Taylor expansion for the transformation $x^{\alpha} \to x'^{\alpha}$:

$$\frac{\partial x^{\alpha}}{\partial x'^{\mu}} \approx \delta^{\alpha}_{\mu} - \partial_{\mu}\xi^{\alpha} \ . \tag{3.5}$$

Substituting this approximation into (3.3):

$$g'_{\mu\nu}(x') = \left(\delta^{\alpha}_{\mu} - \partial_{\mu}\xi^{\alpha}\right)\left(\delta^{\beta}_{\nu} - \partial_{\nu}\xi^{\beta}\right) g_{\alpha\beta}(x) \ . \tag{3.6}$$

Now, simplify the right-hand side:

$$g'_{\mu\nu}(x') = g_{\mu\nu}(x) - \partial_{\mu}\xi^{\alpha} g_{\alpha\nu}(x) - \partial_{\nu}\xi^{\beta} g_{\mu\beta}(x) + \partial_{\mu}\xi^{\alpha}\partial_{\nu}\xi^{\beta} g_{\alpha\beta}(x) \ . \tag{3.7}$$

Remember that $g_{\mu\nu}(x) = \eta_{\mu\nu} + h_{\mu\nu}(x)$, and since, again, we're interested in the linearized theory, we'll neglect terms of $O(h^2)$ and higher:

$$g_{\mu\nu}(x) \approx \eta_{\mu\nu} + h_{\mu\nu}(x) \ . \tag{3.8}$$

Substitute this approximation into the above equation:

$$g'_{\mu\nu}(x') \approx \eta_{\mu\nu} + h_{\mu\nu}(x) - \partial_{\mu}\xi^{\alpha}(\eta_{\alpha\nu} + h_{\alpha\nu}(x)) - \partial_{\nu}\xi^{\beta}(\eta_{\mu\beta} + h_{\mu\beta}(x)) + \partial_{\mu}\xi^{\alpha}\partial_{\nu}\xi^{\beta}(\eta_{\alpha\beta} + h_{\alpha\beta}(x)) \ . \tag{3.9}$$

Now, subtract the Minkowski metric $\eta_{\mu\nu}$ from both sides:

$$h'_{\mu\nu}(x') = h_{\mu\nu}(x) - \partial_{\mu}\xi_{\nu} - \partial_{\nu}\xi_{\mu} + \partial_{\mu}\xi^{\alpha}\partial_{\nu}\xi_{\alpha} \ . \tag{3.10}$$

This equation (3.11) represents how the gravitational wave perturbation $h_{\mu\nu}$ changes under a coordinate transformation ξ^{μ}.

$$h'_{\mu\nu}(x') = h_{\mu\nu}(x) - \partial_{\mu}\xi_{\nu} - \partial_{\nu}\xi_{\mu} \ . \tag{3.11}$$

Expressing Eq. (3.1) in the new system of coordinates gives,

$$g'_{\mu\nu}(x') = \eta_{\mu\nu} + h'_{\mu\nu}(x') \ , \qquad |h'_{\mu\nu}(x')| \ll 1 \ . \tag{3.12}$$

Note that $|\partial_\alpha \xi_\beta|$ must be as small as (or even smaller) $|h_{\alpha\beta}|$.

Now we express the affine connection (Christoffel symbols) to linear order in the tensor perturbation in order to find the expressions for the Riemann tensor, Ricci tensor and Ricci scalar as follows,

$$\Gamma^\alpha{}_{\mu\nu} \equiv \frac{1}{2} g^{\alpha\beta}(\partial_\nu g_{\beta\mu} + \partial_\mu g_{\beta\nu} - \partial_\beta g_{\mu\nu}) = \frac{1}{2}(\partial_\nu h^\alpha{}_\mu + \partial_\mu h^\alpha{}_\nu - \partial^\alpha h_{\mu\nu}) + \mathcal{O}(h^2) \ , \tag{3.13}$$

where,

$$h^\mu{}_\nu \equiv \eta^{\mu\alpha} h_{\alpha\nu} = h_\nu{}^\mu \ , \tag{3.14}$$

and so,

$$R^\alpha{}_{\mu\nu\beta} = \partial_\nu \Gamma^\alpha{}_{\mu\beta} - \partial_\beta \Gamma^\alpha{}_{\mu\nu} = \frac{1}{2}(\partial_\mu \partial_\nu h^\alpha{}_\beta + \partial_\beta \partial^\alpha h_{\mu\nu} - \partial_\nu \partial^\alpha h_{\mu\beta} - \partial_\beta \partial_\mu h^\alpha{}_\nu) \ , \tag{3.15}$$

$$R_{\mu\nu} \equiv -R^\alpha{}_{\mu\nu\alpha} = \frac{1}{2}(\partial_\nu \partial^\alpha h_{\alpha\mu} + \partial_\mu \partial^\alpha h_{\alpha\nu} - \partial_\mu \partial_\nu h - \Box h_{\mu\nu}) \ , \tag{3.16}$$

$$R = R^\mu{}_\mu = (\partial^\alpha \partial^\beta h_{\alpha\beta} - \Box h) \ , \tag{3.17}$$

where $h \equiv h^\alpha{}_\alpha$ is the trace of the metric perturbation, $\partial^\alpha \equiv \eta^{\alpha\beta}\partial_\beta$ and $\Box \equiv \partial_\alpha \partial^\alpha = \eta^{\alpha\beta}\partial_\alpha \partial_\beta$. From these expressions we can construct the Einstein tensor, first defined in Eq. (1.13), again to first order in the metric perturbation, as

$$\begin{aligned} G_{\mu\nu} &\equiv R_{\mu\nu} - \frac{1}{2}\eta_{\mu\nu} R = \frac{1}{2}(\partial_\nu \partial_\alpha h^\alpha{}_\mu + \partial_\mu \partial^\alpha h_{\nu\alpha} - \partial_\mu \partial_\nu h - \Box h_{\mu\nu} - \eta_{\mu\nu}\partial^\alpha \partial_\beta h_\alpha{}^\beta + \eta_{\mu\nu}\Box h) \\ &= \frac{1}{2}(\partial_\alpha \partial_\nu \bar{h}^\alpha{}_\mu + \partial^\alpha \partial_\mu \bar{h}_{\nu\alpha} - \Box \bar{h}_{\mu\nu} - \eta_{\mu\nu}\partial_\alpha \partial^\beta \bar{h}^\alpha{}_\beta) \ , \end{aligned} \tag{3.18}$$

where in the last line, for convenience, we have introduced a new metric perturbation,

$$\bar{h}_{\mu\nu} \equiv h_{\mu\nu} - \frac{1}{2}\eta_{\mu\nu} h \ . \tag{3.19}$$

As the trace of $\bar{h}_{\mu\nu}$ has the opposite sign to that of $h_{\mu\nu}$, $\bar{h} = -h$, $\bar{h}_{\mu\nu}$ is referred to as the trace-reversed metric perturbation. And so, writing $G_{\mu\nu}$ in terms of $\bar{h}_{\mu\nu}$ has the advantage of eliminating the trace.

We can simplify Eq. (3.18) by exploiting the invariance of the linearized theory under slowly varying infinitesimal coordinate transformations. Under the transformation in Eq. (3.4), the metric perturbation $h_{\mu\nu}$ changes as in Eq. (3.11), whereas the trace-reversed perturbation in Eq. (3.19) transforms as,

$$\bar{h}'_{\mu\nu}(x') = \bar{h}_{\mu\nu}(x) + \xi_{\mu\nu}(x), \quad \xi_{\mu\nu}(x) \equiv \eta_{\mu\nu}\partial_\alpha \xi^\alpha - \partial_\mu \xi_\nu - \partial_\nu \xi_\mu \ . \tag{3.20}$$

Having the expression of $G_{\mu\nu}$ in terms of $\bar{h}_{\mu\nu}$, it seems convenient to make a coordinate transformation such that the metric perturbation verifies,

$$\partial^\mu \bar{h}_{\mu\nu}(x) = 0 \ . \tag{3.21}$$

This is the Lorentz gauge choice, which we can prove that it is always possible. This condition ensures that the wave equation for $h_{\mu\nu}$ simplifies to a form that resembles the d'Alembertian wave equation for a massless scalar field, which is easier to work with. Given an arbitrary perturbation $\bar{h}_{\mu\nu}$, for which $\partial^\mu \bar{h}_{\mu\nu} \neq 0$. The Lorentz gauge condition, using Eq. (3.20), transforms as:

$$\partial'^\mu \bar{h}'_{\mu\nu}(x') = \partial^\mu \bar{h}_{\mu\nu}(x) - \Box \xi_\nu \ . \tag{3.22}$$

So that we can always demand that $\partial'^{\mu}\bar{h}'_{\mu\nu}(x') = 0$, as long as,

$$\Box\xi_\nu = f_\nu(x) \ , \qquad f_\nu(x) \equiv \partial^\mu \bar{h}_{\mu\nu}(x) \ . \tag{3.23}$$

One can always find solutions to the above Eq. (3.23), simply because the d'Alembertian operator $\Box$ is invertible. Hence, it is possible to take advantage of the linearized theory's property of remaining unchanged under small coordinate transformations to select the Lorentz gauge.

The advantage of expressing $G_{\mu\nu}$ in terms of the trace-reversed metric becomes now manifest. Restricting the coordinate systems to those verifying the Lorentz-gauge condition Eq. (3.21) leads to, as promised, a very simple expression for the Einstein tensor,

$$G^{(\mathrm{L})}_{\mu\nu} = -\frac{1}{2}\Box\bar{h}_{\mu\nu} \ , \tag{3.24}$$

where $^{(L)}$ refers to the Lorentz gauge. Recall (1.13), in the Lorentz gauge, linearized Einstein gravity reduces therefore to the equation,

$$\Box\bar{h}_{\mu\nu} = -\frac{2}{m_p^2}T_{\mu\nu} \ , \tag{3.25}$$

which is nothing else but a wave equation with a source, and $m_p = 1/\sqrt{8\pi G}$. The general homogeneous solution to the wave equation, based on the superposition of the linearly independent solutions, can be written as,

$$\bar{h}_{\mu\nu}(x) = \int d^3k(\bar{h}_{\mu\nu}(\vec{k})e^{ikx} + \bar{h}^*_{\mu\nu}(\vec{k})e^{-ikx}) \ , \qquad \text{with} \ \ k^\mu\bar{h}_{\mu\nu} = 0 \ , \tag{3.26}$$

where,

$$kx \equiv k^\mu x_\mu \ = \ -\omega(k)t + \vec{k}\cdot\vec{x} \ , \qquad \omega(k) = k \ , \tag{3.27}$$

and $\bar{h}_{\mu\nu}(k)$, are functions that depend solely on the wave vector k. The latter are not free but must rather satisfy,

$$k^\mu\bar{h}_{\mu\nu} = 0 \ . \tag{3.28}$$

This equation essentially expresses that the gravitational wave field $\bar{h}_{\mu\nu}$ is transverse to the direction of propagation given by the vector k^μ. In other words, the components of $\bar{h}_{\mu\nu}$ along the direction of the wave's propagation are zero.

3.1.1 Gravitational Waves in a Curved Background

Now we consider the case of GWs over a curved background. According to General Relativity, matter and energy contribute to the curvature of spacetime. Our goal is to find expressions for the energy and momentum carried by GWs, and so we have to explore in which sense GWs are themselves a source of space-time curvature. In the rest of this chapter we will be dealing with GWs generation processes operating in the early universe, mainly Inflation and Phase Transitions, and hence it is crucial that we determine how to define GWs over a FLRW background, which naturally corresponds to a curved background.

We need to generalize the theory to,

$$g_{\mu\nu}(x) = \bar{g}_{\mu\nu}(x) + \delta g_{\mu\nu}(x) \ , \tag{3.29}$$

with,

$$|\delta g_{\mu\nu}(x)| \ll |\bar{g}_{\mu\nu}(x)| \ , \tag{3.30}$$

and $\bar{g}_{\mu\nu}(x)$ a general metric of a curved spacetime.

The only way to define fluctuations representing gravitational waves in this context is to exploit a possible separation of scales/frequencies, if:

- The background $\bar{g}_{\mu\nu}(x)$ varies over a typical length-scale L_B (or its time variation is characterized by a typical frequency f_B)
- The GWs have a typical reduced wavelength $\bar{\lambda} = \lambda/2\pi$ (or frequency $f = 1/\lambda$)

One can distinguish the GWs from the background if, and only if, $L_B \gg \bar{\lambda}$ ($f_B \ll f$). In this case, the GWs can be viewed as small perturbations on a smooth background, or rapidly varying perturbations over a slowly varying background.

3.2 Stochastic Background of Gravitational Waves

It is basically a sea of gravitational waves that permeates the entire universe. Unlike the discrete and localized gravitational waves produced by individual sources like merging black holes or neutron stars, the stochastic gravitational wave background consists of a superposition of gravitational waves from a multitude of unresolved and randomly distributed sources throughout the cosmos.

The stochastic gravitational wave background is generated by the collective contributions of many astrophysical and cosmological processes, such as the early universe's inflationary phase, cosmic strings, phase transitions, and binary compact object mergers. It is characterized by its frequency spectrum, which describes how the amplitude of gravitational waves varies with frequency. Different astrophysical sources and cosmological events produce gravitational waves at different frequencies, and the SGWB is composed of a wide range of frequencies spanning from extremely low frequencies to very high frequencies.

The SGWB also carries crucial information about the universe's history and evolution. For example, it can provide insights into the nature of the early universe during inflation and other cosmological phase transitions. It can also offer information about the abundance of cosmic strings and the distribution of binary compact object mergers. Researchers are continually developing techniques to improve the sensitivity of gravitational wave detectors and search for the SGWB. Additionally, they are working to distinguish the various contributions to the SGWB and extract valuable cosmological information from it.

3.3 Gravitational Waves from Inflation

In this section, we study the production of GWs from Inflation, since the inflationary scenario predicts also the production of a background of stochastic GW. During the inflationary epoch, quantum fluctuations in the inflaton field can lead to the generation of primordial perturbations. These fluctuations occur on incredibly small scales but are stretched to cosmological scales by the rapid inflation. Just as quantum fluctuations in a field can produce density fluctuations, they can also give rise to gravitational waves. These gravitational waves are the result of fluctuations in the spacetime metric itself. They are sometimes referred to as primordial gravitational waves or inflationary gravitational waves. Gravitational waves in the context of inflation are often described as tensor perturbations. These tensor perturbations represent the perturbations in the metric tensor of spacetime caused by the quantum fluctuations during inflation. Mathematically, they are typically denoted as h_{ij}, where i and j represent spatial indices. Gravitational waves from inflation can leave a specific imprint on the CMB. In particular, they can produce a characteristic pattern of polarization known as B-mode polarization [70][83]. Detecting B-mode polarization in the CMB is a significant goal of observational cosmology because it would provide strong evidence for the existence of primordial

gravitational waves and validate the inflationary theory.

The evolution of the tensor fluctuations is only regulated by the traceless spatial part of the Einstein equation, which, in the presence of perfect fluids does not contain direct influence from the energy content of the universe except for the underlying background solution. We will see later that a coupling between GWs and the content of the Universe grows up only in the presence of anisotropic stress tensor.

Also in this section, we find the expression for the tensor power spectrum, the tensor spectral tilt and the consistency relation for the case of a slow-roll inflationary model.

3.3.1 Power Spectrum

The action of a scalar field minimally coupled to gravity,

$$S = \int d^4x\sqrt{-g}\left[\frac{1}{2}M_{\rm pl}^2 R - \frac{1}{2}g^{\mu\nu}\partial_\mu\varphi\partial_\nu\varphi - \mathbf{V}(\varphi)\right] , \tag{3.31}$$

where M_{pl} is the Planck mass, R is the Ricci scalar, and φ is our scalar field and $a(t)$ is the scale factor. Perturbing it at first order leads to the following action for tensor perturbations [56][57][60], which represents the action for the transverse-traceless (TT) part of the metric perturbation h_{ij} in the framework of cosmological perturbation theory:

$$S_{\rm T}^{(2)} = \frac{M_{\rm pl}^2}{8}\int d^4x\; a^2(t)\left[\dot{h}_{ij}\dot{h}_{ij} - \frac{1}{a^2}(\nabla h_{ij})^2\right] , \tag{3.32}$$

h_{ij} is gauge-invariant, so varying the action with respect to this quantity, we get the required equation of motion,

$$\nabla^2 h_{ij} - a^2\ddot{h}_{ij} - 3a\dot{a}\dot{h}_{ij} = 0 . \tag{3.33}$$

Recalling that h_{ij} is symmetric, transverse and traceless, the solution of Eq. (3.33) is given by,

$$h_{ij}(\vec{x},t) = h(t)e_{ij}^{(+,\times)}(\vec{x}) , \tag{3.34}$$

where $e_{ij}^{(+,\times)}$ is a polarization tensor satisfying the conditions $e_{ij} = e_{ji}$, $k^i e_{ij} = 0$, $e_{ii} = 0$, with $+,\times$ the two GW polarization states [82]. From Eq. (3.34) we can see that tensor modes are left with two physical degrees of freedom. The most general solution of Eq.(3.33) reads,

$$h_{ij}(\vec{x},t) = \sum_{\lambda=(+,\times)} h^{(\lambda)}(t)e_{ij}^{(\lambda)}(\vec{x}) . \tag{3.35}$$

It is now useful to perform the transformation,

$$v_{ij} \equiv \frac{aM_{\rm pl}}{\sqrt{2}}h_{ij} . \tag{3.36}$$

In terms of v_{ij} the action (3.32) reads,

$$S_{\rm T}^{(2)} = \frac{M_{\rm pl}^2}{8}\int d^4x\left[v'_{ij}v'_{ij} - (\nabla v_{ij})^2 + \frac{a''}{a}v_{ij}v_{ij}\right] , \tag{3.37}$$

which can be interpreted as the action for two scalar fields in Minkowski space-time, with effective mass squared equal to a''/a [60]. Being interested in the power-spectrum, we move to Fourier space and write,

$$v_{ij}(\vec{x},t) = \int\frac{d^3\vec{k}}{(2\pi)^3}\sum_{\lambda=(+,\times)} v_{\vec{k}}^{(\lambda)}(t)\; e_{ij}^{(\lambda)}(k)\; e^{i\vec{k}\cdot\vec{x}} , \tag{3.38}$$

where $v_k^{(\lambda)}$ is the Fourier transform of the scalar amplitude. From (3.38), the equation of motion for each mode $v_k^{(\lambda)}$ then reads:

$$v_{\vec{k}}^{(\lambda)\,\prime\prime} + (k^2 - \frac{a''}{a})\, v_{\vec{k}}^{(\lambda)} = 0\,. \tag{3.39}$$

We obtained a wave equation. Let us study the qualitative behavior of its solutions. We can identify two main regimes depending on the relative magnitude of the second and third term.

In the sub-horizon regime ($k \gg aH$):
This implies that $a''/a \ll k^2$ since $a''/a \sim (a'/a)^2$ and in case of de Sitter spacetime $a(\eta) \sim 1/\eta$. So, ignoring the second term in parenthesis, the equation for v_k becomes that of a free harmonic oscillator,

$$v_{\vec{k}}^{(\lambda)\,\prime\prime} + k^2\, v_{\vec{k}}^{(\lambda)} = 0\,, \tag{3.40}$$

so that tensor perturbations h_{ij} oscillate with a damping factor $1/a$. Keeping in this regime, the solution of (3.40) reads,

$$v_k(\eta) = Ae^{-ik\eta}\,, \tag{3.41}$$

which means that the amplitude of the modes of the original field h_{ij} decrease in time with the inverse of the scale-factor as an effect of the Universe expansion.

In the super-horizon regime ($k \ll aH$):
This implies that $a''/a \gg k^2$. In this case the second term is negligible with respect to the third one,

$$v_{\vec{k}}^{(\lambda)\,\prime\prime} - \frac{a''}{a}\, v_{\vec{k}}^{(\lambda)} = 0\,. \tag{3.42}$$

There are two possible solutions of the equation (3.42):

$$v_k(\eta) \propto a\,, \qquad \text{and} \qquad v_k(\eta) \propto 1/a^2\,, \tag{3.43}$$

which corresponds to $h \propto const$ solution and a decreasing in time solution, respectively. We are interested in the solutions with constant amplitude.

Now we calculate more accurately the power-spectrum of tensor perturbations, solving (3.39). We perform the standard quantization of the field writing (similarily to what is done in Chapter 1),

$$v_{\vec{k}}^{(\lambda)} = v_k\,(\eta)\,\hat{a}_{\vec{k}}^{(\lambda)} + v_k^*\,(\eta)\,\hat{a}_{-\vec{k}}^{(\lambda)\dagger}\,, \tag{3.44}$$

where the modes are normalized so that they satisfy $v_k^* v_k' - v_k v_k^{*\prime} = -i$, and this condition ensures that $\hat{a}_k^{(\lambda)}$ and $\hat{a}_{-k}^{(\lambda)\dagger}$ behave as the canonical creation and annihilation operators. Following the simplest and most natural hypothesis, as initial condition, we assume that the Universe was in the vacuum state defined as $\hat{a}_k^{(\lambda)}|0\rangle = 0$ at past infinity, that is the "Bunch-Davies vacuum state" [29].

Equation (3.39) is a Bessel equation, which, in case of de Sitter spacetime, has the following exact solution [2][60]:

$$v_{\vec{k}}\,(\eta) = \sqrt{-\eta}\Big[C_1 H_\nu^{(1)}\,(-k\eta) + C_2 H_\nu^{(2)}\,(-k\eta)\Big]\,, \tag{3.45}$$

where C_1, C_2 are integration constants, $H_v^{(1)}$, $H_v^{(2)}$ are Hankel functions of first and second order and $v \simeq 3/2 + \epsilon$. Remember we have negative sign to η because, from its definition, it lies in $-\infty < \eta < 0$. To determining C_1 and C_2, we impose that in the sub-horizon scales, the solution matches the plane-wave solution $e^{-ik\eta}/\sqrt{2k}$ found before. This hypothesis is a direct consequence of the Bunch-Davies vacuum condition. Using the asymptotic form of Hankel functions:

$$H_\nu^{(1)}\,(x \gg 1) \sim \sqrt{\frac{2}{\pi x}} e^{i(x - \frac{\pi}{2}\nu - \frac{\pi}{4})}\,, \qquad H_\nu^{(2)}(x \gg 1) \sim \sqrt{\frac{2}{\pi x}} e^{-i(x - \frac{\pi}{2}\nu - \frac{\pi}{4})}\,. \tag{3.46}$$

The second term in the solution has negative frequency, so that we have to fit $C_2 = 0$, while matching the asymptotic solution to a plane wave leads to,

$$C_1 = \frac{\sqrt{\pi}}{2} e^{i(\nu+\frac{1}{2})\frac{\pi}{2}} \,. \tag{3.47}$$

Then the exact solution becomes,

$$v_{\vec{k}} = \frac{\sqrt{\pi}}{2} e^{i(\nu+\frac{1}{2})\frac{\pi}{2}} \sqrt{-\eta} H_\nu^{(1)} \left(-k\eta\right) . \tag{3.48}$$

But actually as we mentioned earlier, we are interested in the super-horizon wavelength behaviour, where the Hankel function reads,

$$H_\nu^{(1)} \left(x \ll 1\right) \sim \sqrt{2/\pi} e^{-i\frac{\pi}{2}} 2^{\nu-\frac{3}{2}} \left[\Gamma\left(\nu\right)/\Gamma\left(3/2\right)\right] x^{-\nu} \,, \tag{3.49}$$

so that the fluctuations on such scales become,

$$v_{\vec{k}} = e^{i(\nu-\frac{1}{2})\frac{\pi}{2}} 2^{(\nu-\frac{3}{2})} \frac{\Gamma\left(\nu\right)}{\Gamma\left(3/2\right)} \frac{1}{\sqrt{2k}} \left(-k\eta\right)^{\frac{1}{2}-\nu} \,, \tag{3.50}$$

where Γ is the Euler function.

With the latter equation we can now write the adimensional tensor power-spectrum. Considering that here we deal with two polarization states. Similar to Eq. (1.86), we have,

$$P_{\rm T}\left(k\right) = \frac{k^3}{2\pi^2} \sum_\lambda \left| h_{\vec{k}}^{(\lambda)} \right|^2 \,, \tag{3.51}$$

so that on super-horizon scales, similar to Eq. (1.87) the following power-spectrum holds,

$$P_{\rm T}\left(k\right) = \frac{8}{M_{\rm pl}^2} \left(\frac{H}{2\pi}\right)^2 \left(\frac{k}{aH}\right)^{-2\epsilon} \,. \tag{3.52}$$

Notice that it is almost scale-invariant, which means that all the GW produced, nearly frozen on super-horizon scales, have all the same amplitude. In this case the power-spectrum is called red, where $n_T = -2\epsilon$ and $\epsilon > 0$, while for $n_T > 0$ it is indicated as blue, and the case in which $n_T = 0$ is referred to as scale-invariant. In general, the tensor spectral tilt n_T is given by,

$$n_T = \frac{d\ln\ P_{\rm T}(k)}{d\ln\ k} \,, \tag{3.53}$$

with,

$$P_{\rm T}(k) \propto k^{n_T} \,, \tag{3.54}$$

which is already shown in Eq. (3.52).

3.3.2 Consistency Relation

The relative contribution of GW is often indicated by the tensor-to-scalar ratio r, defined as,

$$r(k_*) \equiv \frac{A_{\rm T}(k_*)}{A_{\rm S}(k_*)} \,, \tag{3.55}$$

where $A_{\rm T}(k_*)$ is the tensor amplitude at some pivot scale k_* and $A_{\rm S}(k_*)$ is the scalar amplitude at the same scale. That yields the amplitude of the GW with respect to that of the scalar perturbations at some fixed pivot scale k_*. We take it to be $k = aH$, i.e. at horizon crossing. From Eq. (3.52), this quantity depends on the time-evolution of the inflaton field, as

$$r = \frac{8}{M_{\rm pl}^2} \left(\frac{\dot{\varphi}}{H}\right)^2 \,, \tag{3.56}$$

that is $r = 16\epsilon$. Furthermore, we have shown that a nearly scale-invariant spectrum of tensor modes is expected, being $n_T = -2\epsilon$. Therefore at the lowest order in slow-roll parameters, one finds the following consistency relation [79]:

$$r = -8n_{\mathrm{T}} \, . \tag{3.57}$$

If this relation really holds true it means that it will be very hard to measure any scale dependence of the tensors, since a large spectral index would invalidate the consistency relation. The consistency relation tells us that if inflation produces a significant amount of gravitational waves (large r), then the tensor perturbations should have a specific spectral tilt, or spectral index (n_T). In particular, if inflation is consistent with observations and produces observable gravitational waves, then r and n_T should be related by the above equation.

3.4 Gravitational Waves from Phase Transitions

We are aware of the concept *Phase Transitions* (PTs), the simplest image we have of phase transitions is that between solid, liquid and gas. PTs can also be cosmological: regions of the universe can abruptly transition from one ground state to another. In this section, we study how gravitational waves are produced by first order phase transitions. We find that there are three process that contribute to the GW production. Before discussing each contribution separately, we define some relevant parameters that parametrize these different contributions. We also obtain an order of magnitude estimate for the characteristic frequency today, which will be shown to be different for each contribution.

3.4.1 First-order Phase Transitions

A first-order cosmological phase transition can occur when two local minima of the free energy coexist for some range of temperatures. In this scenario, the relevant scalar field can quantum mechanically 'tunnel' or thermally fluctuate into the new phase, see the discussion in Section 1.4.1. These quantum or thermal processes involve the nucleation of bubbles in a sea of the metastable phase. These bubbles will then expand and eventually collide with each other. This sequence of events can give rise to a significant stochastic background of gravitational waves. But these bubbles have to collide to source GWs, if they stay isolated, they will not source GWs.

In the production of gravitational waves during a first-order phase transition, three processes play varying roles:

1. **Collisions of bubble walls and (where relevant) shocks in the plasma**: These collisions can be treated using the "envelope approximation" [64][74] and contribute to the GW spectrum from the scalar field itself.

2. **Sound waves in the plasma**: After the bubbles have collided, sound waves can propagate in the plasma until expansion dissipates the kinetic energy. These contribute to the GW background.

3. **Magnetohydrodynamic (MHD) turbulence**: This arises in the plasma formed after the bubble collisions and contributes to the GW background as well.

These three processes typically coexist during a first-order PT, and their contributions to the stochastic GW background combine linearly, at least approximately. So that,

$$h^2\Omega_{\mathrm{GW}} \simeq h^2\Omega_{\phi} + h^2\Omega_{\mathrm{sw}} + h^2\Omega_{\mathrm{turb}} \, . \tag{3.58}$$

During the adiabatic expansion of the universe, it may have undergone several phase transitions driven by the decreasing temperature. These primordial PTs can give rise to various processes that lead to the production of a Stochastic Gravitational Wave Background. In many cases, a relic SGWB

is the only observable remnant after a PT occurs, making it a crucial source of information about the nature of the phase transition itself. Studying the SGWB can provide valuable insights into the physical processes and particles involved in these early universe transitions.

First-order phase transitions are characterized by the presence of a potential barrier within the potential energy landscape associated with an order parameter. This barrier serves as a boundary between two distinct states: the false, symmetric vacuum state and the true, symmetry-breaking vacuum state. As the temperature of the system decreases, the true vacuum state becomes energetically favored over the false vacuum. To make this transition from the false vacuum to the true vacuum possible, the potential barrier must be overcome. This can occur, as we mentioned earlier, through one of two mechanisms: quantum tunneling or thermal fluctuations. In terms of physical space, this transition corresponds to the formation of small bubbles of the true vacuum within the larger, space-filling region of the false vacuum. These bubbles then undergo expansion, driven by the pressure difference acting on their walls. This process ultimately leads to the transformation of the entire system from the false vacuum to the true vacuum state.

In the simplified scenario of a phase transition occurring in a vacuum, the energy released during the transition primarily contributes to the kinetic energy of the expanding bubble walls, causing them to accelerate to nearly the speed of light. However, in the early universe, where these phase transitions take place, the surrounding space is filled with a primordial plasma. In this more realistic setting, a significant portion of the energy released is converted into thermal energy, elevating the temperature of the surrounding plasma. Furthermore, some of the released energy remains invested in the kinetic energy associated with the motion of the bubble walls. Additionally, because the field responsible for the phase transition is often coupled to other fields present in the plasma, a portion of the released energy is transferred to the collective motion of the surrounding fluid. These complex interactions give rise to a diverse range of physical processes and generate sources of gravitational waves linked to first-order phase transitions in the early universe.

In fact, when examining the energy-momentum tensors associated with the gradient energy stored in the expanding bubble walls of the field and the energy-momentum tensor representing the kinetic energy of the bulk plasma motions, if they possess non-zero components of anisotropic stress in their spatial dimensions (typically represented by 'ij'). Then, these non-zero tensor components with spatial anisotropy can serve as origins or sources of gravitational waves. This potential for gravitational wave generation is indicated by [31],

$$\ddot{h}_{ij}(\vec{x},t) + 3\,H\,\dot{h}_{ij}(\vec{x},t) - \frac{\nabla^2}{a^2} h_{ij}(\vec{x},t) = 16\pi G\,\Pi_{ij}^{TT}(\vec{x},t)\ , \tag{3.59}$$

contributing to the stochastic gravitational wave background. The anisotropic stress, when it exists, can be one of the factors contributing to the production of GWs during first-order phase transitions in the early universe. Here $\nabla^2 = \partial_i\partial_i$ is the Laplacian associated to the comoving coordinates x^i, a dot denotes derivative with respect to t, $H = \dot{a}/a$ is the Hubble rate, and Π_{ij}^{TT} is the transverse and traceless part of the anisotropic stress. The anisotropic stress is given by,

$$a^2\Pi_{ij} = T_{ij} - p\,a^2(\delta_{ij} + h_{ij})\ , \tag{3.60}$$

where T_{ij} denotes the spatial components of the energy-momentum tensor of the source, and p is the background pressure. In the RHS of Eq. (3.60), the term in $p\,\delta_{ij}$ is a pure trace that does not contribute to Π_{ij}^{TT}, while the term in $p\,h_{ij}$ cancels out with an identical term of opposite sign that emerges in the derivation of Eq. (3.59).

In general, the detection of a SGWB would serve as a valuable probe for studying the occurrence and nature of cosmological first-order phase transitions, bringing new insights into the underlying high-energy theory describing the primordial universe.

3.4.2 Relevant Parameters and Frequency Shape of the SGWB Spectrum

The gravitational wave signal originating from first-order phase transitions is contingent upon several critical parameters [31][32]. These parameters encompass various aspects of the evolving bubbles within the symmetry-broken phase, including their sizes at the moment of collision and the speed at which their walls expand. Also, an essential factor is the amount of energy available for generating gravitational waves. This energy reservoir is linked to tensor anisotropic stresses, which, in turn, are influenced by a range of contributing factors. Among these factors, the strength of the phase transition itself plays a significant role. The interaction of the field undergoing the phase transition with the surrounding plasma particles is pivotal in determining the energy release and consequent gravitational wave generation as well.

It's important to note that the precise numerical values of these parameters are highly dependent on the specific details and particle physics characteristics of the phase transition in question. However, but the gravitational wave signal can be effectively described in a phenomenological manner that is nearly model-independent, in terms of these parameters. The gravitational wave signal from first-order phase transitions is a complex interplay of bubble dynamics, energy release mechanisms, and the interactions between the transitioning field and the surrounding plasma. Understanding and characterizing these parameters is essential for predicting and interpreting the gravitational wave signatures associated with such phase transitions in the early universe.

Of significance for gravitational wave production is T_*, which represents the temperature of the thermal bath at the moment t_* when GWs are generated. This typically occurs towards the conclusion of the phase transition, coinciding with the time of bubble collisions. For phase transitions that do not involve significant supercooling and reheating, T_* is approximately equivalent to the nucleation temperature, denoted as T_n. The nucleation temperature is determined by the nucleation rate shown below [58] and corresponds to the temperature at which the probability of nucleating one bubble per horizon volume becomes roughly one,

$$\Gamma(t) = A(t)e^{-S(t)} \,, \tag{3.61}$$

where A is a pre-factor with unit of energy to the fourth power, $A(t) \sim \mathcal{M}^4$, where $\mathcal{M} \sim T$ is the typical energy scale of the transition and S is the Euclidean action of a critical bubble [77][90] also a function of T [58]. One can define an approximate inverse time duration of the PT, denoted as β, as the rate of change of the bubble nucleation rate, taking into account that most of the time variation of $\Gamma(t)$ is associated with $S(t)$,

$$\beta \equiv -\frac{dS}{dt}\bigg|_{t_*} \simeq \frac{\dot{\Gamma}}{\Gamma}\bigg|_{t_*} \,. \tag{3.62}$$

The ratio between the inverse duration of the PT, denoted as β, and the inverse characteristic rate of expansion of the universe at the PT time $H(T_*)$, represents a fundamental parameter for the GW signal, as we will demonstrate. From the adiabaticity of the expansion of the universe, $dT/dt = -TH$, therefore,

$$\frac{\beta}{H_*} = T_* \frac{dS}{dT}\bigg|_{T_*} \,. \tag{3.63}$$

This parameter determines R_*, which represents the size of the bubbles near the end of the PT. If v_w is the speed of the bubble wall in the rest frame of the fluid and far from the bubble, then $R_* \simeq v_w/\beta$.

The strength of the PT is quantified by comparing the vacuum energy density released during the transition to the radiation energy density in the universe at the time of the PT. This parameter is sometimes defined in the literature in terms of the latent heat instead of the vacuum energy,

$$\alpha = \frac{\rho_{\rm vac}}{\rho^*_{\rm rad}} \,. \tag{3.64}$$

The magnitude of the gravitational wave signal hinges on the available reservoir of energy capable of generating these waves. In many scenarios, the phase transition takes place within a thermal environment where a substantial portion of the liberated energy is transformed into heat, contributing little to GW production. However, during the phase transition, the process of bubble nucleation unfolds, setting the stage for the motion of bubble walls. Toward the latter stages of the phase transition, as these bubbles collide, they give rise to a non-zero tensor anisotropic stress, which serves as a catalyst for GW generation. As we discussed, this anisotropic stress can emerge from two primary sources: the gradient energy stored within the bubble walls or the collective motion induced within the fluid by the bubbles. This is true assuming that the field responsible for driving the phase transition is coupled to the surrounding plasma. Hence,

$$\kappa_\phi = \frac{\rho_\phi}{\rho_{\rm vac}} \,, \qquad \kappa_v = \frac{\rho_v}{\rho_{\rm vac}} \,. \tag{3.65}$$

From [31], one has,

$$\frac{\rho^*_{\rm GW}}{\rho^*_{\rm tot}} \sim \left(\frac{H_*}{\beta}\right)^2 \left(\frac{\Pi}{\rho^*_{\rm tot}}\right)^2 \,, \tag{3.66}$$

which shows that the GW energy density scales like the square of the ratio of the GW source duration and the Hubble time, and the square of the ratio of the energy density in the source and in the universe at the emission time, which makes sense. Also from [31], the amplitude of the SGWB today becomes,

$$h^2\,\Omega_{\rm GW} \sim 1.6\times 10^{-5} \left(\frac{100}{g_*(T_p)}\right)^{1/3} \left(\frac{H_*}{\beta}\right)^2 \left(\frac{\kappa\,\alpha}{1+\alpha}\right)^2 \,, \tag{3.67}$$

where, to rewrite $\Pi/\rho^*_{\rm tot}$, we have used $\rho^*_{\rm tot} = \rho^*_{\rm rad} + \rho_{\rm vac}$, and we have set $\kappa \sim \Pi/\rho_{\rm vac}$, where κ can be either of the parameters defined in (3.65).

To generate a gravitational wave signal above the sensitivity threshold of a future interferometric detector like LISA ($h^2\Omega_{GW} \gtrsim 10^{-13}$), certain conditions must be met. Typically, detectable signals are produced by very energetic processes involving a substantial fraction of the total energy density in the universe. Simultaneously, these processes need to be relatively slow, minimizing the value of the parameter β/H_*. Specifically, for a GW signal to be detectable, the product $(H_*/\beta)(\Pi/\rho^*_{\rm tot})$ should be greater than or roughly of the order of 10^{-4}. These conditions could be understood looking at Eq. (3.67).

As previously mentioned, the processes leading to the production of the stochastic gravitational wave background primarily occur towards the end of the phase transition when bubble collisions take place. The characteristic wave number k_* of the SGWB generated by these processes corresponds to the inverse of the typical time or length scale of the problem. Specifically, it can be related to either the duration of the PT or the size of the bubbles. Therefore, $k_*/a_* \simeq 2\pi\beta$ or $k_*/a_* \simeq 2\pi/R_* \simeq 2\pi\beta/v_w$, depending on the specific characteristics of the source. In these expressions, a_* represents the scale factor at the time of SGWB production, β is the inverse duration of the PT, and R_* is the size of the bubbles during the late stages of the PT.

If the growth of the bubble proceeds at a highly relativistic speed, the two time/length scales are equal. Setting, for example, $k_*/a_* \simeq 2\pi\beta$, you can [31] obtain an order of magnitude estimate for the characteristic frequency today. This estimate is given by:

$$f \sim 1.6\times 10^{-5}\,{\rm Hz}\,\frac{\beta}{H_*}\left(\frac{g_*(T_*)}{100}\right)^{\frac{1}{6}}\frac{T_*}{100\,{\rm GeV}} \,. \tag{3.68}$$

Since at the end of the PT one expects the entire universe to be converted to the broken phase, i.e. true vacuum, in general the PT must complete faster than a Hubble time, so that $\beta/H_* > 1$.

From the above equation, it appears that indeed, the characteristic frequency of gravitational waves emitted during a phase transition, such as the Electroweak (EW) symmetry breaking at around

100 GeV, can fall within the frequency range of space-based interferometers like LISA. Specifically, for values of $1 \lesssim \beta/H_* \lesssim 10^5$, the characteristic frequency is in the LISA frequency range. This is an interesting feature because it suggests that future space-based interferometers like LISA may have the capability to detect the stochastic gravitational wave background generated during such phase transitions, providing valuable insights into the early universe and the nature of these transitions.

3.4.3 Contribution to the SGWB from the Scalar Field driving the PT: Bubble Wall Collisions

Gravitational wave production resulting from the collision of bubble walls during a phase transition is often analyzed using the *envelope approximation*. This modeling approach streamlines numerical simulations by approximating the bubble walls as spherical, infinitely thin shells, rather than explicitly evolving the scalar field using the Klein-Gordon equation. Under this approximation, gravitational waves originate from the transverse-traceless (TT) component of the energy-momentum tensor associated with the uncollided envelope of these spherical bubbles.

This method has demonstrated its validity in various scenarios, particularly for strongly first-order phase transitions that occur both in vacuum and thermal environments. It is particularly effective when these phase transitions advance at supersonic speeds, a condition often referred to as "detonation". In such cases, the energy-momentum tensor characterizing the collective fluid motions, which are responsible for generating gravitational waves, can be effectively concentrated within a thin shell located near the bubble wall.

Recent numerical simulations using the envelope approximation have provided improved accuracy and a better understanding of a larger portion of the GW spectrum. These simulations have also allowed for a more detailed analysis of the high-frequency behavior of the SGWB spectrum. The resulting SGWB spectrum is [64][102],

$$h^2\Omega_\phi(f) = 1.67 \times 10^{-5} \left(\frac{H_*}{\beta}\right)^2 \left(\frac{\kappa_\phi\, \alpha}{1+\alpha}\right)^2 \left(\frac{100}{g_*(T_*)}\right)^{1/3} \left(\frac{0.11\, v_w^3}{0.42 + v_w^2}\right) \times \frac{3.8(f/f_\phi)^{2.8}}{1 + 2.8(f/f_\phi)^{3.8}}\,, \quad (3.69)$$

where the peak frequency f_ϕ corresponds roughly to the characteristic time-scale of the PT, i.e. its duration $1/\beta$,

$$\frac{f_*}{\beta} = \frac{0.62}{1.8 - 0.1 v_w + v_w^2}\,, \quad (3.70)$$

which becomes, once redshifted to today,

$$f_\phi = 1.65 \times 10^{-2}\,\text{mHz} \left(\frac{f_*}{\beta}\right) \left(\frac{\beta}{H_*}\right) \left(\frac{T_*}{100\,\text{GeV}}\right) \left(\frac{g_*(T_*)}{100}\right)^{\frac{1}{6}}\,. \quad (3.71)$$

3.4.4 Contribution to the SGWB from the Bulk Fluid Motions: Sound Waves

The characteristics of the bulk flow depend on the strength of the coupling of the field driving the PT to the fluid particles: this coupling strongly influences the bubble evolution, as demonstrated by many analyses. In general, it can be assumed that the propagation quickly reaches stability, and the bubble walls expand with a constant velocity, v_w, which can be either subsonic (deflagration) or supersonic (detonation). The bubble wall speed, v_w, should be determined by a full analysis of the microscopic interactions, of the type carried out. However, from the point of view of GW production, the problem can be tackled by introducing a phenomenological parameter, the friction, η, and by studying the bubble evolution as a function of this parameter [49]. Both semi-analytical methods (see e.g., [65]) and numerical simulations (see e.g., [55]) show that the friction modeling the

interactions influences the bubble wall velocity and the transfer of kinetic energy of the scalar field to bulk kinetic energy of the fluid [49], which are important parameters entering the GW production rate.

The most recent and detailed numerical simulations of the full system of the scalar field performing the transition and the surrounding fluid coupled to it via a friction parameter η have been performed in Refs. [62][63]. These have demonstrated that compressional modes, i.e., sound waves, are induced in the surrounding fluid by the expansion of the bubbles due to the coupling between the scalar field and the fluid. At bubble collisions, the sound waves give rise to a non-zero tensor anisotropic stress that is a powerful source of GWs. Simulations have furthermore found that the sound waves continue to act as a source of GWs well after the merging of the bubbles is completed and the scalar field has everywhere settled in the true vacuum. They remain present in the fluid until either they are damped by viscosity or they generate shocks. The long-lasting nature of the sound waves in the primordial fluid enhances the GW signal by a factor β/H_*, making them the most relevant contribution to the SGWB spectrum in the case of PTs that are not very strongly first order and happen in a thermal environment.

The SGWB spectrum from sound waves, fitted from the numerical results of [63], is given by:

$$h^2\Omega_{\rm SW}(f) = 2.65\times10^{-6}\left(\frac{H_*}{\beta}\right)\left(\frac{\kappa_v\,\alpha}{1+\alpha}\right)^2\left(\frac{100}{g_*(T_*)}\right)^{1/3} v_w \times \left(\frac{f}{f_{\rm SW}}\right)^3\left(\frac{7}{4+3(f/f_{\rm SW})^2}\right)^{7/2}, \tag{3.72}$$

where the peak frequency is set by the characteristic size of the bubbles at the end of the transition, and it is approximately given by $f_{\rm sw} \simeq \frac{2}{\sqrt{3}}\left(\frac{\beta}{v_w}\right)$, which, after redshifting, becomes:

$$f_{\rm SW} = 1.9\times10^{-2}\,{\rm mHz}\,\frac{1}{v_w}\left(\frac{\beta}{H_*}\right)\left(\frac{T_*}{100\,{\rm GeV}}\right)\left(\frac{g_*(T_*)}{100}\right)^{\frac{1}{6}}. \tag{3.73}$$

3.4.5 Contribution to the SGWB from the Bulk Fluid Motions: MHD Turbulence

In addition to sound waves, the merging of bubbles during a phase transition could also give rise to swirling or rotational motions within the surrounding fluid. These rotations, or vortical motions, constitute an independent source of gravitational waves. The primordial plasma in the early universe is characterized by an extraordinarily high Reynolds number, which is on the order of 10^{13} at energies around 100 GeV and at the typical scale of the bubbles. This high Reynolds number indicates that when the bubbles collide, they inject energy into the surrounding medium, leading to the formation of what is known as magneto-hydrodynamic (MHD) turbulence and a subsequent generation of GWs through the anisotropic stresses of the chaotic fluid motions and magnetic fields that become prevalent in this energetic environment. It's important to note that turbulence in the early universe is often accompanied by the presence of magnetic fields, as the plasma in this era is fully ionized and exhibits extremely high electrical conductivity. Turbulence can also enhance small magnetic fields that are generated due to charge separation processes at the bubble walls.

In the simulations of [62][63], the vortical component of the bulk fluid motions has been evaluated and was always largely sub-dominant with respect to the compressional one. However, after a characteristic time $\tau_{sh} \sim (v_w/\sqrt{\kappa_v\alpha})\beta^{-1}$ (see e.g., [87]), one expects the formation of shocks that will eventually convert the acoustic signal into a turbulent one. This happens, of course, only if $\tau_{sh} \leq H_*^{-1}$, i.e., if shocks can develop within one Hubble time. From [26][30], the resulting contribution of MHD turbulence to the GW spectrum is,

$$h^2\Omega_{\rm turb}(f) = 3.35\times10^{-4}\left(\frac{H_*}{\beta}\right)\left(\frac{\kappa_{\rm turb}\,\alpha}{1+\alpha}\right)^{\frac{3}{2}}\left(\frac{100}{g_*(T_*)}\right)^{1/3} v_w \times \frac{(f/f_{\rm turb})^3}{[1+(f/f_{\rm turb})]^{\frac{11}{3}}(1+8\pi f/h_*)}, \tag{3.74}$$

where,

$$\kappa_{\rm turb} = \epsilon\, \kappa_v \ , \tag{3.75}$$

represents the (yet unknown) fraction of bulk kinetic energy associated to the vortical motions, as opposed to the compressional modes. Similarly to the sound waves case, the peak frequency is connected to the inverse characteristic length-scale of the source, the bubble size R_* towards the end of the PT: $f_{turb} \simeq (3.5/2)(\beta/v_w)$, which becomes, after red-shifting,

$$f_{\rm turb} = 2.7 \times 10^{-2}\,{\rm mHz}\,\frac{1}{v_w}\left(\frac{\beta}{H_*}\right)\left(\frac{T_*}{100\,{\rm GeV}}\right)\left(\frac{g_*(T_*)}{100}\right)^{\frac{1}{6}} \ . \tag{3.76}$$

Chapter 4

Anisotropies of the Cosmological SGWB

As we discussed earlier in Chapter 3, the Stochastic Gravitational Wave Backrgound consists of a superposition of gravitational waves from many unresolved and randomly distributed sources throughout the cosmos. It could be due to astrophysical and cosmological processes. It is characterized by its frequency spectrum, since different astrophysical sources and cosmological events produce gravitational waves at different frequencies.

This stochastic background showed some degree of anisotropy, that could have been inherited both, at the time of its production, and during its propagation through the perturbed universe. We aim to study and characterize the anisotropies of this background. Studying the directionality dependence of the SGWB will help future dectectors with a better angular resolution of anisotropies of the background, to distinguish among the various backgrounds.

In this chapter, we mainly review what has been done in [14] and [19], and we re-do all the computations but in more details. We follow the Boltzmann approach to study the propagation effects on the SGWB through scalar and tensor perturbations, and we find the expression for the energy density contrast. We write the first order Boltzmann equation in terms of the function Γ, which represents the perturbed part of the distribution function of gravitons, and we find the solution for Γ. We then decompose the solution in Spherical Harmonics for each contribution: the Initial condition term, the Scalar-sourced term, and the Tensor-sourced term. After doing so, we compute the 2-point and 3-point correlation functions of the GW anisotropies, from which we get the angular power spectrum and the angular bispectrum of the GW energy density. Recall that we are interested in the cosmological sources, so after we probe the approach, we will mention two examples, one for Inflation, and the other for Phase Transitions. We then show the imprint of relativistic particles on the anisotropies of the SGWB. Finally, we move our attention to the initial conditions and study the possibility of them being non-adiabatic, instead of the adiabatic assumption we have followed all along.

4.1 Boltzmann Equation for Gravitational Waves

In this discussion, we explore the propagation of gravitons using a Boltzmann approach [39], a method commonly employed in the study of the Cosmic Microwave Background (CMB) (refer to [22][46]). Our analysis considers the distribution f of gravitons within the framework of a FLRW background, incorporating first-order scalar and tensor perturbations. At the unperturbed level, in accordance with the isotropic and homogeneous nature of the background, the graviton distribution relies solely on time and the GW frequency $p/2\pi$ where $\vec{p}$ is the physical momentum of the gravitons

through $q \equiv pa$, where a represents the scale factor of the universe. Essentially, gravitons propagate freely, with their physical momentum experiencing redshift during their journey. This behavior bears a resemblance to that of CMB photons.

However, a fundamental distinction emerges when comparing the SGWB with the CMB: while the temperature anisotropies in the CMB arise exclusively at the last scattering surface or later, the universe remains transparent to GWs at all energy levels below the Planck scale. Consequently, the SGWB offers a snapshot of the universe's conditions immediately following inflation, carrying information about the primordial universe and the mechanisms underlying GW formation. Additionally, in contrast to photon distribution, gravitons' initial population is not expected to be thermal, preserving a 'memory' of the initial state to the distribution. As we demonstrate, the non-thermal nature of the spectrum typically results in angular anisotropies characterized by an order-one dependence on the GW frequency. This stands in contrast to the CMB, where such dependence only manifests at the second order in perturbation theory.

This initial state is inherently anisotropic since no GW production mechanism can be perfectly homogeneous. Furthermore, GW propagation within the perturbed universe introduces additional anisotropies. Our primary focus centers on large scales, operating within a regime where the comoving momentum q of GWs is much larger than the comoving momentum k of large-scale perturbations; $q \gg k$.

We consider first order perturbations around FLRW background in the Poisson gauge,

$$ds^2 = a^2(\eta)[-e^{2\Phi}d\eta^2 + (e^{-2\Psi}\delta_{ij} + h_{ij})dx^i dx^j] \,, \tag{4.1}$$

where a(η) is the scale factor as a function of the conformal time η. Φ and Ψ are scalar perturbations while h_{ij} represent the transverse-traceless (TT) tensor perturbations. Following [14], [19] and [39] we neglect linear vector modes since they are not produced at first order in standard mechanisms for the generation of cosmological perturbations (as scalar field inflation), and we consider tensor modes at linearised order.

We consider a distribution function f such that,

$$f = f(\eta, x^i, q, n^i) \,, \tag{4.2}$$

which is a function the position x^μ and the momentum $p^\mu = dx^\mu/d\lambda$, where λ represents an affine parameter along the trajectory of GWs. This distribution is subject to the Boltzmann equation, which is expressed as $\mathcal{L}[f] = \mathcal{C}[f(\lambda)] + \mathcal{I}[f(\lambda)]$. In this equation, the Liouville term $\mathcal{L}$ corresponds to the derivative with respect to λ. The terms $\mathcal{C}$ and $\mathcal{I}$ respectively account for two distinct processes: the interactions and collisions of GWs within their respective patches and their production from cosmological and astrophysical sources.

The collision interactions among GWs primarily affect the distribution at higher orders (within an expansion series involving the gravitational strength $1/M_{Pl}$) than those we are currently considering. For our purposes, these collision effects can be safely neglected. The term 'emissivity' pertains to the rate at which GWs are emitted and can arise from various sources, including astrophysical phenomena like the merger of black holes in the relatively recent universe, as well as cosmological processes such as inflation or phase transitions. In this particular study, our focus is solely on the stochastic GW background originating from cosmological sources. Consequently, we treat the emissivity term as an initial condition governing the GW distribution. This approach leads us to investigate the free Boltzmann equation, expressed as $df/d\eta = 0$, in the perturbed universe,

$$\frac{df}{d\eta} = \frac{\partial f}{\partial \eta} + \frac{\partial f}{\partial x^i}\frac{dx^i}{d\eta} + \frac{\partial f}{\partial q}\frac{dq}{d\eta} + \frac{\partial f}{\partial n^i}\frac{dn^i}{d\eta} = 0 \,, \tag{4.3}$$

where $\hat{n} \equiv \hat{p}$ is the GW direction of motion, and where we have used the comoving momentum $q \equiv |\vec{p}|a$ (as opposed to the physical one, used in [39],[46]). This simplifies the equations by factorizing out the universe expansion.

The first two terms in Eq. (4.3) encode *free streaming*, that is the propagation of perturbations on all scales. At higher order this term also includes gravitational time delay effects. The third term causes the *red-shifting* of gravitons, including the Sachs-Wolfe (SW) [95], integrated Sachs-Wolfe (ISW) and Rees-Sciama (RS) effects. The fourth term vanishes to first order, and describes the effect of *gravitational lensing*.

Keeping only the terms up to first order in the perturbations, Eq. (4.3) gives,

$$\frac{\partial f}{\partial \eta} + n^i \frac{\partial f}{\partial x^i} + [\frac{\partial \Psi}{\partial \eta} - n^i \frac{\partial \Phi}{\partial x^i} + \frac{1}{2} n^i n^j \frac{\partial h_{ij}}{\partial \eta}] q \frac{\partial f}{\partial q} = 0 \, . \tag{4.4}$$

We now assume that the distribution of GWs consists of two components: a primary, dominant contribution characterized by a distribution function denoted as $\bar{f}$ which is homogeneous and isotropic. Alongside this dominant component, there exists a secondary, subdominant contribution represented by δf These two distribution functions are determined by solving equation (4.4) at both zeroth and first orders within the framework of perturbations. The subdominant anisotropic component δf can be present as an initial condition. However, even if it is initially absent, Eq. (4.4) shows that this anisotropy is produced by the propagation of the isotropic component $\bar{f}$ in the perturbed background. It is convenient to rescale the perturbed part of the distribution function as [14][96],

$$\delta f \equiv -q \frac{\partial \bar{f}}{\partial q} \Gamma(\eta, x^i, q, n^i) \, . \tag{4.5}$$

So, the distribution function f can be expanded as,

$$f(\eta, x^i, q, n^i) = \bar{f}(q) + f^{(1)}(\eta, x^i, q, n^i) + ... \equiv \bar{f}(q) - q \frac{\partial \bar{f}}{\partial q} \Gamma(\eta, x^i, q, n^i) + ... \, . \tag{4.6}$$

In the case of a thermal distribution with temperature T it is observed that the parameter Γ is proportional to $\delta T/T$ This relationship holds true, particularly in the context of the CMB, where the thermalization process ensures that temperature anisotropies remain independent of frequency up to the second order in perturbations. For gravitons, as previously noted, the collisional term is exceedingly small, and in the case of a general production mechanism, the parameter Γ typically exhibits an order-one dependence on frequency. Note that, as we will demonstrate below, also in the case of GWs, the effects of propagation lead to perturbations that are independent of frequency at the linear order.

From the graviton distribution function, evaluated at the present time η_0, we can compute the SGWB energy density,

$$\rho_{GW}(\eta_0, \vec{x}) = \frac{1}{a_0^4} \int d^3q \; q \; f(\eta_0, \vec{x}, q, \hat{n}) \equiv \rho_{crit,0} \int d\ln \; q \; \Omega_{GW}(\vec{x}, q) \, , \tag{4.7}$$

where,

$$\Omega_{GW}(\vec{x}, q) = \frac{1}{\rho_{crit,0}} \frac{d\rho_{GW}}{d\ln \; q} \, , \tag{4.8}$$

with $d\rho_{GW}$ being the energy density in GW contained in the comoving momentum interval q to $q + dq$ [18], and from the chain rule we have,

$$\frac{d \; q}{d\ln \; q} = q \, . \tag{4.9}$$

Substituting Eq. (4.9) and (4.7) into (4.8), we get,

$$\Omega_{GW}(\vec{x}, q) = \frac{1}{\rho_{crit,0}} \frac{1}{a_0^4} \; 4\pi \; q^3 \; dq \; \frac{1}{d\ln \; q} f(\eta_0, \vec{x}, q, \hat{n}) = \frac{4\pi}{\rho_{crit,0}} (\frac{q}{a_0})^4 f(\eta_0, \vec{x}, q, \hat{n}) \, , \tag{4.10}$$

and similarily, its homogenous component,

$$\bar{\Omega}_{GW}(q) \equiv \frac{4\pi}{\rho_{crit,0}}(\frac{q}{a_0})^4 \bar{f}(q) \ . \tag{4.11}$$

For the full spectral energy density, account for a possibly anisotropic dependence, we define,

$$\Omega_{GW}(\vec{x}, q) \equiv \frac{1}{4\pi}\int d^2\hat{n}\ \omega_{GW}(\vec{x}, q, \hat{n}) \ , \tag{4.12}$$

where,

$$\omega_{GW}(\vec{x}, q, \hat{n}) \equiv \frac{4\pi}{\rho_{crit,0}}(\frac{q}{a_0})^4 f(\vec{x}, q, \hat{n}) \ . \tag{4.13}$$

In very good approximation, we can assume that the detector occupies a typical position in the universe where $\Omega_{GW}(\vec{x}, q) = \bar{\Omega}_{GW}(q)$ [96] so that we disregard the dependence on the position. The SGWB density contrast is given by,

$$\delta_{GW} \equiv \delta\omega_{GW}(\vec{x}, q, \hat{n})/\bar{\Omega}_{GW}(q) \equiv \frac{\omega_{GW}(\vec{x}, q, \hat{n}) - \bar{\Omega}_{GW}(q)}{\bar{\Omega}_{GW}(q)} \ . \tag{4.14}$$

From Eqs (4.11) and (4.13), the density contrast can be written as,

$$\delta_{GW} = \frac{\delta f(\vec{x}, q, \hat{n})}{\bar{f}(q)} \ , \tag{4.15}$$

and since,

$$\begin{aligned}
\frac{\partial \ln \bar{\Omega}_{GW}(q)}{\partial \ln q} &= \frac{1}{\bar{\Omega}_{GW}(q)}\frac{\partial \bar{\Omega}_{GW}(q)}{\partial \ln q} \\
&= \frac{q}{\bar{\Omega}_{GW}(q)}\frac{\partial \bar{\Omega}_{GW}(q)}{\partial q} \\
&= \frac{q}{\bar{\Omega}_{GW}(q)}\frac{\bar{\Omega}_{GW}(q)}{\bar{f}(q)}\frac{\partial \bar{f}(q)}{\partial q} + \frac{q}{\bar{\Omega}_{GW}(q)}4\frac{\bar{\Omega}_{GW}(q)}{q} \\
&= \frac{q}{\bar{f}(q)}\frac{\partial \bar{f}(q)}{\partial q} + 4 \ ,
\end{aligned} \tag{4.16}$$

therefore, we have,

$$[4 - \frac{\partial \ln \bar{\Omega}_{GW}(q)}{\partial \ln q}]\Gamma(\eta_0, \vec{x}, q, \hat{n}) = -\frac{q}{\bar{f}(q)}\frac{\partial \bar{f}}{\partial q}\Gamma(\eta_0, \vec{x}, q, \hat{n}) \ , \tag{4.17}$$

and finally,

$$\delta_{GW} = [4 - \frac{\partial \ln \bar{\Omega}_{GW}(q)}{\partial \ln q}]\Gamma(\eta_0, \vec{x}, q, \hat{n}) \ . \tag{4.18}$$

We now aim to write the first order Boltzmann equation in terms of the function Γ, going term by term, using Eq. (4.6),

$$\begin{aligned}
\frac{\partial f}{\partial \eta} &= -q\frac{\partial \bar{f}}{\partial q}\frac{\partial \Gamma}{\partial \eta} \ , \\
n^i\frac{\partial f}{\partial x^i} &= -q\frac{\partial \bar{f}}{\partial q}n^i\frac{\partial \Gamma}{\partial x^i} \ , \\
\frac{\partial \Psi}{\partial \eta}q\frac{\partial f}{\partial q} &= \frac{\partial \Psi}{\partial \eta}q\frac{\partial \bar{f}}{\partial q} - \text{higher orders} \ , \\
n^i\frac{\partial \Phi}{\partial x^i}q\frac{\partial f}{\partial q} &= n^i\frac{\partial \Phi}{\partial x^i}q\frac{\partial \bar{f}}{\partial q} - \text{higher orders} \ , \\
\frac{1}{2}n_i n_j\frac{\partial h_{ij}}{\partial \eta}q\frac{\partial f}{\partial q} &= \frac{1}{2}n_i n_j\frac{\partial h_{ij}}{\partial \eta}q\frac{\partial \bar{f}}{\partial q} - \text{higher orders} \ ,
\end{aligned}$$

collecting all the terms together, neglecting the higher orders,

$$-q\frac{\partial \bar{f}}{\partial q}\frac{\partial \Gamma}{\partial \eta} - q\frac{\partial \bar{f}}{\partial q}n^i\frac{\partial \Gamma}{\partial x^i} + \frac{\partial \Psi}{\partial \eta}q\frac{\partial \bar{f}}{\partial q} - n^i\frac{\partial \Phi}{\partial x^i}q\frac{\partial \bar{f}}{\partial q} + \frac{1}{2}n_i n_j\frac{\partial h_{ij}}{\partial \eta}q\frac{\partial \bar{f}}{\partial q} = 0 \ , \tag{4.19}$$

and we get the desired form,

$$\frac{\partial \Gamma}{\partial \eta} + n^i\frac{\partial \Gamma}{\partial x^i} = S(\eta, x^i, n^i) \ , \tag{4.20}$$

where,

$$S(\eta, x^i, n^i) = \frac{\partial \Psi}{\partial \eta} - n^i\frac{\partial \Phi}{\partial x^i} - \frac{1}{2}n^i n^j\frac{\partial h_{ij}}{\partial \eta} \ , \tag{4.21}$$

is the source function which includes the physical effects due to cosmological scalar and tensor inhomogeneities. Clearly the source is q-independent, confirming what we said earlier about the anisotropies arising at first order from propagation effects being frequency-independent.

It is convenient to Fourier transform with respect to spatial coordinates,

$$\Gamma \equiv \int \frac{d^3k}{(2\pi)^3}e^{i\vec{k}\cdot\vec{x}}\Gamma(\eta, \vec{k}, q, \hat{n}) \ , \tag{4.22}$$

going again term by term,

$$\begin{aligned}
\frac{\partial \Gamma}{\partial \eta} &= \int \frac{d^3k}{(2\pi)^3}e^{i\vec{k}\cdot\vec{x}}\frac{\partial \Gamma}{\partial \eta} \ , \\
n^i\frac{\partial \Gamma}{\partial x^i} &= n^i\int \frac{d^3k}{(2\pi)^3}e^{i\vec{k}\cdot\vec{x}}ik^i\Gamma \ , \\
\frac{\partial \Psi}{\partial \eta} &= \int \frac{d^3k}{(2\pi)^3}e^{i\vec{k}\cdot\vec{x}}\frac{\partial \Psi}{\partial \eta} \ , \\
n^i\frac{\partial \Phi}{\partial x^i} &= n^i\int \frac{d^3k}{(2\pi)^3}e^{i\vec{k}\cdot\vec{x}}ik^i\Phi \ , \\
\frac{1}{2}n^i n^j\frac{\partial h_{ij}}{\partial \eta} &= \frac{1}{2}n^i n^j\int \frac{d^3k}{(2\pi)^3}e^{i\vec{k}\cdot\vec{x}}\frac{\partial h_{ij}}{\partial \eta} \ ,
\end{aligned}$$

so that, the first order Boltzmann equation in terms of the function Γ in fourier space is given by,

$$\Gamma' + ik\mu\Gamma = S(\eta, \vec{k}, \hat{n}) \ , \tag{4.23}$$

where from now on prime denotes a derivative with respect to conformal time, and where we denote by,

$$\mu \equiv \hat{k}\cdot\hat{n} \ , \tag{4.24}$$

the cosine of the angle between the Fourier variable $\vec{k}$ and the direction of motion $\hat{n}$ of the GW. In Fourier space the source term reads,

$$S = \Psi' - ik\mu\Phi - \frac{1}{2}n^i n^j h'_{ij} \ . \tag{4.25}$$

Integrating Eq. (4.23) gives,

$$\begin{aligned}
\Gamma(\eta, \vec{k}, q, \hat{n}) &= e^{ik\mu(\eta_{in}-\eta)}\Gamma(\eta_{in}, \vec{k}, q, \hat{n}) \\
&+ \int_{\eta_{in}}^{\eta} d\eta' e^{ik\mu(\eta'-\eta)}\left[\frac{d\Psi(\eta', \vec{k})}{d\eta'} - ik\mu\Phi(\eta', \vec{k}) - \frac{1}{2}n^i n^j\frac{\partial h_{ij}(\eta', \vec{k})}{\partial \eta'}\right] \ ,
\end{aligned} \tag{4.26}$$

and integrating the second term by parts gives,

$$\Gamma(\eta,\vec{k},q,\hat{n}) = e^{ik\mu(\eta_{in}-\eta)}[\Gamma(\eta_{in},\vec{k},q,\hat{n})+\Phi(\eta_{in},\vec{k})] - \Phi(\eta,\vec{k}) + \int_{\eta_{in}}^{\eta} d\eta' e^{ik\mu(\eta'-\eta)}[\frac{d[\Psi(\eta',\vec{k})+\Phi(\eta',\vec{k})]}{d\eta'} - ik\mu\Phi(\eta',\vec{k}) - \frac{1}{2}n^i n^j \frac{\partial\hat{h}_{ij}(\eta',\vec{k})}{\partial\eta'}] \,, \quad (4.27)$$

with the last two terms in the first line being the boundary terms of this integration. We are not interested in the monopole term, so we can disregard the $-\Phi(\eta,\vec{k})$ contribution to the solution, and write,

$$\Gamma(\eta,\vec{k},q,\hat{n}) = \int_{\eta_{in}}^{\eta} d\eta' e^{ik\mu(\eta'-\eta)}([\Gamma(\eta_{in},\vec{k},q,\hat{n})+\Phi(\eta',\vec{k})]\delta(\eta'-\eta_{in}) + \frac{\partial[\Psi(\eta',\vec{k})+\Phi(\eta',\vec{k})]}{\partial\eta'} - \frac{1}{2}n^i n^j \frac{\partial\hat{h}_{ij}(\eta',\vec{k})}{\partial\eta'}) \,. \quad (4.28)$$

In the following section, we decompose the $\hat{n}$-dependence of that solution in spherical harmonics.

4.2 Spherical Harmonics Decomposition

Now, we separate the different contributions to the solution (4.28) and decompose each by spherical harmonics,

$$\Gamma(\eta,\vec{k},q,\hat{n}) = \Gamma_I(\eta,\vec{k},q,\hat{n}) + \Gamma_S(\eta,\vec{k},\hat{n}) + \Gamma_T(\eta,\vec{k},\hat{n}) \,, \quad (4.29)$$

where I, S, and T stand for Initial, Scalar and Tensor sourced terms respectively and they are given by,

$$\Gamma_I(\eta,\vec{k},q,\hat{n}) = e^{ik\mu(\eta_{in}-\eta)}\Gamma(\eta_{in},\vec{k},q) \,, \quad (4.30)$$

$$\Gamma_S(\eta,\vec{k},\hat{n}) = \int_{\eta_{in}}^{\eta} d\eta' e^{ik\mu(\eta'-\eta)}(\Phi(\eta',\vec{k})]\delta(\eta'-\eta_{in}) + \frac{\partial[\Psi(\eta',\vec{k})+\Phi(\eta',\vec{k})]}{\partial\eta'}) \,, \quad (4.31)$$

$$\Gamma_T(\eta,\vec{k},\hat{n}) = -\frac{1}{2}n^i n^j \int_{\eta_{in}}^{\eta} d\eta' e^{ik\mu(\eta'-\eta)} \frac{\partial\hat{h}_{ij}(\eta',\vec{k})}{\partial\eta'} \,. \quad (4.32)$$

In order to compute the angular power spectrum, in an all-sky analysis we decompose the fluctuations using spin-0 or spin-2 spherical harmonics. Since Γ is a scalar, we can express it as,

$$\Gamma(\hat{n}) = \sum_{\ell}\sum_{m=-\ell}^{\ell} \Gamma_{\ell m} Y_{\ell m}(\hat{n}) \,, \quad (4.33)$$

inverted by,

$$\Gamma_{\ell m} = \int d^2n \Gamma(\hat{n}) Y^*_{\ell m}(\hat{n}) \,. \quad (4.34)$$

So now, we can write,

$$\Gamma_{\ell m} = \int d^2n Y^*_{\ell m}(\hat{n}) \int \frac{d^3k}{(2\pi)^3} e^{i\vec{k}\cdot\vec{x}} \Gamma(\eta,\vec{k},q,\hat{n})[\Gamma_I(\eta,\vec{k},q,\hat{n}) + \Gamma_S(\eta,\vec{k},\hat{n}) + \Gamma_T(\eta,\vec{k},\hat{n})] \equiv \Gamma_{\ell m,I} + \Gamma_{\ell m,S} + \Gamma_{\ell m,T} \,. \quad (4.35)$$

Now, let's evaluate each term.

4.2.1 Initial Condition Term and q-dependent Anisotropies

Let's first evaluate the initial condition term,

$$\Gamma_{\ell m,I} = \int \frac{d^3k}{(2\pi)^3} e^{i\vec{k}\cdot\vec{x_0}} \Gamma(\eta_{in}, \vec{k}, q) \int d^2n Y^*_{\ell m}(\hat{n}) e^{-ik(\eta_0-\eta_{in})\hat{k}\cdot\hat{n}} \ . \tag{4.36}$$

We make use of the identity,

$$e^{-i\vec{k}\cdot\vec{y}} = \sum_\ell (-i)^\ell (2\ell+1) j_\ell(ky) P_\ell(\hat{k}\cdot\hat{y}) = 4\pi \sum_\ell \sum_{m=-\ell}^{\ell} (-i)^\ell j_\ell(ky) Y_{\ell m}(\hat{k}) Y^*_{\ell m}(\hat{y}) \ . \tag{4.37}$$

Since complex conjugation commutes with multiplication, in other words, taking the complex conjugate of the product of two complex numbers is the same as taking the product of their complex conjugates in reverse order, then:

$$\int d^2n \sum_\ell \sum_{m=-\ell}^{\ell} Y_{\ell m}(\hat{k}) Y^*_{\ell m}(\hat{n}) Y^*_{\ell m}(\hat{n}) = \int d^2n \sum_\ell \sum_{m=-\ell}^{\ell} Y_{\ell m}(\hat{n}) Y^*_{\ell m}(\hat{k}) Y^*_{\ell m}(\hat{n}) = Y^*_{\ell m}(\hat{k}) \ . \tag{4.38}$$

Therefore,

$$\Gamma_{\ell m,I} = 4\pi(-i)^\ell \int \frac{d^3k}{(2\pi)^3} e^{i\vec{k}\cdot\vec{x_0}} \Gamma(\eta_{in}, \vec{k}, q) Y^*_{\ell m}(\hat{k}) j_\ell(k(\eta_0-\eta_{in})) \ . \tag{4.39}$$

Here $\vec{x_0}$ denotes our location (that can be set to the origin), η_0 denotes the present time, and η_{in} the initial time. We can clearly see the dependence of the initial condition on the frequency q.

4.2.2 Scalar and Tensor Sourced Terms

Another source of anisotropy arises from the propagation of gravitational waves within the large-scale scalar perturbations present in the universe. These scalar perturbations exhibit much smaller wavenumbers (denoted as k) compared to the frequency of the gravitational waves (q). In that sense, gravitational waves serve as a means to probe these extensive background scalar perturbations. As long as these scalar perturbations remain within the linear regime (which is the case for the large-scale modes that are relevant to the significant anisotropies we are interested in), we can describe them using a transfer function. This transfer function is essentially a deterministic function that encodes how these perturbations change with time, times a stochastic variable ζ However, this description assumes the absence of isocurvature modes, particularly the absence of anisotropic stresses caused by factors like relic neutrinos. Also, this assumption relies on the statistical properties of ζ being well-established prior to the stage of propagation that we are examining. These properties are typically determined during earlier cosmic epochs, such as during inflation or some early phase transition. Therefore, the scalar perturbations are,

$$\Phi(\eta, \vec{k}) = T_\Phi(\eta, k)\zeta(\vec{k}) \ , \qquad \Psi(\eta, \vec{k}) = T_\Psi(\eta, k)\zeta(\vec{k}) \ . \tag{4.40}$$

And so, the scalar sourced term becomes,

$$\begin{aligned} \Gamma_S(\eta_0, \vec{k}, \hat{n}) &= \int_{\eta_{in}}^{\eta_0} d\eta' e^{ik\mu(\eta'-\eta_0)} [T_\Phi(\eta', \vec{k})\delta(\eta'-\eta_{in}) + \frac{\partial[T_\Psi(\eta', k) + T_\Phi(\eta', k)]}{\partial\eta'}]\zeta(\vec{k}) \\ &\equiv \int_{\eta_{in}}^{\eta_0} d\eta' e^{-ik\mu(\eta_0-\eta')} \mathcal{T}_S(\eta', k)\zeta(\vec{k}) \ . \end{aligned} \tag{4.41}$$

Note that we are assuming a single adiabatic mode (i.e. $\zeta(\vec{k})$ is the operator associated with the conserved curvature perturbation at super-horizon scales, see the discussion in the end of Chapter

2). In spherical harmonics,

$$\Gamma_{\ell m,S} = 4\pi(-i)^\ell \int \frac{d^3k}{(2\pi)^3} e^{i\vec{k}\cdot\vec{x_0}} \zeta(\vec{k}) Y^*_{\ell m}(\hat{k}) [T_\Phi(\eta_{in},k) j_\ell(k(\eta_0-\eta_{in})) + \int_{\eta_{in}}^{\eta_0} d\eta' \frac{\partial[T_\Psi(\eta',k)+T_\Phi(\eta',k)]}{\partial\eta'} j_\ell(k(\eta_0-\eta'))] \,. \tag{4.42}$$

From which, it is clear that, also the SGWB, feels, similarly to the CMB, a Sachs-Wolfe and integrated Sachs-Wolfe effect, which are represented by the first and the second term in (4.42), respectively.

The last contribution is due to the GW propagation in the large-scale tensor modes, i.e., perturbations in the metric itself. The tensor sourced term becomes,

$$\Gamma_{\ell m,T} = -\int d^2n Y^*_{\ell m}(\hat{n}) \int \frac{d^3k}{(2\pi)^3} e^{i\vec{k}\cdot\vec{x_0}} \frac{1}{2} n^i n^j \int_{\eta_{in}}^{\eta} d\eta' e^{ik\mu(\eta'-\eta_0)} \frac{\partial h_{ij}(\eta',\vec{k})}{\partial\eta'} \tag{4.43}$$

To evaluate such term we decompose the tensor modes in right and left-handed (respectively $\lambda = \pm 2$) circular polarizations [21],

$$h_{ij} \equiv \sum_{\lambda=\pm 2} e_{ij,\lambda}(\hat{k}) h(\eta,k) \xi_\lambda(k^i) \,. \tag{4.44}$$

The three factors involved in each term are, respectively, the tensor circular polarization operator, the tensor mode function (equal for the two polarizations), and the stochastic variable for that tensor polarization. Using the computations in Appendix A of [19], we get,

$$\Gamma_{\ell m,T} = \pi(-i)^\ell \sqrt{\frac{(\ell+2)!}{(\ell-2)!}} \int \frac{d^3k}{(2\pi)^3} e^{i\vec{k}\cdot\vec{x_0}} \sum_{\lambda=\pm 2} {}_{-\lambda}Y^*_{\ell m}(\Omega_k) \xi_\lambda(\vec{k}) \int_{\eta_{in}}^{\eta_0} d\eta h'(\eta,k) \frac{j_\ell(k(\eta_0-\eta))}{k^2(\eta_0-\eta)^2} \,. \tag{4.45}$$

It is better to write the three contributions in a more compact form as,

$$\begin{aligned}
\Gamma_{\ell m,I} &= 4\pi(-i)^\ell \int \frac{d^3k}{(2\pi)^3} e^{i\vec{k}\cdot\vec{x_0}} \Gamma(\eta_{in},\vec{k},q) Y^*_{\ell m}(\hat{k}) j_\ell(k(\eta_0-\eta_{in})) \,, \\
\Gamma_{\ell m,S} &= 4\pi(-i)^\ell \int \frac{d^3k}{(2\pi)^3} e^{i\vec{k}\cdot\vec{x_0}} \zeta(\vec{k}) Y^*_{\ell m}(\hat{k}) \mathcal{T}^S_\ell(k,\eta_0,\eta_{in}) \,, \\
\Gamma_{\ell m,T} &= 4\pi(-i)^\ell \int \frac{d^3k}{(2\pi)^3} e^{i\vec{k}\cdot\vec{x_0}} \sum_{\lambda=\pm 2} {}_{-\lambda}Y^*_{\ell m}(\Omega_k) \xi_\lambda(\vec{k}) \mathcal{T}^T_\ell(k,\eta_0,\eta_{in}) \,,
\end{aligned} \tag{4.46}$$

where,

$$\begin{aligned}
\mathcal{T}^S_\ell(k,\eta_0,\eta_{in}) &\equiv T_\Phi(\eta_{in},k) j_\ell(k(\eta_0-\eta_{in})) + \int_{\eta_{in}}^{\eta_0} d\eta' \frac{\partial[T_\Psi(\eta,k)+T_\Phi(\eta,k)]}{\partial\eta} j_\ell(k(\eta-\eta_{in}))] \,, \\
\mathcal{T}^T_\ell(k,\eta_0,\eta_{in}) &\equiv \sqrt{\frac{(\ell+2)!}{(\ell-2)!}} \frac{1}{4} \int_{\eta_{in}}^{\eta_0} d\eta \frac{\partial h(\eta,k)}{\partial\eta} \frac{j_\ell(k(\eta_0-\eta))}{k^2(\eta_0-\eta)^2} \,,
\end{aligned} \tag{4.47}$$

are linear transfer functions which represent the time evolution of the graviton fluctuations originated from the primordial perturbation.

4.3 Correlators of GW Anisotropies

We now compute the 2-point and the 3-point angular correlators of the solutions (4.46). We

assume that the stochastic variables are nearly Gaussian, with the 2-point functions,

$$\begin{aligned}\left\langle \Gamma(\eta_{in},\vec{k},q)\Gamma^*(\eta_{in},\vec{k}',q)\right\rangle &= \frac{2\pi^2}{k^3}P_I(q,k)(2\pi)^3\delta(\vec{k}-\vec{k}')\ ,\\ \left\langle \zeta(\vec{k})\zeta^*(\vec{k}')\right\rangle &= \frac{2\pi^2}{k^3}P_\zeta(k)(2\pi)^3\delta(\vec{k}-\vec{k}')\ ,\\ \left\langle \xi_\lambda(\vec{k})\xi^*_{\lambda'}(\vec{k}')\right\rangle &= \frac{2\pi^2}{k^3}P_\lambda(k)\delta_{\lambda,\lambda'}(2\pi)^3\delta(\vec{k}-\vec{k}')\ ,\end{aligned} \tag{4.48}$$

and the 3-point functions,

$$\begin{aligned}\left\langle \Gamma(\eta_{in},\vec{k},q)\Gamma^*(\eta_{in},\vec{k}',q)\Gamma^*(\eta_{in},\vec{k}'',q)\right\rangle &= B_I(q,k,k',k'')(2\pi)^3\delta(\vec{k}+\vec{k}'+\vec{k}'')\ ,\\ \left\langle \zeta(\vec{k})\zeta(\vec{k}')\zeta(\vec{k}'')\right\rangle &= B_\zeta(k,k',k'')(2\pi)^3\delta(\vec{k}+\vec{k}'+\vec{k}'')\ ,\\ \left\langle \xi_\lambda(\vec{k})\xi_{\lambda'}(\vec{k}')\xi_{\lambda''}(\vec{k}'')\right\rangle &= B_\lambda(k,k',k'')\delta_{\lambda,\lambda'}\delta_{\lambda,\lambda''}(2\pi)^3\delta(\vec{k}+\vec{k}'+\vec{k}'')\ .\end{aligned} \tag{4.49}$$

The assumption of nearly Gaussian modes is experimentally verified for the large-scale perturbations of ζ and of ξ_λ, as obtained from the CMB data [37]. We assume that this is the case also for the initial condition term. For simplicity of exposition, we have here assumed that the various terms are not cross-correlated.

The computations performed so far assume statistical isotropy. Correspondingly, when we combine (4.48) and (4.49) with (4.46) we obtain angular correlators with well specific dependence on the multipole indices. Specifically, the two point correlators have the dependence,

$$\left\langle \Gamma_{\ell m}\Gamma^*_{\ell' m'}\right\rangle \equiv \delta_{\ell\ell'}\delta_{mm'}\tilde{C}_\ell\ , \qquad \left\langle \Gamma_{\ell_1 m_1}\Gamma_{\ell_2 m_2}\Gamma_{\ell_3 m_3}\right\rangle \equiv \begin{pmatrix}\ell_1 & \ell_2 & \ell_3\\ m_1 & m_2 & m_3\end{pmatrix}\tilde{b}_{\ell\ell'\ell''}\ , \tag{4.50}$$

while, under the above assumption, the angular power spectrum and the reduced bispectrum consists of the three separate contributions,

$$\tilde{C}_\ell = \tilde{C}_{\ell,I}(q)+\tilde{C}_{\ell,S}+\tilde{C}_{\ell,T}\ , \qquad \tilde{b}_{\ell_1\ell_2\ell_3} = \tilde{b}_{\ell_1\ell_2\ell_3,I}(q)+\tilde{b}_{\ell_1\ell_2\ell_3,S}+\tilde{b}_{\ell_1\ell_2\ell_3,T}\ . \tag{4.51}$$

We recall that the form of the bispectrum factorizes the Wigner-3j symbols [73], which are nonvanishing only provided that $\sum_i m_i = 0$ and that the three ℓ_i satisfy the triangular inequalities,

$$\begin{aligned}&|\ell_1-\ell_2|\le\ell_3\le\ell_1+\ell_2\ ,\\ &|m_1|\le\ell_1\ ,\quad |m_2|\le\ell_2\ ,\quad |m_3|\le\ell_3\ .\end{aligned}$$

4.3.1 Angular Power Spectrum of GW Energy Density

We now compute the 2-point function for the initial condition term, using (4.46),

$$\begin{aligned}\left\langle \Gamma_{\ell m,I}(q)\Gamma^*_{\ell' m',I}(q)\right\rangle =&(4\pi)^2(-i)^{(\ell-\ell')}\int\frac{d^3k}{(2\pi)^3}e^{i\vec{k}\cdot\vec{x}_0}\int\frac{d^3k'}{(2\pi)^3}e^{-i\vec{k}'\cdot\vec{x}_0}\left\langle \Gamma(\eta_{in},\vec{k},q)\Gamma^*(\eta_{in},\vec{k}',q)\right\rangle\\ &\times Y^*_{\ell m}(\hat{k})Y_{\ell' m'}(\hat{k}')j_\ell(k(\eta_0-\eta_{in}))j_{\ell'}(k'(\eta_0-\eta_{in}))\ .\end{aligned} \tag{4.52}$$

we make use of the orthonormality condition of the spherical harmonics, $\int d^2\hat{n}_s Y_{\ell m s}Y^*_{\ell' m'}=\delta_{\ell\ell'}\delta_{mm'}$, and using (4.48), we compute the angular power spectrum as follows,

$$\begin{aligned}&\int\frac{d^3k}{(2\pi)^3}e^{i\vec{k}\cdot\vec{x}_0}\int\frac{d^3k'}{(2\pi)^3}e^{-i\vec{k}'\cdot\vec{x}_0}\left\langle \Gamma(\eta_{in},\vec{k},q)\Gamma^*(\eta_{in},\vec{k}',q)\right\rangle\\ &\qquad=\int\frac{d^3k}{(2\pi)^3}e^{i\vec{k}\cdot\vec{x}_0}\int\frac{d^3k'}{(2\pi)^3}e^{-i\vec{k}'\cdot\vec{x}_0}\times\frac{2\pi^2}{k^3}P_I(q,k)(2\pi)^3\delta(\vec{k}-\vec{k}')\\ &\qquad=\int\frac{4\pi k^2dk}{(2\pi)^3}\frac{1}{(2\pi)^3}\frac{2\pi^2}{k^3}P_I(q,k)(2\pi)^3\\ &\qquad=\int\frac{dk}{k}P_I(q,k)\ ,\end{aligned}$$

which leads to,

$$\left\langle \Gamma_{\ell m,I}(q)\Gamma^{*}_{\ell' m',I}(q)\right\rangle = \delta_{\ell\ell'}\delta_{mm'}4\pi\int\frac{dk}{k}[j_\ell(k(\eta_0-\eta_{in}))]^2 P_I(q,k)\ . \tag{4.53}$$

And using (4.50) we finally find,

$$\tilde{C}_{\ell,I}(q) = 4\pi\int\frac{dk}{k}[j_\ell(k(\eta_0-\eta_{in}))]^2 P_I(q,k)\ , \tag{4.54}$$

and analogously for the other terms,

$$\begin{aligned}\tilde{C}_{\ell,S} &= 4\pi\int\frac{dk}{k}\mathcal{T}^{(S)2}_\ell(k,\eta_0,\eta_{in})P_\zeta(k)\ ,\\ \tilde{C}_{\ell,T} &= 4\pi\int\frac{dk}{k}\mathcal{T}^{(T)2}_\ell(k,\eta_0,\eta_{in})\sum_{\lambda=\pm2}P_\lambda(k)\ .\end{aligned} \tag{4.55}$$

4.3.2 Angular Bispectrum of GW Energy Density

The characterization of the non-Gaussian properties of the SGWB is a potential tool to discriminate whether a SGWB has a primordial or astrophysical origin. The primoridal 3-point function of the GW field, $\langle h^3\rangle$, is unobservable, due to the decoherence of the associated phase (because of the propagation, and the finite duration of the measurement [16][17]), with, possibly, the exception of very specific shapes [45][88]. It is more convenient to consider the non-gaussianity associated to the GW energy density angular distribution, which is not affected by this problem [13].

Starting from the initial conditions again, using (4.46) and the first of (4.49) we get,

$$\begin{aligned}\left\langle\prod_{i=1}^{3}\Gamma_{\ell_i m_i,I}(q)\right\rangle = \prod_{i=1}^{3}[4\pi(-i)^{\ell_i}\int\frac{d^3k_i}{(2\pi)^3}Y^{*}_{\ell_i m_i}(\hat{k_i})j_{\ell_i}(k_i(\eta_0-\eta_{in}))]\\ \times B_I(q,k_1,k_2,k_3)(2\pi)^3\delta^{(3)}(\vec{k_1}+\vec{k_2}+\vec{k_3})\ .\end{aligned} \tag{4.56}$$

And using the representation of the Dirac δ-function,

$$\delta^{(3)}(\vec{k_1}+\vec{k_2}+\vec{k_3}) = \int\frac{d^3y}{(2\pi)^3}e^{i(\vec{k_1}+\vec{k_2}+\vec{k_3})\cdot\vec{y}}\ , \tag{4.57}$$

where $d^3y = y^2dyd\Omega_y$, and so,

$$\int\frac{d^3y}{(2\pi)^3}e^{i\vec{k}\cdot\vec{y}} = \frac{1}{(2\pi)^3}\int_0^\infty y^2dy\int d\Omega_y\ e^{i\vec{k}\cdot\vec{y}}\ , \tag{4.58}$$

and from (4.37),

$$e^{i\vec{k}\cdot\vec{y}} = 4\pi\sum_{L_iM_i}i^L j_L(ky)Y_{L_iM_i}(\hat{k})Y^{*}_{L_iM_i}(\Omega_y)\ , \tag{4.59}$$

therefore,

$$\begin{aligned}\frac{1}{(2\pi)^3}\int_0^\infty y^2dy\int d\Omega_y\ e^{i\vec{k}\cdot\vec{y}} &= \int_0^\infty y^2dy\int d\Omega_y\ \frac{1}{(2\pi)^3}4\pi\sum_{L_iM_i}i^{L_i}j_{Li}(k_iy)Y_{L_iM_i}(\hat{k_i})Y^{*}_{L_iM_i}(\Omega_y)\\ &= \int_0^\infty y^2dy\int d\Omega_y\frac{1}{2\pi^2}\sum_{L_iM_i}i^{L_i}j_{Li}(k_iy)Y^{*}_{L_iM_i}(\Omega_y)Y_{L_iM_i}(\hat{k_i})\ .\end{aligned} \tag{4.60}$$

And using the orthonormality of the spherical harmonics again, we arrive to,

$$\left\langle \prod_{i=1}^{3} \Gamma_{\ell_i m_i, I}(q) \right\rangle = \int d^2\hat{n} Y_{\ell_1 m_1}(\hat{n}) Y_{\ell_2 m_2}(\hat{n}) Y_{\ell_3 m_3}(\hat{n}) \times \int_0^\infty dr r^2 \prod_{i=1}^{3} [4\pi \int \frac{4\pi k_i^2 dk_i}{(2\pi)^3} j_{\ell_i}(k_i(\eta_0 - \eta_{in})) \frac{1}{2\pi^2} j_{\ell_i}(k_i r)] (2\pi)^3 B_I(q, k, k', k'') \,, \tag{4.61}$$

where we have made use of the property $Y^*_{\ell_i m_i}(\hat{n}) Y_{\ell_i m_i}(\hat{k_i}) = Y_{\ell_i m_i}(\hat{n}) Y^*_{\ell_i m_i}(\hat{k_i})$. Therefore,

$$\left\langle \prod_{i=1}^{3} \Gamma_{\ell_i m_i, I}(q) \right\rangle = \mathcal{G}^{m_1 m_2 m_3}_{\ell_1 \ell_2 \ell_3} \int_0^\infty dr r^2 \prod_{i=1}^{3} [\frac{2}{\pi} \int dk_i k_i^2 j_{\ell_i}(k_i(\eta_0 - \eta_{in})) j_{\ell_i}(k_i r)] B_I(q, k, k', k'') \,, \tag{4.62}$$

where we have introduced the Gaunt integrals,

$$\mathcal{G}^{m_1 m_2 m_3}_{\ell_1 \ell_2 \ell_3} \equiv \int d^2\hat{n} Y_{\ell_1 m_1}(\hat{n}) Y_{\ell_2 m_2}(\hat{n}) Y_{\ell_3 m_3}(\hat{n}) = \sqrt{\frac{(2\ell_1+1)(2\ell_2+1)(2\ell_3+1)}{4\pi}} \begin{pmatrix} \ell_1 & \ell_2 & \ell_3 \\ 0 & 0 & 0 \end{pmatrix} \begin{pmatrix} \ell_1 & \ell_2 & \ell_3 \\ m_1 & m_2 & m_3 \end{pmatrix} . \tag{4.63}$$

We remark that also the bispectrum from the initial condition also generally as an $O(1)$ dependence on the GW frequency.

Similarily for the Scalar and Tensor sourced contributions we get,

$$\left\langle \prod_{i=1}^{3} \Gamma_{\ell_i m_i, S} \right\rangle = \mathcal{G}^{m_1 m_2 m_3}_{\ell_1 \ell_2 \ell_3} \int_0^\infty dr r^2 \prod_{i=1}^{3} [\frac{2}{\pi} \int dk_i k_i^2 \mathcal{T}^S_{\ell_i}(k_i, \eta_0, \eta_{in}) j_{\ell_i}(k_i r)] B_\zeta(k, k', k'') \,,$$
$$\left\langle \prod_{i=1}^{3} \Gamma_{\ell_i m_i, T} \right\rangle = \sum_{\lambda=\pm 2} \prod_{i=1}^{3} [4\pi(-i)^{\ell_i} \int \frac{k_i^2 dk_i}{(2\pi)^3} \mathcal{T}^T_{\ell,i}(k_i, \eta_0, \eta_{in}) \int d\Omega_{k_i} {}_{-\lambda}Y^*_{\ell_i m_i}(\Omega_{k_i})] \left\langle \prod_{i=1}^{3} \xi_\lambda(\vec{k_i}) \right\rangle . \tag{4.64}$$

The tensor sourced contribution can be also written in the form:

$$\left\langle \prod_{i=1}^{3} \Gamma_{\ell_i m_i, T} \right\rangle = \mathcal{G}^{m_1 m_2 m_3}_{\ell_1 \ell_2 \ell_3} [\prod_{i=1}^{3} [4\pi(-i)^{\ell_i} \int \frac{k_i^2 dk_i}{(2\pi)^3} \mathcal{T}^T_{\ell,i}(k_i, \eta_0, \eta_{in})] \sum_{\lambda=\pm 2} \tilde{\mathcal{F}}^\lambda_{\ell_1 \ell_2 \ell_3}(k_1, k_2, k_3) \,, \tag{4.65}$$

where,

$$\tilde{\mathcal{F}}^\lambda_{\ell_1 \ell_2 \ell_3}(k_1, k_2, k_3) \equiv \sqrt{4\pi} \begin{pmatrix} \ell_1 & \ell_2 & \ell_3 \\ 0 & 0 & 0 \end{pmatrix}^{-1} \sum_{m_1, m_2, m_3} \begin{pmatrix} \ell_1 & \ell_2 & \ell_3 \\ m_1 & m_2 & m_3 \end{pmatrix} \times [\prod_{i=1}^{3} \int d\Omega_{k_i} \frac{-\lambda Y^*_{\ell_i m_i}(\Omega_{k_i})}{\sqrt{2\ell_i + 1}}] \left\langle \xi_\lambda(\vec{k}_1) \xi_\lambda(\vec{k}_2) \xi_\lambda(\vec{k}_3) \right\rangle . \tag{4.66}$$

Note that we have neglected for simplicity all the mixed scalar-tensor correlators.

4.3.3 Reduced Bispectrum

We now write the explicit form of the reduced bispectra contributing to (4.51),

$$\tilde{b}_{\ell_1\ell_2\ell_3,I} = \int_0^\infty dr r^2 \prod_{i=1}^3 [\frac{2}{\pi}\int dk_i k_i^2 j_{\ell_i}(k_i(\eta_0-\eta_{in}))j_{\ell_i}(k_i r)]B_I(q,k_1,k_2,k_3)\ ,$$
$$\tilde{b}_{\ell_1\ell_2\ell_3,S} = \int_0^\infty dr r^2 \prod_{i=1}^3 [\frac{2}{\pi}\int dk_i k_i^2 \mathcal{T}^S_{\ell_i}(k_i,\eta_0,\eta_{in})j_{\ell_i}(k_i r)]B_\zeta(k,k',k'')\ , \tag{4.67}$$

and for the tensor bispectrum,

$$\left\langle \prod_{i=1}^3 \Gamma_{\ell_i m_i,T}\right\rangle = \mathcal{G}^{m_1m_2m_3}_{\ell_1\ell_2\ell_3}[\prod_{i=1}^3[4\pi(-i)^{\ell_i}\int \frac{k_i^2 dk_i}{(2\pi)^3}\mathcal{T}^T_{\ell,i}(k_i,\eta_0,\eta_{in})]\sum_{\lambda=\pm2}\sqrt{4\pi}\begin{pmatrix}\ell_1 & \ell_2 & \ell_3\\ 0 & 0 & 0\end{pmatrix}^{-1}$$
$$\times \sum_{m_1,m_2,m_3}\begin{pmatrix}\ell_1 & \ell_2 & \ell_3\\ m_1 & m_2 & m_3\end{pmatrix}[\prod_{i=1}^3\int d\Omega_{k_i}\frac{-{}_\lambda Y^*_{\ell_i m_i}(\Omega_{k_i})}{\sqrt{2\ell_i+1}}]\left\langle \xi_\lambda(\vec{k}_1)\xi_\lambda(\vec{k}_2)\xi_\lambda(\vec{k}_3)\right\rangle\ . \tag{4.68}$$

Therefore,

$$\tilde{b}_{\ell_1\ell_2\ell_3,T} = \frac{4}{\pi^2}\sum_{\lambda=\pm2}\sum_{m_i}\begin{pmatrix}\ell_1 & \ell_2 & \ell_3\\ 0 & 0 & 0\end{pmatrix}^{-2}\mathcal{G}^{m_1m_2m_3}_{\ell_1\ell_2\ell_3}[\prod_{i=1}^3\frac{(-i)^{\ell_i}}{2\ell_i+1}\int d^3k_i \mathcal{T}^T_{\ell,i}(k_i)\,{}_{-\lambda}Y^*_{\ell_i m_i}(\Omega_{k_i})]$$
$$\times\,\delta(\vec{k}+\vec{k}'+\vec{k}'')B_\lambda(\vec{k},\vec{k}',\vec{k}'') \tag{4.69}$$

4.4 First Example: The Axion-Inflaton

As we previously mentioned, we will give two examples, one being on Inflation. Our goal here is to understand under which conditions the initial term $\Gamma_I(q)$ has a nontrivial q-dependence, making it distinct from other contributions to the anisotropy. We are specifically examining a scenario where an axion inflaton ϕ sources gauge fields, which in turn generates a large GW background. In particular we consider the specific evolution shown in Figure 4 of [52]. In this scenario, the inflaton potential is chosen in such a way that it results in peak in the GW signal at frequencies that are relevant for LISA, without overproducing scalar perturbations and primordial black holes. The amount of GWs sourced in this mechanism is controlled by the parameter $\xi \equiv (\dot{\phi}/2f_\phi H)$, where f_ϕ is the decay constant of the axion inflaton. The present fractional energy in GW, $\Omega_{GW}(\eta_0,q)$, is related to the primordial GW power spectrum $P_\lambda(\eta_{in},q)$ by [31],

$$\Omega_{GW}(\eta_0,q) = \frac{3}{128}\Omega_{rad}\sum_\lambda P_\lambda(\eta_{in},q)[\frac{1}{2}(\frac{q_{eq}}{q})^2+\frac{4}{9}(\sqrt{2}-1)]\ . \tag{4.70}$$

Since we are interested in the modes with $q \gg q_{eq}$, that entered the horizon during radiation domination, we consider only the second term in the square bracket, and we find,

$$\Omega_{GW}(\eta_0,q) = \text{constant}\times\sum_\lambda \mathrm{P}_\lambda(\eta_{\mathrm{in}},\mathrm{q})\ . \tag{4.71}$$

We are studying here the contribution from the initial condition, so we can safely neglect the scalar and tensor modes. We therefore assume that the value of the energy density that arrives to the location $\vec{x}$ from the direction $\hat{n}$ is controlled by the parameter,

$$\xi = \bar{\xi} + \delta\xi(\vec{x}+d\hat{n})\ , \tag{4.72}$$

where ξ is the value that this parameter had during inflation at the location $\vec{x}+d\hat{n}$, and d is the distance covered by the gravitons between the initial and the present time (equal for all directions, since we are disregarding the effect of the long scale modes ζ). In writing this relation, we have assumed that the parameter ξ is in turn controlled by a dynamical field (the rolling axion, in the

example of [52]), which results in the background value $\bar{\xi}$, and in the perturbation $\delta\xi$.
We generalize Eq. (4.1) to,

$$\omega_{GW}(\eta_0, \vec{x}, q, \hat{n}) = \text{constant} \times \sum_{\lambda} \mathrm{P}_{\lambda}(\mathrm{q}, \xi(\eta_0, \tilde{\mathrm{x}}, \hat{\mathrm{n}})) \,, \tag{4.73}$$

which has the background value $\bar{\Omega}_{GW}(\eta_0, q) = constant \times \sum_\lambda P_\lambda(q, \bar{\xi})$. Therefore we have,

$$4 - \frac{\partial \ln \bar{\Omega}_{GW}(\eta_0, q)}{\partial \ln q} = 4 - \frac{\partial \ln[\sum_\lambda P_\lambda(q, \bar{\xi})]}{\partial \ln q}. \tag{4.74}$$

The density contrast is given by,

$$\delta_{GW}(\eta_0, \vec{x}, q, \hat{n}) = \frac{\sum P_\lambda(q, \xi(\eta_0, \vec{x}, \hat{n})) - \sum P_\lambda(q, \bar{\xi})}{\sum P_\lambda(q, \bar{\xi})} \,. \tag{4.75}$$

The numerator can be written as,

$$\sum P_\lambda(q, \xi(\eta_0, \vec{x}, \hat{n})) - \sum P_\lambda(q, \bar{\xi}) = \sum P_\lambda(q, \bar{\xi} + \delta\xi(\vec{x} + d\hat{n})) - \sum P_\lambda(q, \bar{\xi}) \,. \tag{4.76}$$

Taylor expanding the first term on the R.H.S, we get,

$$P_\lambda(q, \bar{\xi} + \delta\xi(\vec{x} + d\hat{n})) = P_\lambda(q, \bar{\xi}) + \frac{\partial P_\lambda}{\partial \bar{\xi}} \delta\xi(\vec{x} + d\hat{n}) + \dots \,. \tag{4.77}$$

Therefore,

$$\begin{aligned} \sum P_\lambda(q, \bar{\xi} + \delta\xi(\vec{x} + d\hat{n})) - \sum P_\lambda(q, \bar{\xi}) &= \sum \left(P_\lambda(q, \bar{\xi}) + \frac{\partial P_\lambda}{\partial \bar{\xi}} \delta\xi(\vec{x} + d\hat{n}) + \dots \right) - \sum P_\lambda(q, \bar{\xi}) \\ &= \sum \frac{\partial P_\lambda}{\partial \bar{\xi}} \delta\xi(\vec{x} + d\hat{n}) + \dots \,. \end{aligned} \tag{4.78}$$

Substituting this result back into the density contrast expression, we find,

$$\frac{\sum \frac{\partial P_\lambda}{\partial \bar{\xi}} \delta\xi(\vec{x} + d\hat{n})}{\sum P_\lambda(q, \bar{\xi})} = \frac{\partial \ln[\sum_\lambda P_\lambda(q, \bar{\xi})]}{\partial \bar{\xi}} \delta\xi(\vec{x} + d\hat{n}) \,. \tag{4.79}$$

And the final expression is,

$$\delta_{GW}(\eta_0, \vec{x}, q, \hat{n}) = \frac{\sum P_\lambda(q, \xi(\eta_0, \vec{x}, \hat{n})) - \sum P_\lambda(q, \bar{\xi})}{\sum P_\lambda(q, \bar{\xi})} = \frac{\partial \ln[\sum_\lambda P_\lambda(q, \bar{\xi})]}{\partial \bar{\xi}} \delta\xi(\vec{x} + d\hat{n}) \,. \tag{4.80}$$

From Eq. (4.18) we can write,

$$\Gamma_I(\eta_0, \vec{x}_0, q, \hat{n}) \equiv \mathcal{F}(q, \bar{\xi}) \delta\xi(\vec{x}_0 + d\hat{n}) \,, \tag{4.81}$$

with,

$$\mathcal{F}(q, \bar{\xi}) \equiv \frac{1}{4 - n_T} \frac{\partial \ln[\sum_\lambda P_\lambda(q, \bar{\xi})]}{\partial \bar{\xi}} \,, \qquad n_T \equiv \frac{\partial \ln[\sum_\lambda P_\lambda(q, \bar{\xi})]}{\partial \ln q} \,, \tag{4.82}$$

where we used the definition of the tensor spectral tilt n_T mentioned earlier in (3.53). So, basically, the question of whether we have or have not spectral distortion depends on whether the quantity $\mathcal{F}(q, \bar{\xi})$ is or is not q-dependent. This provides an immediate criterion for evaluating whether and how much the GW anisotropies depend on frequency.

We show in Figure 4.1 (taken from [19]) the evolution of the function $\mathcal{F}$ corresponding to the GW production shown in Figure 4 of [52]. We see that indeed this quantity presents a nontrivial scale dependence, and therefore the correlators of the anisotropies will be different at different frequencies.

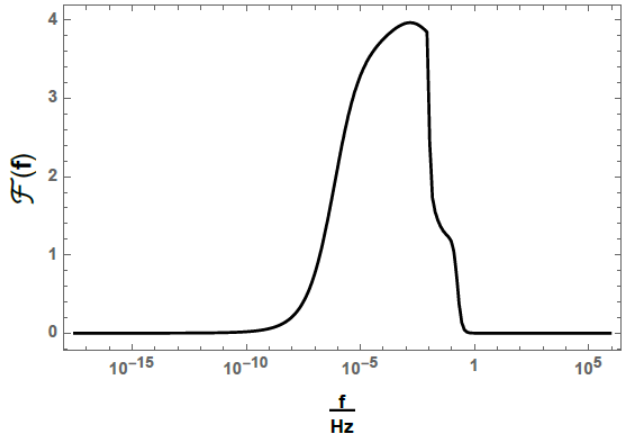

Figure 4.1: Quantity $\mathcal{F}$ as a function of the frequency $f = q/2\pi$ of the GW signal for the model of axion inflation described in the text. Taken from [19].

4.5 Second Example: First-Order Phase Transitions

In Chapter 3, we have described how first order phase transitions can produce GWs, contributing to the background. This gravitational wave background bears a similarity to the CMB, which consists of 3K photons. Similar to how CMB radiation originates from the surface of the last scattering, gravitational waves effectively originate from a remote surface at the outer reaches of our universe during the primordial times. These gravitational waves subsequently journey toward us, experiencing substantial cosmological redshift along the way. Hence, they exhibit frequencies in the range of mHz to Hz, along with signal strengths that could potentially be detected by some gravitational wave observatories. The detailed frequency spectrum of this stochastic GW background would reflect the physics of the PT, during a cosmological era otherwise difficult to access. The SGWB generated by PTs also have anisotropies due to the primordial fluctuations, which could be generated during a possible inflationary era well before the PT itself.

Following [53] and [75], we can define the two-point correlation function of GW perturbation as:

$$C^{GW}(\theta) \equiv \frac{\langle \rho_{GW}(1)\rho_{GW}(2)\rangle_\theta}{\bar{\rho}^2_{GW}} \,, \tag{4.83}$$

where we are averaging over all pairs of points on the sphere, 1, 2, separated by a fixed angle θ. And with $\delta_{GW} \equiv \delta\rho_{GW}/\rho_{GW}$, it can also be written as,

$$C^{GW}(\theta) \equiv \langle \delta_{GW}(\hat{n}_1)\delta_{GW}(\hat{n}_2)\rangle \,. \tag{4.84}$$

We expand the anisotropies in Legendre polynomials,

$$C^{GW}(\theta) = \frac{1}{4\pi}\sum_\ell (2\ell+1) C_\ell^{GW} P_\ell(\cos\theta) \,, \tag{4.85}$$

with $\hat{n_1}\cdot\hat{n_2} = \cos\theta$. From the CMB observation, besides small deviations coming from the physics of inflation/reheating [24], we expect the large-scale GWB perturbation should be almost scale-invariant. An exact scale invariant spectrum would correspond to,

$$C_\ell^{GW} \propto [\ell(\ell+1)]^{-1} \,. \tag{4.86}$$

Our ability to observe such GW anisotropies will be limited by detector sensitivity (which we will discuss briefly in Chapter 6), as well as our understanding and ability to subtract the GW "foregrounds" arising from astrophysical mergers and to account for the peculiar motion of the Earth.

In [53], they assumed the bubble wall moves at the speed of light, and all of the latent heat goes into GW and expressed the energy in GW in terms of the energy in CMB photons today as follows,

$$\rho_{GW}^{today} = 0.06 \frac{\rho_{PT}^2}{\rho_{tot}^2} \left(\frac{H_*}{\beta} \right)^2 \rho_\gamma \ , \tag{4.87}$$

where ρ_{PT} is the energy density in the sector undergoing the PT, but clearly the largest signal would arise if the entire contents of the universe undergoes the PT such that, $\rho_{tot} = \rho_{PT}$. This is what they assumed and they have also assumed a single source of primordial fluctuations, and so $(\delta\rho/\rho)_{\rm GW} = (\delta\rho/\rho)_{\rm CMB} = 4.6 \times 10^{-5}$. And so, from (4.87) the anisotropy is,

$$\delta\rho_{_{GW}} = 2.8 \times 10^{-6} \left(\frac{H_*}{\beta} \right)^2 \rho_\gamma \ . \tag{4.88}$$

While in [75], they used $(\delta\rho/\rho)_{\rm GW} = 6 \times 10^{-5}$, which would give,

$$\delta\rho_{_{GW}} = 3.6 \times 10^{-6} \left(\frac{H_*}{\beta} \right)^2 \rho_\gamma \ , \tag{4.89}$$

which is of the same order anyways.

The Planck satellite CMB data [36] put isocurvature constraint is on the anisotropy such that,

$$\delta\rho_{_{GW}} \lesssim 10^{-6} \rho_\gamma \ . \tag{4.90}$$

4.6 The Imprint of Relativistic Particles on the Anisotropies of the SGWB

In this section, we explore how the presence and motion of high-energy, relativistic particles, such as photons and neutrinos, influence the observed variations in the SGWB across different directions in the universe. Relativistic particles can interact with gravitational waves in various ways. For instance, gravitational waves passing through a medium containing relativistic particles may experience scattering or other interactions that modify their properties. The motion of relativistic particles relative to an observer can also introduce a Doppler effect on gravitational waves. The presence of relativistic particles can also lead to energy transfer between the particles and gravitational waves. As a result, the energy content and spectrum of the SGWB can be influenced by these interactions. In the early universe, when relativistic particles were abundant, their interactions with gravitational waves could have had a significant impact on the observed anisotropies in the SGWB. This can provide insights into the conditions and processes that prevailed during the cosmic history.

It was shown in [43] and [101], that the energy density is sensitive to the evolution of the relativistic degrees of freedom g_* before matter-radiation equality ($k > k_{eq}$). The effective number relativistic degrees of freedom is then given by the temperature-weighted sum of all particle contributions is,

$$g_*(T) = \sum_i g_{*,i} \left(\frac{T_i}{T} \right)^4 \ , \tag{4.91}$$

where $g_{*,i}$ is the intrinsic degrees of freedom of the different species, and T_i is their temperature. The term $(T_i/T)^4$ accounts for the temperature dependence of the contribution of each of the species i to the energy density. It reflects the fact that as the universe expands and cools, the energy density of relativistic particles decreases as T^4.

The energy density of relativistic particles can be written then in terms of g_* as,

$$\rho(T) = \frac{\pi^2}{30} g_*(T) T^4 \ . \tag{4.92}$$

From the end of inflation until the present epoch, the temperature of the different particle species decreases, and some particles would become non-relativistic before the others [101] and stop contributing to the radiation energy density. In that sense, $T_\alpha \lesssim m_\alpha$, giving no more contribution to g_*, which changes from $g_*(T \geq 10^4 \text{ MeV}) \simeq 106$, when all the SM particles contribute, to $g_*(T \leq 0.1 \text{ MeV}) \simeq 3.36$, when only photons and relativistic neutrinos contribute [43].

When relativistic particles are present in the universe, they can contribute to the anisotropic stress. The transverse-traceless part of Einstein's equations focuses on the behavior of gravitational waves in the presence of perturbations in the stress-energy tensor, including the anisotropic stress. The anisotropic stress, $\sigma_{\rm dec}$, associated with certain species of relativistic particles can affect the evolution of scalar metric perturbations through its influence on the gravitational field, as described by the transverse-traceless part of Einstein's equations [96],

$$k^2(\phi - \psi) = 16\pi G a^2 \bar{\rho}_r^{\rm dec} \sigma_{\rm dec} \ . \tag{4.93}$$

The fractional energy density of decoupled relativistic particles is given by [43][96],

$$f_{\rm dec}(\eta_{in}) \equiv \frac{\bar{\rho}_r^{\rm dec}(\eta_{in})}{\bar{\rho}_{\rm tot}(\eta_{in})} = \frac{g_*^{\rm dec}(T_i)}{g_*(T_i)} \ , \tag{4.94}$$

where $g_*^{\rm dec}(T_i)$ are the relativistic degrees of freedom of decoupled particles evaluated at temperature T_i at the end of inflation, corresponding to conformal time η_{in}.

This influences the initial conditions for the scalar metric perturbations at the end of inflation, such that it sets the value of the transfer function $T_\psi(\eta_{in}, k)$ in the expressions of $\Delta_\ell^{\rm AD}$ and $\Delta_\ell^{\rm SW}$ in (5.9). Plus, any variation of $f_{\rm dec}(\eta_{in})$ over time leads to a nonzero derivative $(\phi' + \psi')$, and thus contributes to the ISW transfer function $\Delta_\ell^{\rm ISW}$ of (5.9). So, you see now how it affects the scalar metric perturbations.

According to [43], [80] and [96], the solution of the perturbation equations on super-Hubble scales and for the adiabatic mode gives,

$$\psi(\eta_{in}, k) = \left(1 + \frac{2}{5} f_{\rm dec}(\eta_{in})\right) \phi(\eta_{in}, k) \ , \tag{4.95}$$

$$\phi(\eta_{in}, k) = -\frac{2}{3}\left(1 + \frac{4}{15} f_{\rm dec}(\eta_{in})\right)^{-1} \zeta(\vec{k}) \ , \tag{4.96}$$

where $\zeta(\vec{k})$ is the the gauge-invariant curvature perturbation of comoving spatial hyper-surfaces at the end of inflation we defined before.

The fractional energy density of decoupled relativistic particles varies since η_{in} down to temperatures around 0.1 MeV, when it reaches a constant value which depends on the chosen N_{eff}; for instance for 3 light neutrino species that are free-streaming it corresponds to $f_{\rm dec}(\eta_{T<0.1MeV}) = 0.4$ [43][96]. That means that, in this interval ϕ and ψ evolve for different $f_{\rm dec}(\eta_{in})$ values.

Now, we quantify the effect of the extra relativistic species on the angular power spectrum of the scalar perturbation-induced anisotropies given in the first of Eqs (4.55) and (4.47), which dominate on large scales, and as such they are the ones which can be probed by GW interferometers considering their limited angular resolution. Rewriting the equation,

$$\tilde{C}_{\ell,S} = 4\pi \int \frac{dk}{k} \left(T_\Phi(\eta_{in}, k) j_\ell(k(\eta_0 - \eta_{in})) + \int_{\eta_{in}}^{\eta_0} d\eta \frac{\partial [T_\Psi(\eta, k) + T_\Phi(\eta, k)]}{\partial \eta} j_\ell(k(\eta - \eta_{in})) \right)^2 P_\zeta(k) \ . \tag{4.97}$$

The authors of [43] modified the public code CLASS for the computation of CMB anisotropies [78] adapting it to the SGWB. Then they have plotted $\tilde{C}_{\ell,S}$, showing how different values of $f_{\rm dec}(\eta_{in})$ (and thus different choices for the end of inflation energy scale and implicitly for the number of relativistic

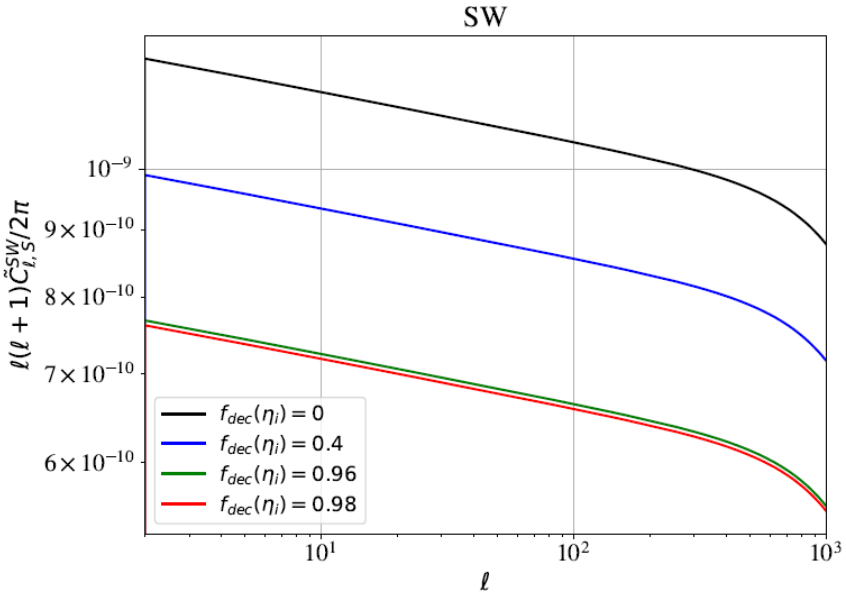

Figure 4.2: SW contribution to the angular power-spectrum of the SGWB. We can see that by increasing $f_{\rm dec}(\eta_{in})$ we are decreasing more and more the amplitude of the angular power spectrum. For values of $f_{\rm dec}(\eta_{in})$ close to 1 we observe a saturation. Taken from [43].

particles present at that time) affect differently the spectra. The plot is shown if Fig. 4.2 and it shows the effect on the SW contribution. Values of $f_{\rm dec}(\eta_{in})$ close to 1 are only considered for illustrative purposes; as such a large fraction is not physically achievable. They then Considered that the effect is generated by particles which are relativistic at their decoupling ($T_{\rm dec} > m$), a simple estimate of the damping at low ℓ is given by,

$$\frac{\tilde{C}_{\ell,S}^{SW}}{4\pi} = \frac{4}{9}\left(1+\frac{4}{15}f_{\rm dec}(\eta_{in})\right)^{-2}\int\frac{dk}{k}P_\zeta(k)j_\ell^2(k(\eta_0-\eta_{in}))\ . \tag{4.98}$$

But why low multipoles? because measuring deviations in the SGWB anisotropies at low ℓ from the angular power-spectrum for $f_{\rm dec}(\eta_{in}) = 0$ would be a proof that at early epochs there were decoupled relativistic particle species contributing to the total energy density by an amount $f_{\rm dec}(\eta_{in})$.

As for the ISW contribution, it depends upon the variation of the potentials between η_{in} and η_0; so it is sensitive the evolution of $f_{\rm dec}(\eta_{in})$ up to low energies scales ($T \lesssim 0.1$ MeV). Thus measurements of the anisotropies of the SGWB anisotropies can constrain extra particles species both at high and low energy scales. The effect of the change of number of relativistic degrees of freedom on the ISW contribution to the angular power-spectrum is represented in Fig. 4.3 also plotted by the authors of [43]. As anticipated, a higher number of relativistic species suppresses the ISW contribution at the largest angular scales through its effect on the early ISW contribution.

They also summed up the two *scalar* contributions to show the main effect on large angular scales that, in the future, can be probed by GW interferometers. They plotted the result and it is shown in Fig. 4.4, where the impact of a varying number of decoupled relativistic species is evident. Note that they did not consider the contribution coming from the tensor background perturbations since they found that they do not alter the spectrum at scales that can be probed in the future by GW direct detection experiments.

We conclude that, the anisotropies observed in the SGWB, which originate from gravitational waves produced during their propagation through the universe, starting from their decoupling at the end of inflation and extending to the present day, are influenced by the presence of relativistic particle species that have decoupled from the thermal bath. Given the limited angular resolution of

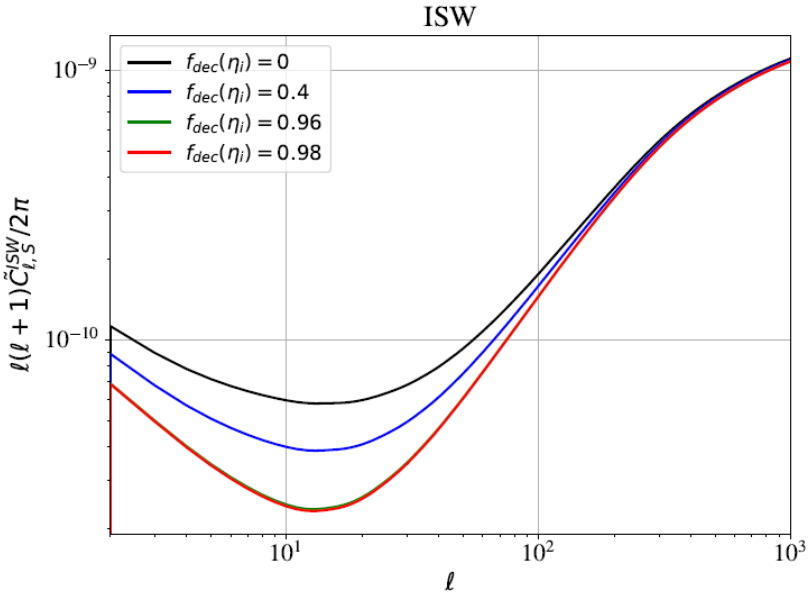

Figure 4.3: ISW contribution to $\tilde{C}_{\ell,S}$. We observe a bump at large ℓ due to the fact that the potentials at large ℓ have the maximum variation. Taken from [43].

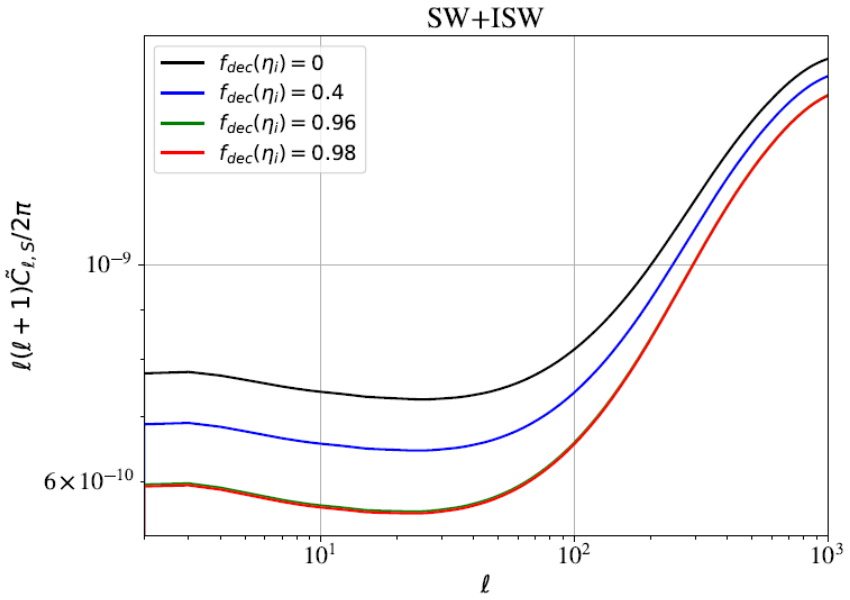

Figure 4.4: Total scalar contribution to the SGWB angular power spectrum, sum of the SW and the ISW terms. Taken from [43].

future gravitational wave detectors, our focus has been on understanding the most significant effects on large cosmic scales. Similar to the CMB, the SGWB at these large scales is subject to two main effects: the Sachs-Wolfe (SW) effect and the Integrated Sachs-Wolfe (ISW) effect. Previous works have undertaken a quantitative analysis to assess the impact of various decoupled particle species on both the SW and ISW effects, and have calculated the SGWB angular power spectrum. These findings reveal that the collective influence of a greater number of decoupled relativistic particle species leads to a suppression of anisotropies at larger cosmic scales in the angular power spectrum of the SGWB. This suppression effect holds the potential to become an observable phenomenon as soon as advanced instruments detect these anisotropies.

4.7 Adiabaticity vs Non-adiabaticity of the Initial Conditions

So far we have focused much more on the propagation effects than the initial conditions, so, maybe it is time we give our attention to those initial conditions. During our discussion, we have always assumed the initial conditions, or the primordial fluctuations, to be adiabatic. But what if they are not? In this section we investigate that possibility, but please put in mind that this is a recently proposed research point, and so, not a lot of work has been done on it. We review what has been done so far, in a brief way.

Recently, the authors of [96] have assumed that the monopole Γ_0 is dominant over the dipole Γ_1 and hence neglected the dipole for the non-adiabatic case just like in the adiabatic case. Consequently, they defined the initial perturbation of Γ of the graviton phase-space distribution as follows,

$$\Gamma(\eta_{\rm in},\vec{k},q,\hat{n}) = \Gamma_0(\eta_{\rm in},\vec{k},q) = T_\Gamma^{\rm AD}(\eta_{\rm in},k,q)\,\mathcal{R}(\vec{k}) + \Gamma_0^{\rm NAD}(\eta_{\rm in},\vec{k},q)\,. \tag{4.99}$$

And, in the Newtonian gauge and for the adiabatic contribution, they used,

$$\Gamma_0(\eta_{\rm in},\vec{k},q) = -\frac{2}{4-n_{\rm gwb}(q)}\psi(\eta_{\rm in},\vec{k})\,, \tag{4.100}$$

and expressed the adiabatic transfer function of Γ at a given frequency q as follows,

$$T_\Gamma^{\rm AD}(\eta_{\rm in},k,q) = -\frac{2}{4-n_{\rm gwb}(q)}T_\psi(\eta_{\rm in},k)\,. \tag{4.101}$$

These expressions allowed them to write the total angular power spectrum of the CGWB auto-correlation, including both, the adiabatic and non-adiabatic initial condition terms,

$$\begin{aligned}\frac{C_\ell^{\rm CGWB\times CGWB}}{(4-n_{\rm gwb})^2} = 4\pi\int\frac{dk}{k}\Big\{&\left[\Delta_\ell^{\rm AD}(k,\eta_0,\eta_{\rm in},q)+\Delta_\ell^{\rm SW}(k,\eta_0,\eta_{\rm in})+\Delta_\ell^{\rm ISW}(k,\eta_0,\eta_{\rm in})\right]^2 P_{\mathcal{R}}(k)\\ &+\left[j_\ell(k(\eta_0-\eta_{\rm in}))\right]^2 P_\Gamma^{\rm NAD}(k,q)\\ &+j_\ell(k(\eta_0-\eta_{\rm in}))\left[\Delta_\ell^{\rm AD}+\Delta_\ell^{\rm SW}+\Delta_\ell^{\rm ISW}\right]P^\times(k,q)\\ &+\left[\Delta_\ell^{T}(k,\eta_0,\eta_{\rm in})\right]^2\sum_{\lambda=\pm2}P_{h_\lambda}(k)\Big\}\,,\end{aligned} \tag{4.102}$$

where,

$$\begin{aligned}\Delta_\ell^{\rm AD}(k,\eta_0,\eta_{\rm in},q) &\equiv -\frac{2}{4-n_{gwb}(q)}T_\psi(\eta_{in},k)j_\ell(k(\eta_0-\eta_{in}))\,,\\ \Delta_\ell^{\rm SW}(k,\eta_0,\eta_{\rm in}) &\equiv T_\psi(\eta_{in},k)j_\ell(k(\eta_0-\eta_{in}))\,,\\ \Delta_\ell^{\rm ISW}(k,\eta_0,\eta_{\rm in}) &\equiv \int_{\eta_{in}}^{\eta_0}d\eta\frac{\partial[T_\psi(\eta,k)+T_\phi(\eta,k)]}{\partial\eta}j_\ell(k(\eta_0-\eta))\,.\end{aligned} \tag{4.103}$$

and the one for the tensor term is given before in Eq. (4.47). They also expressed the non-adiabatic and cross-correlation primordial spectra,

$$P_{\Gamma}^{\rm NAD}(k,q) = \left\langle \left| \Gamma_0^{\rm NAD}(\eta_{\rm in},\vec{k},q) \right|^2 \right\rangle , \tag{4.104}$$

$$P^{\times}(k,q) = \left\langle \mathcal{R}(\vec{k})\,\Gamma_0^{\rm NAD*}(\eta_{\rm in},\vec{k},q) + \mathcal{R}^*(\vec{k})\,\Gamma_0^{\rm NAD}(\eta_{\rm in},\vec{k},q) \right\rangle . \tag{4.105}$$

Few months later, the authors of [44] proposed that the adiabaticity of the initial conditions is no longer valid, and that the such non-adiabaticity arises from the presence of independent tensor perturbations during inflation, which behave as two extra fields that affect the standard single-clock argument. Their argument was that: in cases where the CGWB originates directly from the inflaton field, such as during the decay of the inflaton into GWs in processes like reheating, the initial conditions are adiabatic. This adiabatic nature occurs particularly in single-field models of inflation because the characteristics of the energy spectrum of the source (in this case, the inflaton) are inherited by the decay products. This adiabatic behavior aligns with the "separate universe assumption", a concept that ensures that when a single cosmic clock governs the evolution of the Universe, the presence of adiabatic modes, where quantities like entropy remain constant, is practically inevitable. However, a different scenario arises when stochastic GWs are generated by the intrinsic quantum fluctuations of the metric. In this case, these fluctuations represent two additional independent degrees of freedom, corresponding to the two polarizations of tensor perturbations. Under these circumstances, non-adiabatic modes may emerge, even within the framework of single-field inflation.

In the case of the production of the CGWB by the decay of the inflaton during reheating, along with other particle species, the initial conditions for the energy density of the CGWB are connected to the perturbations of the inflaton, because the inhomogeneities in the inflaton field propagate to its decay products. And so, they are adiabatic. They finally arrived to the same equation in (4.100).

In the case of the production of the CGWB by quantum fluctuations of the metric during inflation, the scenario differs significantly. To apply the short-wave approximation, it is crucial that the initial conditions for the CGWB are set when the high-frequency GWs have already crossed the cosmological horizon. This is because it is important that the initial conditions for the CGWB are set when the high-frequency GWs have already experienced multiple cosmic expansion phases. This ensures that their wavelengths are considerably shorter than the current cosmological horizon size. Another condition is thet the energy produced in the form of gravitational radiation is relatively minor when compared to the energy from standard radiation sources because, according to Big-Bang Nucleosynthesis and Planck constraints [31], one has the upper bound,

$$\frac{\bar{\rho}_{\rm GW}(\eta_{\rm in})}{\bar{\rho}_{\rm rad}(\eta_{\rm in})} \lesssim \left(\frac{g_S(T_0)}{g_S(T_{\rm in})}\right)^{4/3} \frac{7}{8}\Delta N_{eff} \approx 4\times 10^{-3}\Delta N_{eff} , \tag{4.106}$$

where the effective numbers of degrees of freedom are $g_S(T_0) = 3.91$ and $g_S(T_{in}) = 106.75$, while $\Delta N_{eff} = 0.046$ [38]. Einstein's equations exhibit a high degree of insensitivity to the presence of the CGWB due to its relatively minor energy density contribution compared to other forms of radiation, where $\bar{\rho}_{_{GW}}/\bar{\rho}_{_{rad}} \ll 1$. Moreover, the (0, 0) of Einstein equation, carries minimal information about $\delta_{_{GW}}$. Also, the perturbations of gravitons are not directly linked to the perturbations of photons, since they originate from two different sources. Therefore, the authors computed the energy-momentum tensor of GWs in a perturbed FLRW metric, using the definition given in [66]. They found that,

$$\bar{\rho}_{\rm GW} = \frac{1}{32\pi G a^2}\langle h'_{ij}h^{ij\prime}\rangle , \tag{4.107}$$

$$\frac{\delta\rho_{\rm GW}}{\bar{\rho}_{\rm GW}} = -2\Phi + 4\Psi + 2H_n^k \frac{\langle h'_{ik}h^{in\prime}\rangle}{\langle h'_{ij}h^{ij\prime}\rangle} , \tag{4.108}$$

which then they related to the perturbation of the distribution function of gravitons, showing the most important features that this new initial condition produces on the anisotropies of the cosmological

background. Here h_{ij} is the small-scale mode of the transverse-traceless tensor perturbation. The result is,

$$\Gamma(\eta_{\rm in},\vec{k},\vec{q}) = \frac{1}{4-n_{\rm gwb}(q)}\Big[-2\Phi(\eta_{\rm in},\vec{k})+4\Psi(\eta_{\rm in},\vec{k})+2H(\eta_{\rm in},\vec{k})(1-\mu^2)\Big]\,, \tag{4.109}$$

considering the expansion for an unpolarized background $H_{ij}(\eta,\vec{k}) = \sum_\lambda H(\eta,\vec{k})e^\lambda_{ij}(\hat{k})$. H_{ij} is the large-scale mode of the transverse-traceless tensor perturbation

Expanding in spherical harmonics gives,

$$\Gamma_{\ell m,I} = 4\pi(-i)^\ell\int\frac{d^3k}{(2\pi)^3}\Big[Y^*_{\ell m}(\hat{k})\mathcal{R}(\vec{k})\Delta^{I-S}_\ell(\eta_0,k,\eta_{\rm in}) + \sum_\lambda Y^{*-\lambda}_{\ell m}(\hat{k})H_\lambda(\vec{k})\Delta^{I-T}_\ell(\eta_0,k,\eta_{\rm in})\Big]\,, \tag{4.110}$$

where,

$$\Delta^{I-S}_\ell = \frac{1}{4-n_{\rm gwb}(q)}[-2T_\Phi(\eta_{\rm in},k)+4T_\Psi(\eta_{\rm in},k)]j_\ell[k(\eta_0-\eta_{\rm in})]\,, \tag{4.111}$$

$$\Delta^{I-T}_\ell = -\frac{1}{4-n_{\rm gwb}(q)}T_H(\eta_{\rm in},k)\frac{1}{2}\sqrt{\frac{(\ell+2)!}{(\ell-2)!}}\frac{j_\ell[k(\eta_0-\eta_{\rm in})]}{k^2(\eta_0-\eta_{\rm in})^2}\,. \tag{4.112}$$

From which, the angular power-spectrum of the CGWB is given by,

$$\frac{C^{\rm GW}_\ell}{4\pi(4-n_{\rm gwb})^2} = \int\frac{dk}{k}\Big[P_\mathcal{R}(k)(\Delta^{I-S}_\ell+\Delta^{\rm SW}_\ell+\Delta^{\rm ISW}_\ell)^2+P_T(k)\,(\Delta^{I-T}_\ell+\Delta^{\rm ISW-T}_\ell)^2\Big]\,. \tag{4.113}$$

Neglecting the tensor perturbations, which are not so relevant here, it is clear that the contribution to the anisotropy of the CGWB from the initial conditions in the case of single-field inflation, for example, enhances the angular power-spectrum w.r.t adiabatic case by a factor,

$$\frac{C^{\rm SFI+SW}_\ell}{C^{\rm AD+SW}_\ell} \approx \left(\frac{4T_\Psi+[2-n_{\rm gwb}(q)]T_\Phi}{-2T_\Phi}\right)^2\,. \tag{4.114}$$

Therefore, if $n_{gwb}=0$, the angular power-spectrum is enhanced by a factor 10. Another important finding, is that, the angular power-spectrum of the CGWB at large angular scales is sensitive to the fractional energy density of relativistic and decoupled species [43], as we already discussed in the previous section, since the impact of these parameters depends on the choice of the initial conditions.

Finally, they plotted the angular power-spectrum of the CGWB with initial conditions in the case of single-field inflation and for the standard adiabatic case, for $n_{gwb}=0.35$ considering the two cases in which all relativistic particles are coupled, $f_{dec}=0$, and decoupled, $f_{dec}=1$. Their plot is shown in Fig. 4.5. From that plot, it is clear that for the case of single-field inflation, the sensitivity to this extra parameter is larger than in the case of standard adiabatic, i.e., the deviation of the dashed line from the solid one is larger.

Okay but how can we test the nature of these initial conditions? and how can we use the result to our benefit? Well, one way is by cross-correlating the CGWB with CMB (which we will study in more details in the next chapter, but only considering adiabatic scalar perturbations). Focusing more on the initial conditions and the scalar perturbations, since they are the dominant effects on large angular scales for both backgrounds, and considering the constraints on the angular power spectrum of CMB anisotropies that show that the initial condition for photons is adiabatic [92], we have two cases:

- When we consider adiabatic initial conditions of the CGWB, the correlation is very large. Because they are also exposed to the same scalar perturbations.

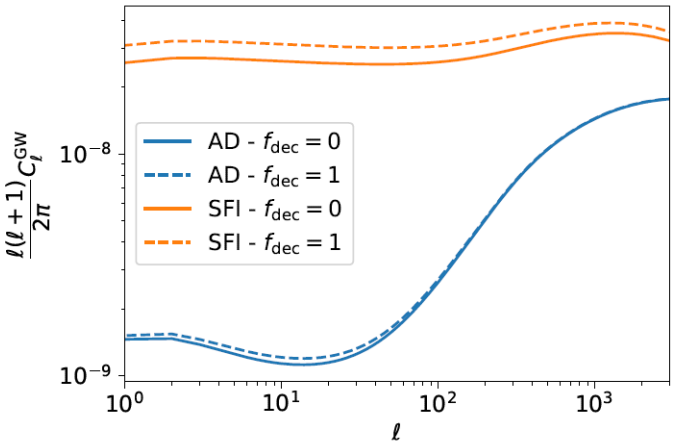

Figure 4.5: Plot of the angular power-spectrum of the CGWB for adiabatic (blue) and single-field inflation (orange) initial conditions, with $n_{gwb} = 0.35$, in the case in which all the relativistic particles at η_{in} are coupled (solid) and decoupled (dashed). Taken from [44].

- When we consider also non-adiabatic initial conditions of the CGWB, i.e., the case of single-field inflation, they are still correlated with large-scale CMB anisotropies at last scattering, because they are still exposed to the same the scalar perturbations, but since the initial conditions combine differently with the other contributions to the angular power-spectrum, the correlation decreases by a small fraction.

This fraction can be quantified using a correlation parameter defined as follows,

$$r_\ell^{CMB\times CGWB} \equiv \frac{C_\ell^{CMB\times CGWB}}{\sqrt{C_\ell^{CMB} C_\ell^{CGWB}}} \,. \tag{4.115}$$

From which, it is possible to show that, on large scales, in the case of adiabatic initial conditions, $r \approx 0.98$ while in the case of single-field inflation, $r \approx 0.8 - 0.9$ [44]. So, if this parameter has a different value for each case, then measuring it would be a way to test the nature of the initial conditions, once the CGWB is detected.

Chapter 5

Cross-correlating Gravitational Wave Backgrounds with the Cosmic Microwave Background

The cross-correlation between the cosmic microwave background (CMB) and gravitational waves (GWs) involves studying the correlation between the temperature or polarization patterns of the CMB and the gravitational wave signals from various sources, such as cosmic inflation or astrophysical events. The correlation between the CMB and inflationary GWs can provide evidence for or constraints on inflationary models. This cross-correlation can also reveal the amplitude and shape of the primordial GW power spectrum. However, it can be challenging due to the presence of various astrophysical foregrounds and instrumental noise in CMB observations. Careful data processing and analysis are required to extract the gravitational wave signals. This cross-correlation give us information about the primordial perturbations and the initial conditions as we will show in the following sections.

In this chapter, we study the cross-correlation between CGWB and CMB, define the different contributions, and study each of them separately at different multipoles.

5.1 CMB x CGWB

At this point we know that the gravitational wave background has both, astrophysical and cosmological origins. We are only interested in the cosmological background, and so, we will not consider the astrophysical one here. The physics that governs SGWB anisotropies (at least in the geometric optics limit) displays strong analogies with that underlying CMB fluctuations. General Relativity predicts a non-zero spatial correlation between the SGWB and the CMB, since gravitons share their perturbed geodesics with CMB photons. We study this correlation considering only the perturbations induced by scalar fluctuations on cosmological scales, which provide the dominant contribution.

Assuming adiabatic scalar perturbations only, we can write the CMB x CGWB cross-correlation angular power spectrum as [96],

$$\delta_{\ell\ell'}\delta_{mm'}C_\ell^{\mathrm{CMB}\times\mathrm{CGWB}}(q) \equiv \frac{1}{2}\langle \delta_{\mathrm{GW},\ell m}(\eta,q)a^*_{\ell' m'}(\eta) + \delta^*_{\mathrm{GW},\ell m}(\eta,q)a_{\ell' m'}(\eta)\rangle \ , \tag{5.1}$$

in which,

$$a_{\ell m} = 4\pi(-i)^{\ell} \int \frac{d^3k}{(2\pi)^3}\, e^{i\vec{k}\cdot\vec{x}_0}\, Y^*_{\ell m}(\hat{k})\, \mathcal{R}(\vec{k})\, \Theta^S_{\ell}(k,\eta_0)\ , \tag{5.2}$$

$$\begin{aligned}\Theta^S_{\ell}(k,\eta_0) = \int_{\eta_{\rm min}}^{\eta_0} d\eta \Big[& g(\eta)\Big(T_{\Theta_0}(\eta,k) + T_{\psi}(\eta,k)\Big) j_{\ell}[k(\eta_0-\eta)] && \text{(SW)} \\ & + g(\eta)\ k^{-1} T_{\theta_b}(\eta,k) j'_{\ell}[k(\eta_0-\eta)] && \text{(DOP)} \\ & + e^{-\kappa(\eta)}\ \frac{\partial[T_{\psi}(\eta,k)+T_{\phi}(\eta,k)]}{\partial\eta} j_{\ell}[k(\eta_0-\eta)]\Big]\ , && \text{(ISW)}\end{aligned} \tag{5.3}$$

where $\kappa(\eta)$ is the photon optical depth, $g(\eta)$ the visibility function, T_{Θ_0} the transfer function of the photon temperature monopole, and $T_{\theta_b}(\eta,k)$ the transfer function of the divergence of the baryon bulk velocity [96]. The line-of-sight integral features three terms standing for the Sachs-Wolfe (SW), Doppler (DOP) and Integrated Sachs-Wolfe (ISW) contributions.

And,

$$\begin{aligned}\delta_{{\rm GW},\ell m} = 4\pi(-i)^{\ell}(4-n_{\rm gwb}) \int \frac{d^3k}{(2\pi)^3}\, e^{i\vec{k}\cdot\vec{x}_0}\, Y^*_{\ell m}(\hat{k})\, \mathcal{R}(\vec{k}) \\ \times\ \left[\Delta^{\rm AD}_{\ell}(k,\eta_0,\eta_{\rm in}) + \Delta^{\rm SW}_{\ell}(k,\eta_0,\eta_{\rm in}) + \Delta^{\rm ISW}_{\ell}(k,\eta_0,\eta_{\rm in})\right]\end{aligned} \tag{5.4}$$

Recall from Eqs (4.39) (4.42) that,

$$\Gamma_{\ell m,I} = 4\pi(-i)^{\ell} \int \frac{d^3k}{(2\pi)^3} e^{i\vec{k}\cdot\vec{x_0}} \Gamma(\eta_{in},\vec{k},q) Y^*_{\ell m}(\hat{k}) j_{\ell}(k(\eta_0-\eta_{in}))\ , \tag{5.5}$$

and,

$$\begin{aligned}\Gamma_{\ell m,S} = 4\pi(-i)^{\ell} \int \frac{d^3k}{(2\pi)^3} e^{i\vec{k}\cdot\vec{x_0}} \zeta(\vec{k}) Y^*_{\ell m}(\hat{k}) [T_{\phi}(\eta_{in},k) j_{\ell}(k(\eta_0-\eta_{in})) \\ + \int_{\eta_{in}}^{\eta_0} d\eta \frac{\partial[T_{\psi}(\eta,k)+T_{\phi}(\eta,k)]}{\partial\eta} j_{\ell}(k(\eta_0-\eta))]\ .\end{aligned} \tag{5.6}$$

And since we are assuming adiabatic initial conditions, we can use the relation [96],

$$\Gamma(\eta_{in},\vec{k},q) = -\frac{2}{4-n_{gwb}(q)} \psi(\eta_{in},\vec{k})\ . \tag{5.7}$$

We express [96] the adiabatic transfer function of Γ at a given momentum/frequency q as,

$$T^{\rm AD}_{\Gamma}(\eta_{in},k,q) = -\frac{2}{4-n_{gwb}(q)} T_{\psi}(\eta_{in},k)\ . \tag{5.8}$$

Then, recalling Eqs (4.81) and (4.82), we conclude again that,

$$\begin{aligned}\Delta^{\rm AD}_{\ell}(k,\eta_0,\eta_{\rm in},q) &\equiv -\frac{2}{4-n_{gwb}(q)} T_{\psi}(\eta_{in},k) j_{\ell}(k(\eta_0-\eta_{in}))\ , \\ \Delta^{\rm SW}_{\ell}(k,\eta_0,\eta_{\rm in}) &\equiv T_{\psi}(\eta_{in},k) j_{\ell}(k(\eta_0-\eta_{in}))\ , \\ \Delta^{\rm ISW}_{\ell}(k,\eta_0,\eta_{\rm in}) &\equiv \int_{\eta_{in}}^{\eta_0} d\eta \frac{\partial[T_{\psi}(\eta,k)+T_{\phi}(\eta,k)]}{\partial\eta} j_{\ell}(k(\eta_0-\eta))\ .\end{aligned} \tag{5.9}$$

And $\zeta(\vec{k})$ being equal to $\mathcal{R}(\vec{k})$.

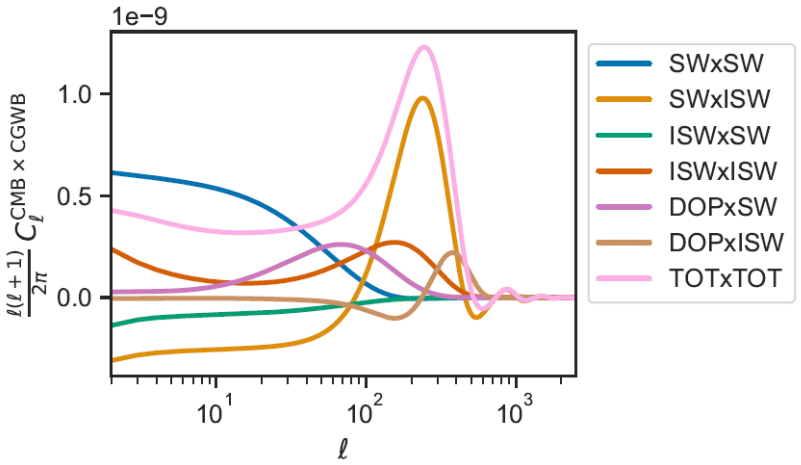

Figure 5.1: Contributions to the CMB x CGWB cross-correlation angular power spectrum. Taken from [96].

5.2 Contributions to the Cross-Correlation Spectrum

The cross-correlation spectrum can be expanded as the sum of six terms,

$$C_\ell^{\mathrm{CMB\times CGWB}} = C_\ell^{\mathrm{SW\times SW}} + C_\ell^{\mathrm{SW\times ISW}} + C_\ell^{\mathrm{ISW\times SW}} + C_\ell^{\mathrm{ISW\times ISW}} + C_\ell^{\mathrm{DOP\times SW}} + C_\ell^{\mathrm{DOP\times ISW}} \,, \quad (5.10)$$

since for CMB we are including the effects of SW, Doppler, and ISW, and for GW we are including the effecrs of Adiabatic initial conditions, SW, and ISW. But here, we refer to both the SW of the CGWB and the monopole of the adiabatic initial anisotropies, called AD in previous equations, as SW.

We give approximate expressions for these six terms, based on the instantaneous decoupling approximation $g(\eta) = \delta(\eta - \eta_*)$, where η_* is the conformal age of the universe at the time of photon decoupling, i.e. last scattering surface. This assumption implies that the optical depth is given by the Heaviside function $\kappa(\eta) = H(\eta - \eta_0)$. The six contributions of Eq. (5.10) to the cross-correlation spectrum are plotted in Fig. 5.1 (taken from [96]), as well as the total cross-correlation spectrum. It can be shown that, when we compute the angular power spectrum, the product of the two Spherical Bessel integrated over k, differs from zero only if the Bessels are peaked in the same time interval [92], which becomes more and more narrow by increasing the multipole considered. This means that if two anisotropies are generated at different times, the cross-correlation between them is non-vanishing only if the spatial separation of the events that generated the anisotropies is much smaller than the scale of the perturbation considered, otherwise the two events are uncorrelated. Let us now study each contribution separately.

5.2.1 SW x SW

Similarily to what is done in Section 4.3.1, we find by cross-correlating the SW anisotropies of the CMB to those of the CGWB,

$$\frac{C_\ell^{\mathrm{SW\times SW}}}{4 - n_{\mathrm{gwb}}} = 4\pi \int \frac{dk}{k} P_{\mathcal{R}}(k) j_\ell[k(\eta_0 - \eta_*)] j_\ell[k(\eta_0 - \eta_{\mathrm{in}})] \times \Big[T_{\Theta_0}(\eta_*, k) + T_\psi(\eta_*, k)\Big] \left[T_\Gamma^{\mathrm{AD}}(\eta_{\mathrm{in}}, k, q) + T_\psi(\eta_{\mathrm{in}}, k)\right] \quad (5.11)$$

The contributions here originate from two different last scattering spheres, since as we know, the decoupling time for the CMB is at η_* while for CGWB is at η_{in}, such that $\eta_* \gg \eta_{in}$. Such a difference would make you think that these fluctuations cannot be correlated, but that's not true. Indeed,

primordial perturbations with a comoving wavelength $2\pi/k$ larger than the radii difference $(\eta_* - \eta_{in})$ imprint nearly the same patterns on the two spheres, and lead potentially to strong correlations. The correlation induced by each of these wavelengths in the early universe is visible to us today at a specific angle, denoted as $\theta \simeq \pi/k\eta_0$. Here, k is the comoving wavenumber of the perturbations, and η_0 is the conformal time at the present epoch. This angle θ describes how the perturbations, originating from a particular wavelength, are observed in the sky today. It corresponds to a multipole moment, $\ell \simeq k\eta_0$. Thus, we expect that for $\ell \ll 2\pi\eta_0/(\eta_* - \eta_{in}) \sim 300$ the angular spectrum is expected to be prominent and observable. Conversely, primordial perturbations with a comoving wavelength $2\pi/k$ smaller than $(\eta_* - \eta_{in})$ imprint different patterns on the two spheres and should leave negligible correlations. Thus, the angular spectrum should be suppressed for $\ell \gg 2\pi\eta_0/(\eta_* - \eta_{in})$.

This expectation has been confirmed analytically in [96]. In the expression of $C_\ell^{\rm SW\times SW}$ in Eq. (5.11), the transfer functions $T_{\Theta_0}, T_\psi, T_\Gamma^{\rm AD}$, which are independent of k on super-Hubble scales, can be pulled out of the integral in first approximation. We can do the same with the primordial curvature spectrum $P_{\mathcal{R}}(k) \simeq A_s$, assuming a tilt n_s close to one. Then, the shape of $C_\ell^{\rm SW\times SW}$ as a function of ℓ depends on,

$$I_\ell = \int \frac{dk}{k} j_\ell[k(\eta_0 - \eta_*)] j_\ell[k(\eta_0 - \eta_{in})] \propto \frac{1}{\sqrt{\ell}(\ell + \frac{1}{2})} e^{-\frac{\eta_* - \eta_{in}}{\eta_0}\ell}\,, \tag{5.12}$$

which, obviously, gets suppressed exponentially for $\ell \gg \eta_0/(\eta_* - \eta_{in})$. This can clearly be seen in Fig. 5.1.

5.2.2 SW x ISW

In this case we have,

$$\frac{C_\ell^{\rm SW\times ISW}}{4 - n_{\rm gwb}} = 4\pi \int \frac{dk}{k} P_{\mathcal{R}}(k) j_\ell[k(\eta_0 - \eta_*)] \Big[T_{\Theta_0}(\eta_*, k) + T_\psi(\eta_*, k)\Big] \times \int_{\eta_{\rm in}}^{\eta_0} d\eta \Big[T'_\psi(\eta, k) + T'_\phi(\eta, k)\Big] j_\ell[k(\eta_0 - \eta)] \tag{5.13}$$

In this term, CMB perturbations contribute at the time η_* (at photon decoupling) and GW perturbations at all times in the range $\eta_{in} \leq \eta' \leq \eta_0$ (from the end of inflation to the present epoch). The correlation between the CMB and GW perturbations peaks when the two types of perturbations are probed on the same sphere, that is, when $\eta' \sim \eta_*$. The behavior of this term is governed by the product of transfer functions $[T_{\Theta_0}(\eta_*, k) + T_\psi(\eta_*, k)][T'_\psi(\eta_*, k) + T'_\phi(\eta_*, k)]$, all evaluated around the time of photon decoupling. The connection between the behavior of this product term and the observed anisotropies i.e., the shape of $C_\ell^{\rm SW\times ISW}$ as a function of ℓ, is described by the angular projection relation $\theta \sim \pi/k\eta_0$ or $\ell \sim k\eta_0$.

The factor $[T_{\Theta_0}(\eta_*, k) + T_\psi(\eta_*, k)]$ exhibits distinct characteristics on various angular scales. It remains nearly constant on very large cosmic scales, where $(k\eta_* \ll 1)$, and then has damped oscillations. The factor $[T'_\psi(\eta_*, k) + T'_\phi(\eta_*, k)]$, however, exhibits a broad peak in its behavior on scales similar to those of the first acoustic peak in the CMB power spectrum. Consequently, $C_\ell^{\rm SW\times ISW}$ possesses distinctive features (see Fig. 5.1):

- On large angular scales, this spectrum has a plateau, indicating relatively constant values. This plateau arises from the nearly constant behavior of the factor $[T_{\Theta_0}(\eta_*, k) + T_\psi(\eta_*, k)]$ on very large cosmic scales.
- In addition to the plateau, there is a prominent peak in the spectrum that aligns with the first acoustic oscillation in the CMB power spectrum. This peak is a consequence of the broad peak exhibited by the factor $[T'_\psi(\eta_*, k) + T'_\phi(\eta_*, k)]$ on similar scales.
- Beyond the peak, the spectrum exhibits smaller damped oscillations. These oscillations stem from the oscillatory nature of both factors $[T_{\Theta_0}(\eta_*, k) + T_\psi(\eta_*, k)]$ and $[T'_\psi(\eta_*, k) + T'_\phi(\eta_*, k)]$ as a function of $k\eta_*$.

The reason behind the plateau and the peak having opposite signs lies [92] in the nature of the transfer functions associated with SW and ISW effects. These transfer functions have opposite signs, because the SW effect in the CGWB relates to the energy lost by a graviton as it escapes from a gravitational potential well, while the ISW effect in the CMB corresponds to the energy gained by photons as they traverse through regions affected by the decay of scalar perturbations. The cross-correlation between these effects is negative because when one background (CGWB) experiences an increase in energy, the other background (CMB) undergoes a decrease in energy.

5.2.3 ISW x SW

In this case we have,

$$\frac{C_\ell^{\rm ISW\times SW}}{4-n_{\rm gwb}} = 4\pi \int \frac{dk}{k} P_{\mathcal{R}}(k) j_\ell[k(\eta_0-\eta_{\rm in})]\left[T_\Gamma^{\rm AD}(\eta_{\rm in},k,q)+T_\psi(\eta_{\rm in},k)\right] \times \int_{\eta_*}^{\eta_0} d\eta \Big[T'_\psi(\eta,k)+T'_\phi(\eta,k)\Big] j_\ell[k(\eta_0-\eta)] \tag{5.14}$$

In this term, the contributions of CMB perturbations and GW perturbations are over different time intervals. The CMB perturbations contribute over the entire range of times $\eta_* \leq \eta \leq \eta_0$, while the GW perturbations, on the other hand, contribute only at a specific moment, precisely at η_{in}, which corresponds to the end of the inflationary period. Clearly, the times at which these contributions occur do not overlap. This lack of temporal overlap significantly affects the correlation between the two.

Although the correlation is not exactly zero, it remains exceedingly small. This small non-zero value arises from the fact that, on the largest angular scales, the same initial primordial fluctuations contribute to the anisotropies observed on both last scattering spheres. However, despite the shared primordial fluctuations, the correlation remains very small. This is primarily due to the behavior of the transfer function $[T'_\psi(\eta_*,k)+T'_\phi(\eta_*,k)]$ in the super-Hubble limit. In this limit, the scalar fields ϕ and ψ essentially remain constant over time. As a result, the correlation term $C_\ell^{\rm ISW\times SW}$ is sub-dominant compared to other contributions (see Fig. 5.1).

5.2.4 ISW x ISW

In this case we have,

$$\frac{C_\ell^{\rm ISW\times ISW}}{4-n_{\rm gwb}} = 4\pi \int \frac{dk}{k} P_{\mathcal{R}}(k) \int_{\eta_*}^{\eta_0} d\eta \Big[T'_\psi(\eta,k)+T'_\phi(\eta,k)\Big] j_\ell[k(\eta_0-\eta)] \times \int_{\eta_{\rm in}}^{\eta_0} d\tilde{\eta} \Big[T'_\psi(\tilde{\eta},k)+T'_\phi(\tilde{\eta},k)\Big] j_\ell[k(\eta_0-\tilde{\eta})] \tag{5.15}$$

In this term, CMB perturbations contribute at times in the range $\eta_* \leq \eta \leq \eta_0$ and GW perturbations are all times in the range $\eta_{in} \leq \eta' \leq \eta_0$. The primary source of correlation between CMB and GW perturbations occurs when their respective time intervals overlap. Specifically, the correlation is most significant when $\eta \simeq \eta'$ with $\eta_* \leq \eta \leq \eta_0$. This term includes a tilted plateau (see Fig. 5.1) in the angular power spectrum for small values of ℓ. The presence of this plateau corresponds to the late-ISW effect, which in the case of CMB, reflects the influence of evolving large-scale structures on its temperature anisotropies, leading to a characteristic plateau in the spectrum. Additionally, the term features a prominent peak in the angular power spectrum, and this peak aligns closely with the scale associated with the first acoustic peak in the CMB power spectrum. This peak arises from the early-ISW effect, which results from the evolution of density perturbations in the early universe.

5.2.5 DOP x SW

In this case we have,

$$\frac{C_\ell^{\mathrm{DOP}\times\mathrm{SW}}}{4-n_{\mathrm{gwb}}} = 4\pi \int \frac{dk}{k} P_{\mathcal{R}}(k)\, j'_\ell[k(\eta_0-\eta_*)]\, j_\ell[k(\eta_0-\eta_{\mathrm{in}})] \times k^{-1} T_{\theta_b}(\eta_*,k)\, \left[T_\Gamma^{\mathrm{AD}}(\eta_{\mathrm{in}},k,q) + T_\psi(\eta_{\mathrm{in}},k)\right] \tag{5.16}$$

The analysis of this term is similar to the SW x SW case. The difference lies in the fact that the transfer function associated with the Doppler term, T_{θ_b}, vanishes on super-Hubble scales, unlike $[T_{\Theta_0}+T_\psi]$. This is because on super-Hubble scales perturbations are subject to the dominant influence of cosmic expansion. In that sense, the redshift due to cosmic expansion becomes the dominant factor affecting the observed frequencies of photons, overshadowing the frequency shifts induced by Doppler effects. Thus, this term only has a broad peak for $\ell \sim 100$ (see Fig. 5.1).

5.2.6 DOP x ISW

In this case we have,

$$\frac{C_\ell^{\mathrm{DOP}\times\mathrm{ISW}}}{4-n_{\mathrm{gwb}}} = 4\pi \int \frac{dk}{k} P_{\mathcal{R}}(k)\, j'_\ell[k(\eta_0-\eta_*)]\, k^{-1} T_{\theta_b}(\eta_*,k) \times \int_{\eta_{\mathrm{in}}}^{\eta_0} d\eta \Big[T'_\psi(\eta,k) + T'_\phi(\eta,k)\Big] j_\ell[k(\eta_0-\eta)] \tag{5.17}$$

A reasoning similar to the SW x ISW case shows that the correlation now depends on the product of the transfer functions $T_{\theta_b}(\eta_*,k)[T'_\psi(\eta_*,k)+T'_\phi(\eta_*,k)]$, all evaluated around the time of photon decoupling. They show distinctive behaviour at different scales:

- $T_{\theta_b}(\eta_*,k)$ vanishes on scales larger than the sound horizon. Meaning that its effect is negligible for perturbations with wavelengths larger than the sound horizon at the time of photon decoupling. But, on smaller scales, it has oscillations due to the interplay between the motion of baryonic matter and the overall cosmological conditions at η_*.
- $T'_\psi(\eta_*,k)+T'_\phi(\eta_*,k)$ are suppressed on scales smaller than the sound horizon.

Consequently, $C_\ell^{\mathrm{DOP}\times\mathrm{ISW}}$ displays two small peaks on intermediate scales (see Fig. 5.1). These peaks are comparable to the scales associated with the first two acoustic peaks observed in the CMB spectrum. However, they exhibit a different phase compared to the SW case.

5.2.7 Total Contribution

The total contribution $C_\ell^{\mathrm{CMB}\times\mathrm{CGWB}}$ is dominated by the SW x SW and SW x ISW contributions, as their effect is larger and dominant over the others, but the others still contribute of course. We therefore have (see Fig. 5.1):

- On large scales: a tilted plateau, mainly due to the contributions of the plateaus of SW x SW, SW x ISW, and ISW x ISW.
- On intermediate scales: a peak, mainly due to the contributions of the peaks of SW x SW and ISW x ISW.
- On small scales: a few damped oscillations, mainly due to the contributions of the damped oscillations of SW x ISW.

Note that, because of its origin in the SW x ISW contribution, the main peak does not originate simply for the first oscillation of the photon density transfer function, and reaches its maximum at a slightly larger ℓ than the first CMB peak.

Although our work is focused only on the CGWB, it is really important to explore such cross-correlation between the CMB and the CGWB, because the future GW detectors, such as LISA or BBO, have the ability to measure such cross-correlation signals. The detectibility of these signals is explored by performing a SNR, as we will see in the next chapter.

Chapter 6

Detection Possibilities of the SGWB and its Anisotropies

In this chapter, we will discuss the sensitivity of some detectors to the SGWB and its anisotropies. We will not go through the details of detectors and how they work, which is a more observational approach than a theoretical one, and we are mostly interested in the latter. We will consider detectors like LISA, Big Bang Observer (BBO), and Einstein Telescope (ET). We will explore the sensitivity of LISA to the SGWB itself and its anisotropies, then we will explore the sensitivity of BBO and ET to the anisotropies. We will review briefly the use of Fisher Analysis for the anisotropies.

6.1 LISA

The Laser Interferometer Space Antenna (LISA) mission [8] is a planned space-based observatory designed to detect and observe gravitational waves in the low-frequency range (from millihertz to a few hertz) $\sim 10^{-5} - 0.1$ Hz with high sensitivity [47]. LISA is a collaborative effort involving the European Space Agency (ESA) and NASA. LISA's primary goal is to detect and study gravitational waves in a frequency range that cannot be observed from Earth-based detectors like LIGO and Virgo. LISA consists of three identical spacecraft, 5 million kilometers apart, positioned in a triangular formation (shown in Fig. 6.1), following the Earth in its orbit around the Sun. The spacecraft are connected by laser beams, forming a Michelson interferometer in space. This configuration allows LISA to detect tiny changes in the distances between the spacecraft caused by passing gravitational waves. The mission involves cutting-edge technology, including high-precision laser interferometry, drag-free spacecraft, and advanced data analysis techniques. The spacecraft are equipped with inertial sensors and thrusters to maintain their precise positions relative to each other. LISA is planned for launch in the 2030s. Once in space, it will operate as an observatory, continuously monitoring gravitational wave signals from distant cosmic events.

The variable characteristics of the (e)LISA (evolved LISA) configuration analysed in some papers were the low-frequency noise level (N1 and N2, see [71]), the number of laser links (4 or 6), the length of the interferometer arm (1, 2 or 5 million km), and the duration of the mission (2 or 5 years). Since then, a major achievement has been reached: the LISA Pathfinder satellite has own and demonstrated that the expected instrumental noise in (e)LISA can be reduced six times below the original requirement [12]. The noise that we adopt in this analysis is therefore the so-called N2 noise level [71]: this has been tested by the pathfinder at frequencies $f > 1$ mHz, but the forecast is that it will be finally achieved over the whole frequency spectrum. Moreover, the outcome of the GOAT study accompanied by the renewed international interest in the (e)LISA mission, in particular from NASA, following both the first GW direct detection by the LIGO and Virgo collaborations and the successful flight of the Pathflnder, prompted the community to anticipate that the number of

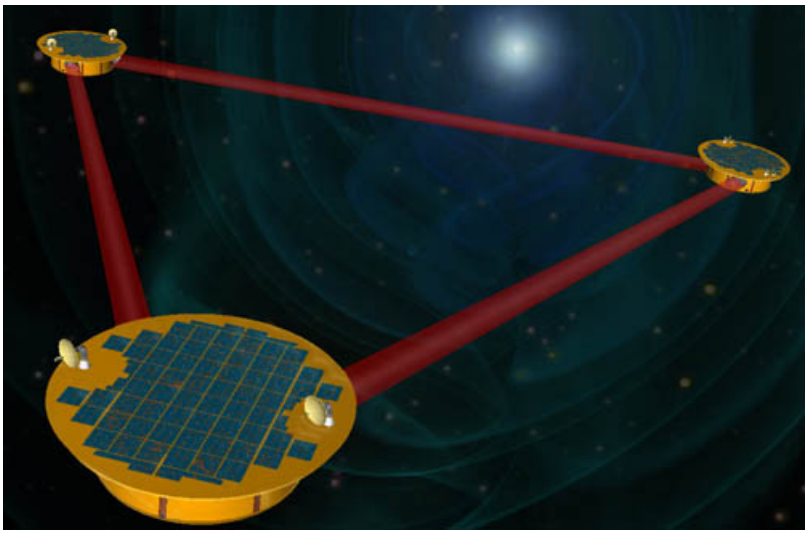

Figure 6.1: LISA's configuration. *Photo Credit:* NASA

laser links of the future GW Observer can be six. Correspondingly, the name goes back to LISA. Therefore, in this work we consider six LISA configurations: having fixed the number of laser links to six (L6) and the best low-frequency noise level (N2), we let vary the length of the arms (A1, A2, and A5 for respectively 1, 2, and 5 million km) and the mission duration (M2 and M5, for respectively 2 and 5 years).

6.1.1 Sensitivity Forecast

In 2013, applying a Bayesian method, refs. [3] and [4] found that, over one year, the best 6-link configuration (with N2 noise level and 5 million km arms) can detect a white noise background at the level of $h^2\Omega_{GW} = 10^{-13}$. One can use this result and convert it into a threshold SNR above which the signal is visible. In order to do so, in 2016, the authors of [20] computed for every LISA configuration the power law sensitivity curve defined in [98]. With respect to the power law sensitivity curve, the SNR corresponding to a white noise spectrum with $h^2\Omega_{GW} = 10^{-13}$ is $SNR = 10$; we therefore classify every signal with $SNR > 10$ as visible by a six-link LISA configuration. They plotted the power law sensitivity curves for the six configurations, as shown in Fig. 6.2. It is clear from the plot that the configurations with A5 (arm length of 5 million km) has the highest sensitivity. They also presented, in Fig. 6.3, the detectability by the six LISA configurations, of a generic GW background parametrised by a single power law, $\Omega_{GW} = A(f/f_*)^{n_T}$. The regions in parameter space (n_T, A), for several values of the pivot frequency f_*, have been derived applying the strategy described above, in particular they represent values of the parameters for which the signal is visible with $SNR > 10$. They have chosen representative values of the pivot frequency f_*, ranging from far smaller to far larger than the frequency of maximal sensitivity of the instrument configurations. Values of the spectral index close to zero are only visible for high enough amplitudes.

In 2016, the authors of [32] have studied eLISA's sensitivity considering the three cases related to first order PTs:

1. Non-runaway Bubbles
2. Runaway Bubbles in a Plasma
3. Runaway Bubbles in Vacuum

For case 1, they plotted (Fig. 6.4) the GW spectra that can arise if the PT proceeds through non-runaway bubbles, for fixed T_*, α and v_w, and varying β/H_*. In this case, the bubbles expanding in a plasma can reach a relativistic terminal velocity. Consequently, the energy in the scalar field

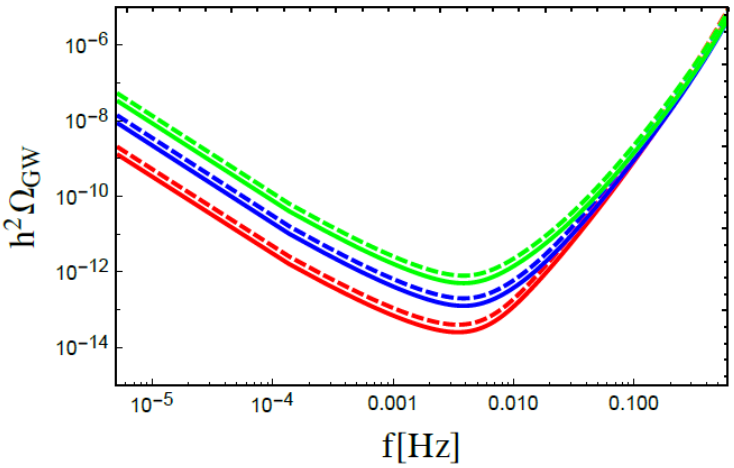

Figure 6.2: Power law sensitivity curves for the six LISA configurations considered in this work: red A5M5, red dashed A5M2, blue A2M5, blue dashed A2M2, green A1M5, green dashed A1M2. Taken from [20].

is negligible and the bulk motion of the fluid contributes the most to the signal. This can be in the form of sound waves and/or MHD turbulence. Setting $\epsilon = 0.05$ in Eq. (3.75), makes the signal from sound waves is dominant. Turbulence can play a role at high frequencies, because the signal from sound waves decays faster and the peak positions are not that different. Increasing β/H_* at fixed T_* and v_w causes the peak position to shift towards larger frequencies, and the overall amplitude to decrease. Correspondingly, the contribution from turbulence becomes less and less important.

For case 2, they plotted (Fig. 6.5) the GW spectra that can arise if the PT proceeds through runaway bubbles in a plasma, for fixed T_*, α, v_w and α_∞ and varying β/H_*. In that case, If a model predicts a first-order PT already at the mean-field level, it is possible for the bubble wall to accelerate indefinitely and hence run away, with $v_w \to c$. Bubbles can run away even if expanding in a thermal plasma. This time, the energy density stored in the scalar field cannot be neglected. The gradients of the scalar field also act as a source of GW together with sound waves and MHD turbulence. Note that fixing α_∞, the minimum value of α such that bubbles run away, sets the relative amplitude of the scalar field-related and the fluid-related contributions. For small β/H_* the contribution from the scalar field can dominate the GW spectrum, since the β/H_* enhancement of the amplitude that operates for long-lasting sources is less relevant. As β/H_* increases, the sound wave contribution gains importance (provided that α_∞ is large enough). At sufficiently high frequencies however the scalar field contribution always dominates because of its shallow decay.

The highest GW signals are expected for runaway bubbles in vacuum (Case 3) for which the GW spectrum has the simplest shape, being determined only by the scalar field contribution. Since in that case, plasma effects are negligible, and the bubble wall will accelerate indefinitely, with v_w quickly approaching c.

In 2022, the authors of [18] have estimated the relative sensitivity of LISA to different ℓ-multipoles by assuming that only one multipole dominates the SGWB and that multipoles with the same ℓ but different m are obtained from the same Gaussian statistics. This amounts to assuming a statistically isotropic SGWB, with correlators given by Eq. (4.50). Summing over the 3 channels A,E and T, they obtained a relation for the sensitivity and plotted the total sensitivity to the ℓ-multipole for multipoles up to $\ell = 10$. The plot is shown in Fig. 6.6.

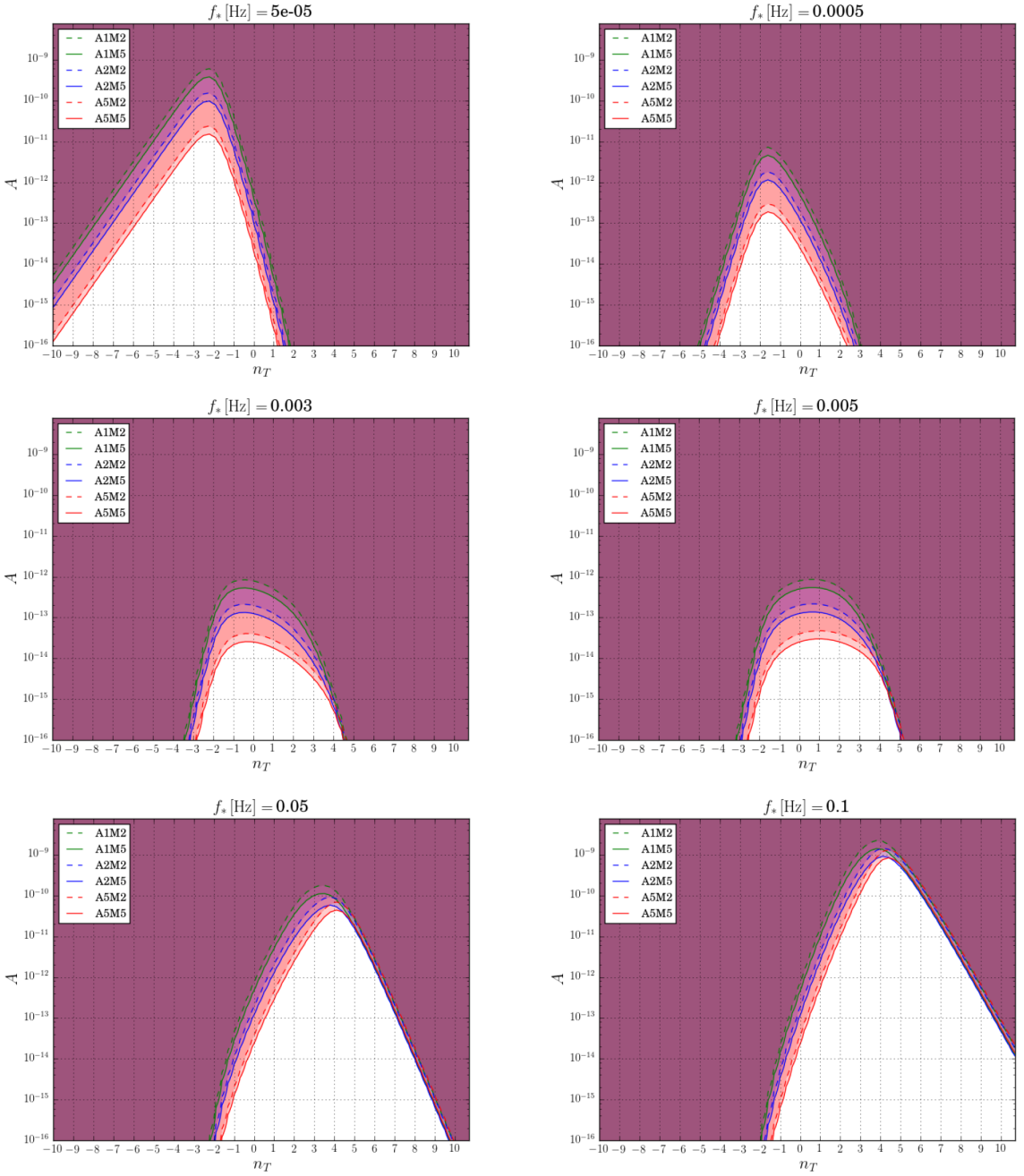

Figure 6.3: For a power-law stochastic background of the form $\Omega_{GW} = A(f/f_*)^{n_T}$, the shaded regions represent the detectable regions in the (n_T, A) parameter space visible by the six LISA configurations under analysis: red A5M5, red dashed A5M2, blue A2M5, blue dashed A2M2, green A1M5, green dashed A1M2. We have chosen six representative pivot frequencies, $f_* = 0.05, 0.5, 3, 5, 50, 100$ mHz. Taken from [20].

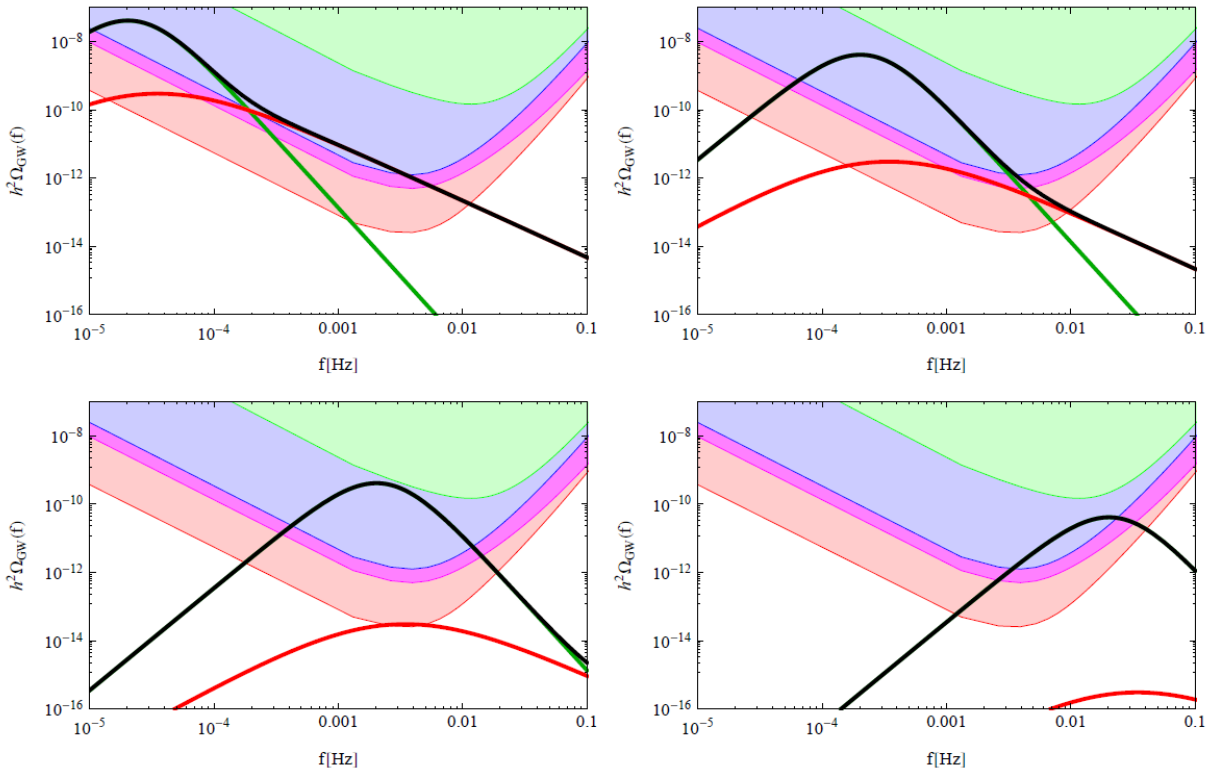

Figure 6.4: Example of GW spectra in Case 1, for fixed $T_* = 100$ GeV, $\alpha = 0.5$, $v_w = 0.95$, and varying β/H_*: from left to right, $\beta/H_* = 1$ and $\beta/H_* = 10$ (top), $\beta/H_* = 100$ and $\beta/H_* = 1000$ (bottom). The black line denotes the total GW spectrum, the green line the contribution from sound waves, the red line the contribution from MHD turbulence. The shaded areas represent the regions detectable by the C1 (red), C2 (magenta), C3 (blue) and C4 (green) configurations. Taken from [32].

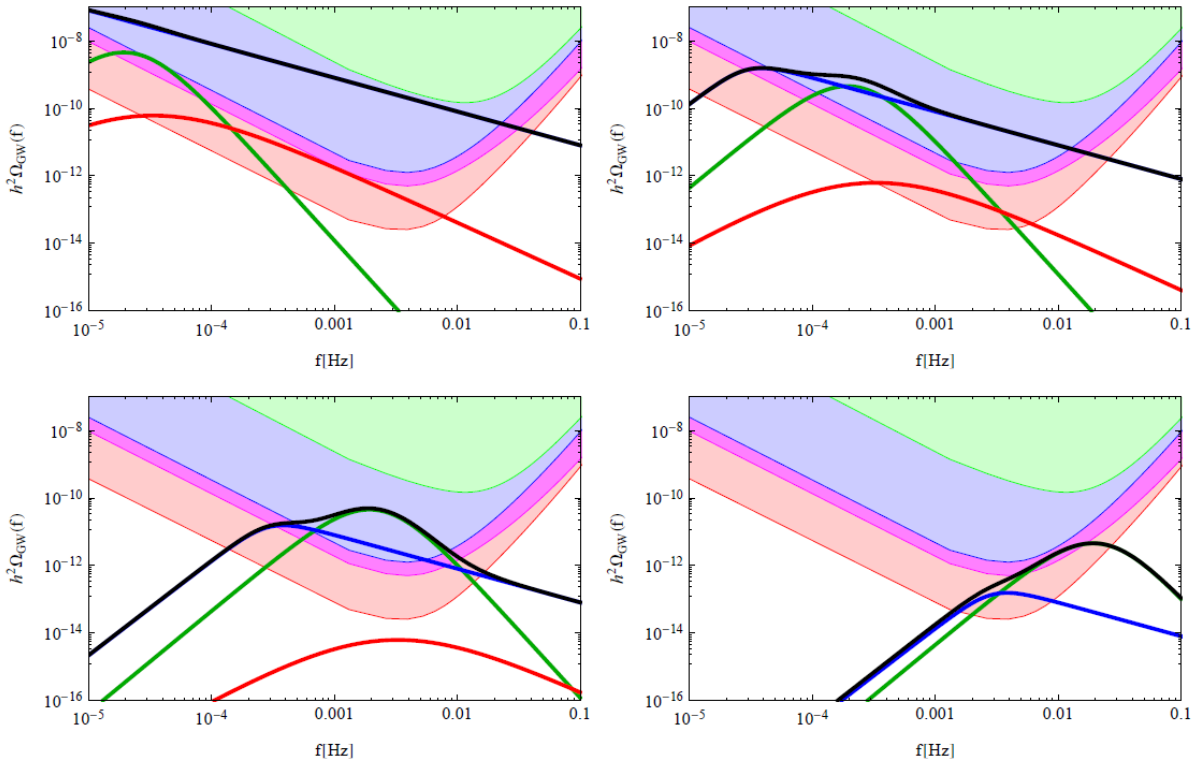

Figure 6.5: Example of GW spectra in Case 1, for fixed $T_* = 100GeV$, $\alpha = 1$, $v_w = 1$, $\alpha_\infty = 0.3$, and varying β/H_*: from left to right, $\beta/H_* = 1$ and $\beta/H_* = 10$ (top), $\beta/H_* = 100$ and $\beta/H_* = 1000$ (bottom). The black line denotes the total GW spectrum, the blue line the contribution from the scalar field, the green line the contribution from sound waves, the red line the contribution from MHD turbulence. The shaded areas represent the regions detectable by the C1 (red), C2 (magenta), C3 (blue) and C4 (green) configurations. Taken from [32].

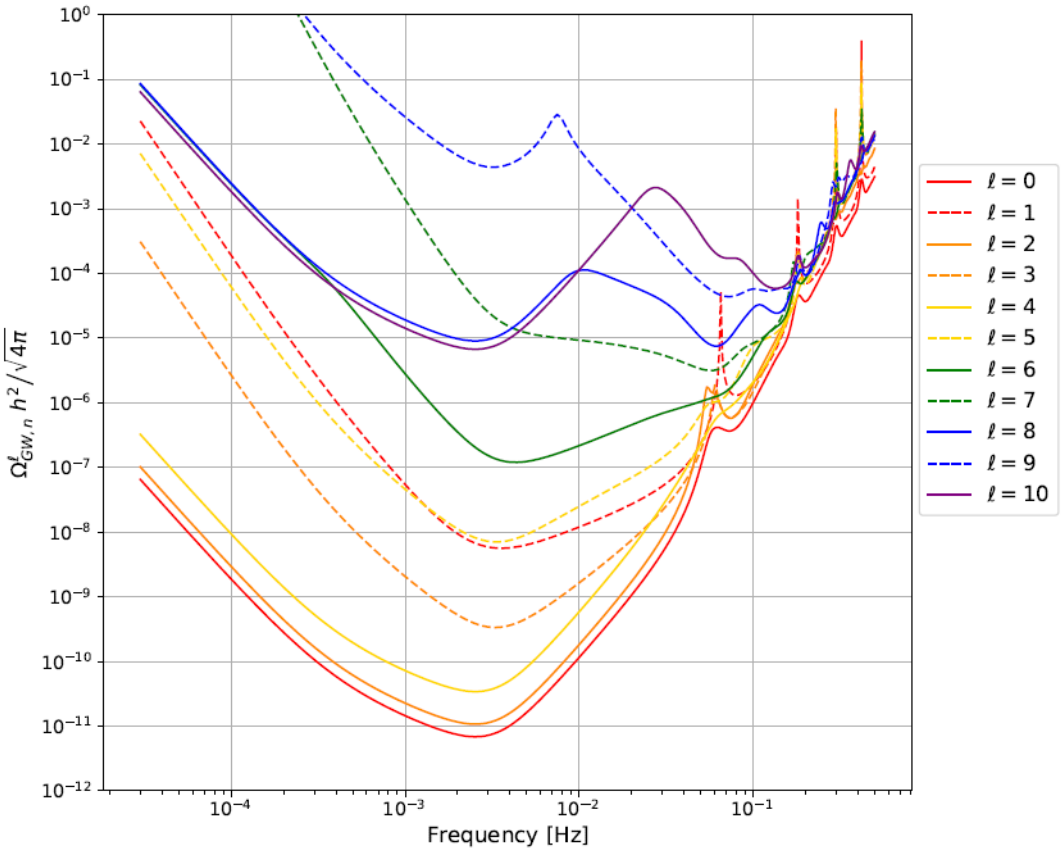

Figure 6.6: Estimated LISA sensitivity to a given multipole ℓ of the SGWB, for multipoles up to $\ell = 10$. Even (odd) multipoles are shown with solid (dashed) lines. The sensitivity is obtained by optimally summing over the LISA channels. Taken from [18].

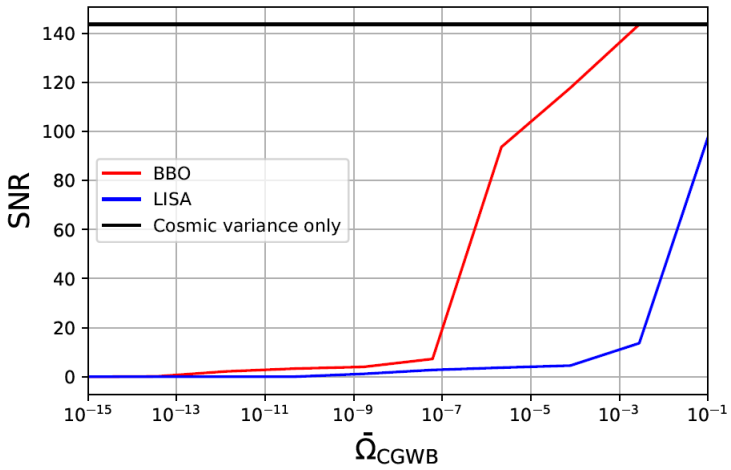

Figure 6.7: SNR of the angular power spectrum of the cross-correlation versus monopole energy density of the CGWB, in the case of BBO (blue line), LISA (red line), and noiseless (black line) cases. Taken from [92].

6.1.2 Signal-to-Noise Ratio

The Signal-to-Noise Ratio (SNR) is a measure of the strength of a signal relative to the background noise or uncertainty. The SNR is a fundamental parameter in signal processing and analysis. The general mathematical expression for SNR is:

$$SNR = \frac{\text{Signal Power}}{\text{Noise Power}} \,, \tag{6.1}$$

where the Signal Power represents the power or strength of the desired signal. In our case, it is the amplitude or power of the signal of the gravitational wave. Noise Power represents the power or intensity of the background noise or uncertainty that interferes with the signal. For GWs, it is the noise level in the detector, which includes various sources of noise like electronic noise, thermal noise, and environmental noise. So, basically, the SNR is a dimensionless value that quantifies how well the signal can be distinguished from the noise. A higher SNR indicates a stronger, more distinguishable signal. Conversely, a lower SNR suggests that the signal is weaker or less distinguishable from the noise.

In 2021, the authors of [92] have studied the detectability of the CMB x CGWB signal calculated earlier in Chapter 5 by performing a SNR analysis. The expression for the SNR is,

$$\mathrm{SNR}^2 = \sum_{\ell=2}^{\ell_{\max}} \frac{\left(C_\ell^{\mathrm{CMB}\times\mathrm{CGWB}}\right)^2}{\sigma_\ell^2} \,, \tag{6.2}$$

where the angular spectrum of the noise N_ℓ is given by the sum of instrumental noise and cosmic variance,

$$\sigma_\ell^2 = \frac{\left(C_\ell^{\mathrm{CMB}\times\mathrm{CGWB}}\right)^2 + \left(C_\ell^{\mathrm{CGWB}} + N_\ell^{\mathrm{CGWB}}\right) C_\ell^{\mathrm{CMB}}}{2\ell + 1} \,. \tag{6.3}$$

In their study, they have neglected the instrumental noise of the CMB experiment, considering that at the multipoles we are interested in ($\ell \lesssim 100$), available CMB data are completely cosmic variance dominated. They have estimated the SNR as a function of the GW background energy density $\bar{\Omega}_{CGWB}$, considering either an ideal, noiseless case scenario, or noise levels expected by e.g. LISA or BBO, and plotted the result (shown in Fig. 6.7). It can be clearly seen from the figure that, for the LISA detector, if the amplitude of the monopole GW signal is large enough ($\bar{\Omega}_{CGWB} \approx 10^{-8}$), the SNR for the cross-correlation can be of order unity. In the BBO case, due the the better sensitivity, a lower GW signal is instead suffcient ($\bar{\Omega}_{CGWB} \approx 10^{-12} - 10^{-11}$) to produce a detectable signal ($SNR \sim 2 - 5$). Such GW monopole amplitudes can be generated by many primordial mechanisms characterized by a blue (i.e., $n_T > 0$) tensor power spectrum, like axion-inflation models and other post-inflationary mechanisms including phase transition.

In 2022, the authors of [18] estimated and plotted the SNR for LISA to detect the kinematic dipole and quadrupole induced by a scale-invariant profile of $\Omega'_{GW}(f) =$ constant in the SGWB rest frame. Doppler anisotropies induced by the motion of the detector with respect to the SGWB rest frame count among the guaranteed features of the SGWB. Following [6], which sets the basis for the analysis of SGWB anisotropies with ground-based GW interferometers, estimated the prospects for ground-based detectors to measure the kinematic dipole of the SGWB, they considered the same for LISA. The plot is shown in Fig. 6.8, which shows clearly that LISA has a better sensitivity to detecting a quadrupole (i.e., $\ell = 2$) than it does for the dipole (i.e., $\ell = 1$) by a factor of $\sim 10^3$.

6.1.3 Fisher Analysis

We will not discuss the details of this analysis/forecasting, but we will give the basics of what it is, how it works, and the forecast results for our case.

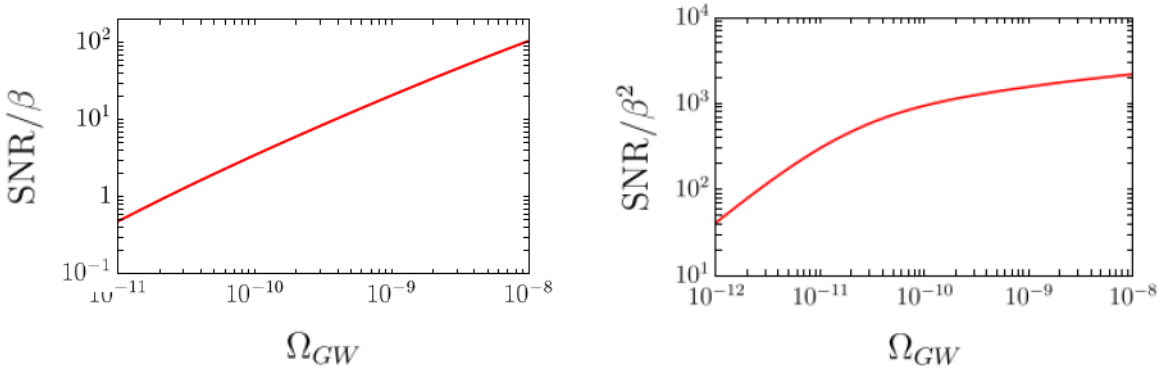

Figure 6.8: The SNR for the dipole (left) and the quadrupole (right) induced by boosting an isotropic SGWB with fractional energy density GW, assumed to be scale free across the LISA band. An observation time of $T = 1$ year is assumed. Taken from [18].

We start be defining what is Fisher Forecast. It is a statistical technique used to estimate the precision with which cosmological parameters can be measured from a future astronomical survey or experiment. In cosmology, researchers are interested in measuring a set of parameters that describe various aspects of the Universe. These parameters may include things like the density of dark matter, the density of dark energy, the amplitude of primordial fluctuations, the Hubble constant, and many others. The Fisher forecast focuses on how precisely these parameters can be determined. The likelihood function quantifies the probability of obtaining a set of observational data given a particular set of model parameters. It essentially describes how well the data constrains the parameters. Practically, the likelihood function is often approximated as a Gaussian distribution around the best-fit model. The Fisher information matrix is constructed using the second derivatives of the logarithm of the likelihood function with respect to the model parameters. It encodes information about how sensitive the likelihood function is to changes in the parameters. This matrix is a square matrix whose elements represent the covariances and variances of the parameters. Once calculated, it can be inverted to obtain the covariance matrix of the parameter estimates. From which one can determine the uncertainties associated with each parameter.

Recently in 2023, the authors of [40] have used Fisher Analysis to study different detectors' sensitivity to an anisotropic GW sky. In this section we will focus on LISA and LISA-Taiji, in Section 6.2 we review their results for BBO, and in Section 6.3 we review those for ET. For cosmological SGWB, the power in a single ℓ-mode (averaged over m-modes) is given by,

$$\Omega^{\ell}_{\rm GW}(f) \equiv \sqrt{C_{\ell,\rm GW}}\bar{\Omega}_{\rm GW}(f)\,, \tag{6.4}$$

where $\bar{\Omega}_{GW}(f)$ is the monopole of the fractional energy density, and $C_{\ell,GW}$ is the anisotropy power spectrum. Using Fisher Analysis, they calculated Fisher Matrix [40], F_ℓ, and from which they got the fractional precision with which the multipoles can be measured,

$$\sigma^2_{C^c_{\ell,\rm GW}} = \left[F^{-1}_\ell\right]_{11}\,, \tag{6.5}$$

and,

$$\frac{1}{\sigma^2_\kappa} = \sum_\ell \frac{(\ln\,\ell)^2}{\sigma^2_{C^c_{\ell,\rm GW}} + \frac{1}{2\ell+1}}\,, \tag{6.6}$$

where κ is the spectral tilt [40].

That being said, for LISA and LISA-Taiji they computed $\sigma^2_{C^c_{\ell,\rm GW}}$ as as a function of various values of $C^c_{\ell,\rm GW}(\bar{\Omega}^c_{\rm GW})^2$. The result is shown in Fig. 6.9. The vertical Band shows the isocurvature constraint [54] that rules out regions with $\sqrt{C^c_{\ell,\rm GW}(\bar{\Omega}^c_{\rm GW})^2} > 10^{-10}$, and consider only the regions

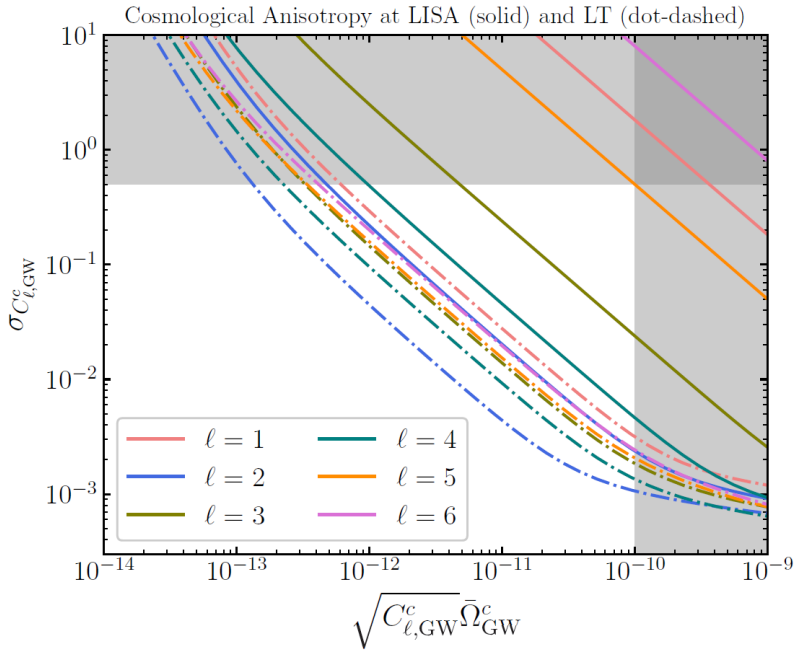

Figure 6.9: Precision on cosmological uncertainties from a Fisher analysis. We assume a PT centered around a frequency of 4 mHz. Taken from [40].

with $\sigma_{C^c_{\ell,\mathrm{GW}}} < 0.5$. The fact is that, LISA has the necessary sensitivity to only the $\ell = 2, 3, 4$ modes, while LT has powerful sensitivity to the other ℓ modes as well, $\ell = 1$ through $\ell = 6$. This can be seen clearly in the plot.

For the case of Phase Transitions, assuming adiabatic perturbation, we have [75] in general,

$$\delta\Omega^{\mathrm{peak}}_{\mathrm{GW}} h^2 = 8 \times 10^{-11} \left(\frac{H_{\mathrm{PT}}}{\beta_{\mathrm{PT}}}\right)^2 \left(\frac{\alpha}{1+\alpha}\right)^2 \tag{6.7}$$

For $\alpha \gtrsim 1$ and $(\beta_{\mathrm{PT}}/H_{\mathrm{PT}})^2 < 10^3$ we have $\delta\Omega^{\mathrm{peak}}_{\mathrm{GW}} h^2 \sim 10^{-14} - 10^{-11}$. However, assuming the presence of primordial isocurvature perturbations, we can have $\delta\Omega^{\mathrm{peak}}_{\mathrm{GW}} \sim 10^{-12}$ for $\alpha \sim 1$ and just $\beta_{\mathrm{PT}}/H_{\mathrm{PT}} \sim 30$. So, we don't need a strong SGWB, weaker PT can still give rise to observable anisotropies if the GW signal carries these isocurvature perturbations. For LISA, in the case of adiabatic perturbations, the result shows that LISA can observe cosmological SGWB anisotropies ($\ell = 2, 4$) only for a strong SGWB, for example, from those with $(\beta_{\mathrm{PT}}/H_{\mathrm{PT}})^2 \simeq 10$ and $\alpha \simeq 1$. But as we discussed, provided the presence of isocurvature perturbations, we can detect signals arising from weaker PT. LT, on the other hand, can access weaker signals such as with $(\beta_{\mathrm{PT}}/H_{\mathrm{PT}})^2 \simeq 100$ and $\alpha \simeq 1$ even for adiabatic perturbations.

What if we deviate from LISA's and LT's favourite frequency, 4 mHz? How will that affect the precision? The answer is shown in Fig. 6.10, where we considered the case of 10 mHz. It clear that the cosmological anisotropies can now be measured with less precision.

6.2 Big Bang Observer (BBO)

Now we turn to the case for BBO. BBO is designed to detect and study gravitational waves from the early universe, particularly those generated during cosmic inflation, a period of rapid cosmic expansion shortly after the Big Bang, and to detect gravitational waves at higher frequencies than other gravitational wave detectors like LIGO and Virgo. This allows it to target gravitational waves associated with inflation, which are expected to be at higher frequencies. The frequency range of

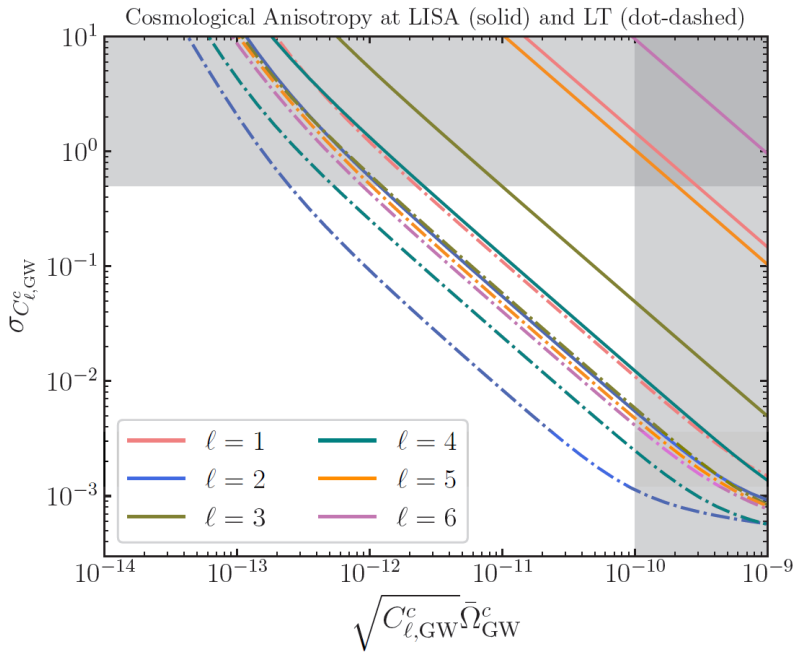

Figure 6.10: Same as Fig. 6.9, except the cosmological signal has a peak at 10 mHz, instead of 4 mHz. Taken from [40].

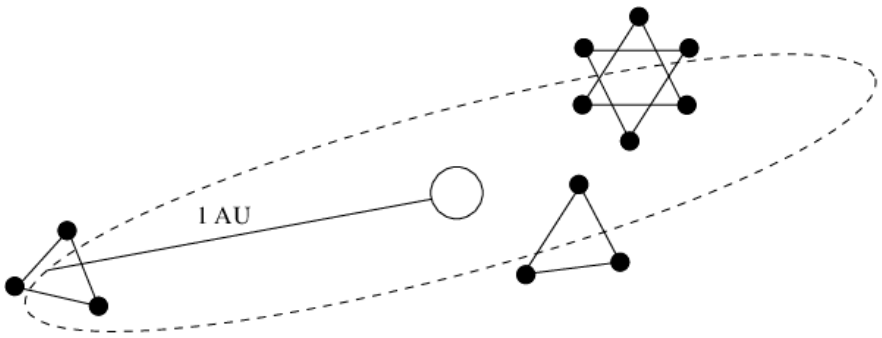

Figure 6.11: BBO's Configuration. Taken from [42].

BBO is $\sim 0.1 - 1$ Hz [41]. It consists of four LISA-like triangular constellations orbiting the Sun at 1 AU. The GW background is measured by cross-correlating the outputs of the two overlapping constellations. This configuration is shown in Fig. 6.11.

The authors of [40] have also used Fisher Analysis to study this detector's sensitivity to an anisotropic GW sky. Again, they computed $\sigma^2_{C^c_{\ell,\mathrm{GW}}}$ as as a function of various values of $C^c_{\ell,\mathrm{GW}}(\bar{\Omega}^c_{\mathrm{GW}})^2$. The result is shown in Fig. 6.12. It is pretty clear that, in contrast to LISA and LT, BBO can probe the cosmological anisotropies with more precision.

For the case of Phase Transitions, assuming adiabatic perturbation, BBO can detect the anisotropies for which $(\beta_{\mathrm{PT}}/H_{\mathrm{PT}})^2 \simeq 10^3$ and $\alpha \simeq 1$ with $\mathcal{O}(10\%)$ precision, unlike the case of LISA and LT where for $(\beta_{\mathrm{PT}}/H_{\mathrm{PT}})^2 \gtrsim 10^3$ and/or $\alpha \ll 1$, anisotropies become smaller than this, and so is the ability to detect it. And if SGWB anisotropies carry isocurvature perturbations, BBO can detect anisotropies for which $(\beta_{\mathrm{PT}}/H_{\mathrm{PT}})^2 \simeq 10^4$ and $\alpha \simeq 1$ with $\mathcal{O}(10\%)$ precision as well.

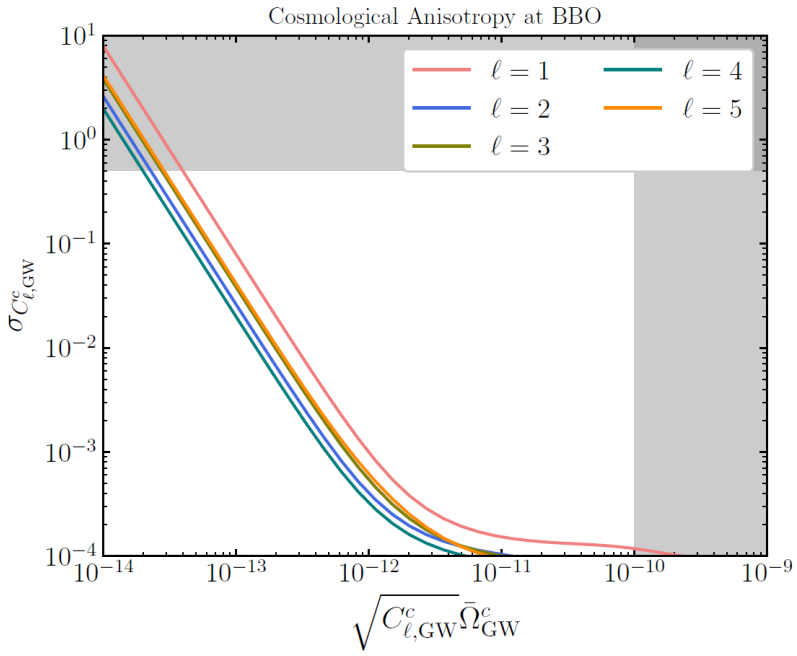

Figure 6.12: Precision on cosmological uncertainties from a Fisher analysis. We assume a PT centered around a frequency of 0.25 Hz. Taken from [40].

6.3 Einstein Telescope (ET)

The Einstein Telescope (ET) is a proposed underground infrastructure to host a third-generation, gravitational-wave observatory. It builds on the success of current, second-generation laser-interferometric detectors Advanced Virgo and Advanced LIGO. The Einstein Telescope will achieve a greatly improved sensitivity by increasing the size of the interferometer from the 3 km arm length of the Virgo detector to 10 km, and by implementing a series of new technologies.

Following the same procedure again but for ET, the authors of [40] have focused on frequencies in the range of $\sim 1 - 100$ Hz. And although in that range, temporal shot noise is significant [69], they have assumed that the temporal shot noise can be fully reduced and considered only the actual astrophysical anisotropies. Their result is shown in Fig. 6.13. Note that they also included the Cosmic Explorer (CE), since while ET or CE alone does not have powerful sensitivity to odd ℓ modes, ET+CE significantly improves that, making the combination sensitive to all modes between $\ell = 1$ and $\ell = 6$.

For the case of Phase Transitions, assuming adiabatic perturbation, ET+CE can detect the anisotropies associated with a strong SGWB corresponding to $(\beta_{\mathrm{PT}}/H_{\mathrm{PT}})^2 \simeq 10$ and $\alpha \simeq 1$, with $\mathcal{O}(10\%)$ precision. And if it carries isocurvature perturbations, then they can detect anisotropies for which $(\beta_{\mathrm{PT}}/H_{\mathrm{PT}})^2 \simeq 10^3$ and $\alpha \simeq 1$ with $\mathcal{O}(10\%)$ precision as well.

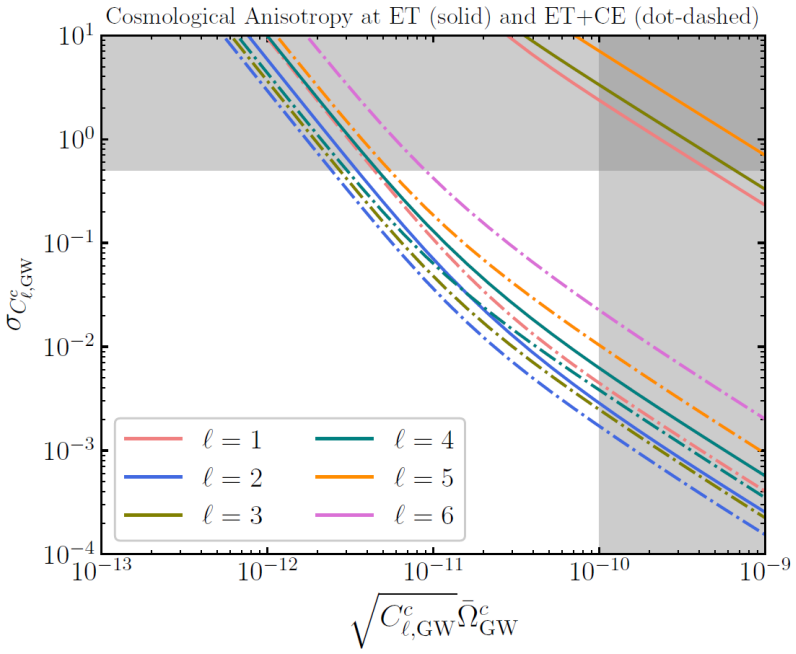

Figure 6.13: Precision on cosmological uncertainties from a Fisher analysis. We assume a PT centered around a frequency of 7 Hz. Taken from [40].

Conclusion and Future Prospects

In this work, we have given an introduction to Cosmology, where we have briefly reviewed the cosmological principle, the expansion of the universe, the cosmic microwave background (CMB) radiation, the FLRW spacetime which was of important use later, and Friedmann's and Einstein's equations. Since the goal of this thesis is to investigate the cosmological gravitational wave background anisotropies, focusing on the case of Inflation and that of Phase Transitions, introducing them was a must. We also reviewed the theory of cosmological perturbations, as we are mainly dealing with perturbations, and it is the main source of the anisotropies we are discussing. We then introduced the gravitational waves (GWs) and how they can be described mathematically. Stochastic Gravitational Wave Background (SGWB) is a superposition of gravitational waves from many unresolved and randomly distributed sources throughout the cosmos. We focused on the cosmological sources, specifically Inflation and Phase Transitions. For inflation, GWs are produced by quantum vacuum fluctuations of the metric. We have shown that on sub-horizon scales, the amplitude of the modes of the GWs decrease in time with the inverse of the scale-factor as an effect of the Universe expansion, while on super-horizon scales, we consider the solution where the amplitude is constant in time, and we have shown an expression for the power spectrum and the consistency relation [79]. For first-order phase transitions, GWs are produced through three processes: collisions of bubble walls, sound waves, and MHD turbulence. We have shown that each has a different characteristic frequency and a different SGWB amplitude, with sound waves and MHD turbulence contributing the most.

We have studied and investigated the spatial anisotropies of the SGWB that arise from cosmological sources [14] [19]. These anisotropies could have been inherited both, at the time of the SGWB production, and during its propagation through the perturbed universe. We followed the Boltzmann approach [14][19][39][96] to study the propagation effects on the SGWB through scalar and tensor perturbations. Our primary focus was on large scales, operating within a regime where the comoving momentum q of GWs is much larger than the comoving momentum k of large-scale perturbations; $q \gg k$. In doing so, we considered first order perturbations around FLRW background in the Poisson gauge which includes the scalar and tensor perturbations. By solving for the function Γ which is related to the anisotropies and separating the solution into initial, scalar, and tensor terms, we found that the anisotropies that come from the initial conditions have an order-one dependence on the frequency, but those due to propagation are independent of the frequency at linear order. We computed the 2-point correlation function for the anisotropies, and showed the non-Gaussianity of the SGWB by computing the 3-point correlation function, such non-Gaussianity is a potential tool to discriminate whether a SGWB has a primordial or astrophysical origin. After characterizing these anisotropies, we considered giving two examples of the possible SGWB sources. Through the example of the Axion-Inflaton [52], we showed that also the correlators of the SGWB anisotropies will be different at different frequencies. We also discussed the example of anisotropies due to first-order phase transitions [53][75] and expressed the SGWB anisotropies in terms of the photon energy density, and by assuming the entire contents of the universe undergoes the PT, we got $\delta\rho_{GW} \sim 10^{-6}\rho_{\gamma}$ [36]. So far we haven't considered that the presence of relativistic particles would have an effect on these anisotropies, and so for a complete characterization, we explored how the presence and motion of such high-energy, relativistic particles, such as photons and neutrinos, influence the observed variations in the SGWB across different directions in the universe [43][96][101]. Our focus has been on understanding the most significant effects on large cosmic scales. And since SW and ISW effects operate on such large scales, we studied the impact of various decoupled particle species on both effects. We found that a greater number of decoupled relativistic particle species leads to a suppression of

anisotropies at larger cosmic scales in the angular power spectrum of the SGWB. This is important because the suppression effect holds the potential to become an observable phenomenon as soon as advanced instruments detect these anisotropies. We also explored the recently proposed possibility of non-adiabaticity of the initial conditions [44][96]. We have shown that the contribution to the anisotropy of the CGWB from the initial conditions in the case of single-field inflation which includes non-adiabatic initial conditions, for example, enhances the angular power-spectrum w.r.t adiabatic case by a factor of 10. We then showed how we can test that nature of the initial conditions through a CGWB x CMB correlation parameter, where on large scales, in the case of adiabatic initial conditions, the value was 0.98, while in the case of single-field inflation it was 0.8 – 0.9, showing a smaller correlation in the case of non-adiabatic initial conditions [44]. We then studied the cross-correlation between CGWB and CMB in more details [92][96], incorporating the effects of the SW, ISW and Doppler for the CMB, and the effects of SW (including the adiabatic initial conditions) and ISW for the CGWB. We showed that the total contribution $C_\ell^{\mathrm{CMB}\times\mathrm{CGWB}}$ is dominated by the SW x SW and SW x ISW contributions, as their effect is larger and dominant over the others, but the others still contribute as well. The total cross-correlation spectrum featured a tilted plateau on large scales, a peak on intermediate scales, and few damped oscillations on small scales.

Finally, we have discussed the sensitivity of some detectors to the SGWB and its anisotropies. This is just a forecast which is to be confirmed later in the future once we have an actual detection. We have explored the sensitivity of LISA to the SGWB itself using many LISA configurations in the sense of the arm length and the mission duration, and we showed that [20] the configurations with A5M5 (arm length of 5 million km and duration of 5 years) has the highest sensitivity to the SGWB. We then showed [20] the detectability by the six LISA configurations, of a generic GW background parametrised by a single power law, $\Omega_{GW} = A(f/f_*)^{n_T}$, using a driven parameter space (n_T, A) with values for which the signal is visible with $SNR > 10$, for several values of the pivot frequency f_*. We then studied the LISA's sensitivity [32] with four different configurations to the SGWB considering the three cases related to first order PTs: Non-runaway Bubbles, Runaway Bubbles in a Plasma, and Runaway Bubbles in Vacuum. We showed how the different contributions dominate over each other and the behaviour of their amplitudes in LISA's favourite frequency range, and how the peaks shift by changing the value of β/H_*, i.e., the duration of the PT. We also showed [18] an estimation for the relative sensitivity of LISA to different ℓ-multipoles by assuming that only one multipole dominates the SGWB, and using SNR analysis, also the SNR for LISA to detect the kinematic dipole and quadrupole induced by a scale-invariant profile of $\Omega'_{GW}(f) =$ constant in the SGWB rest frame, due to Doppler anisotropies induced by the motion of the detector with respect to the SGWB rest frame. We found that LISA has a better sensitivity to detecting a quadrupole (i.e., $\ell = 2$) than it does for the dipole (i.e., $\ell = 1$) by a factor of $\sim 10^3$. Using the SNR analysis, we have studied [92] the detectability of the CMB x CGWB signal as well, showing that for LISA, the SNR for the cross-correlation can be of order unity if the amplitude of the monopole GW signal is large enough ($\bar{\Omega}_{CGWB} \approx 10^{-8}$), while for BBO, a lower GW signal is instead suffcient ($\bar{\Omega}_{CGWB} \approx 10^{-12} - 10^{-11}$) to produce a detectable signal ($SNR \sim 2-5$). For exploring the sensitivity to the anisotropies of the SGWB, we showed the results given by Fisher Analysis [40] to study different detectors' sensitivity to an anisotropic GW sky. For LISA and LISA-Taiji, we have shown the precision $\sigma^2_{C^c_{\ell,\mathrm{GW}}}$ as a function of various values of $C^c_{\ell,\mathrm{GW}}(\bar{\Omega}^c_{\mathrm{GW}})^2$, considering the isocurvature constraint [54] that rules out regions with $\sqrt{C^c_{\ell,\mathrm{GW}}(\bar{\Omega}^c_{\mathrm{GW}})^2} > 10^{-10}$, and consider only the regions with $\sigma_{C^c_{\ell,\mathrm{GW}}} < 0.5$ and assuming a PT centered on around a frequency of 4 mHz. We found that LISA has the necessary sensitivity to only the $\ell = 2, 3, 4$ modes, while LT has powerful sensitivity to the other ℓ modes as well, $\ell = 1$ through $\ell = 6$. In the case of adiabatic perturbations, the result shows that LISA can observe cosmological SGWB anisotropies ($\ell = 2, 4$) only for a strong SGWB, for example, from those with $(\beta_{\mathrm{PT}}/H_{\mathrm{PT}})^2 \simeq 10$ and $\alpha \simeq 1$, but with the presence of isocurvature perturbations, it can detect signals arising from weaker PT. LT, on the other hand, can access weaker signals such as with $(\beta_{\mathrm{PT}}/H_{\mathrm{PT}})^2 \simeq 100$ and $\alpha \simeq 1$ even for adiabatic perturbations. We also showed that when we changed the frequency from 4 mHz to 10 mHz, the cosmological anisotropies can then be measured but with less precision. For BBO, following the same analysis, we showed that in contrast to LISA and LT, BBO can probe the cosmological anisotropies with more precision. For the case of Phase Transitions, assuming adiabatic perturbation, BBO can detect the anisotropies for which $(\beta_{\mathrm{PT}}/H_{\mathrm{PT}})^2 \simeq 10^3$ and $\alpha \simeq 1$ with $\mathcal{O}(10\%)$

precision and if SGWB anisotropies carry isocurvature perturbations, BBO can detect anisotropies for which $(\beta_{\rm PT}/H_{\rm PT})^2 \simeq 10^4$ and $\alpha \simeq 1$ with $\mathcal{O}(10\%)$ precision as well. Similarly for ET, focusing on frequencies in the range of $\sim 1-100$ Hz and assuming a PT centered around a frequency of 7 Hz, also assuming that the temporal shot noise [69] can be fully reduced, we found that ET alone does not have powerful sensitivity to odd ℓ modes, but a combination ET+CE significantly improves that, making it sensitive to all modes between $\ell = 1$ and $\ell = 6$. Assuming adiabatic perturbation, ET+CE can detect the anisotropies associated with a strong SGWB corresponding to $(\beta_{\rm PT}/H_{\rm PT})^2 \simeq 10$ and $\alpha \simeq 1$, with $\mathcal{O}(10\%)$ precision. And if it carries isocurvature perturbations, then they can detect anisotropies for which $(\beta_{\rm PT}/H_{\rm PT})^2 \simeq 10^3$ and $\alpha \simeq 1$ with $\mathcal{O}(10\%)$ precision as well.

In addition to the discussion we made on the sensitivity forecast for the SGWB and its anisotropies, two possible ideas for investigating the Cosmological Gravitational Wave Background Anisotropies can be followed in future work. As we mentioned before, these anisotropies are inherited during the production of the GWs and due to propagation effects, which we have studied using Boltzmann approach. Another approach for studying the propagation effects is by studying the perturbed geodesics for the gravitons. A similar study has been done for the CMB in [84][89] where they studied the behavior of light rays in perturbed RW cosmologies, calculating the redshift between an observer and the surface of last scattering to second order in the metric perturbation, and [84], where they also considered the second order perturbations of the metric itself obtaining them, for a universe dominated by a collision-less fluid, in the Poisson gauge. They found that second order terms of potential observational interest may be interpreted as transverse and longitudinal lensing by scalar perturbations, and a correction to the ISW effect. So, for gravitons, following a different approach will either confirm our results, provide some corrections, or both. The other idea is for the initial conditions, which we mostly assume to be adiabatic, until recently. But we have shown that the initial conditions for the cosmological background, generated by quantum fluctuations of the metric during inflation, even in the single-field case depart from the adiabaticity. The idea is to explore such possibility but considering other mechanisms, for example, perturbations induced by other decoupled particle species that fluctuate during inflation, or any inflationary mechanism that gives rise to adiabatic initial conditions for radiation and matter perturbations. For example, one can consider the Axion-Inflaton case.

Bibliography

[1] B. P. Abbott et al. Observation of Gravitational Waves from a Binary Black Hole Merger. *Phys. Rev. Lett.*, 116(6):061102, 2016.

[2] L. F. Abbott and Mark B. Wise. Constraints on Generalized Inflationary Cosmologies. *Nucl. Phys. B*, 244:541–548, 1984.

[3] Matthew R. Adams and Neil J. Cornish. Discriminating between a stochastic gravitational wave background and instrument noise. *Phys. Rev. D*, 82:022002, Jul 2010.

[4] Matthew R. Adams and Neil J. Cornish. Detecting a stochastic gravitational wave background in the presence of a galactic foreground and instrument noise. *Phys. Rev. D*, 89:022001, Jan 2014.

[5] Gabriella Agazie, Akash Anumarlapudi, Anne M Archibald, Paul T Baker, Bence Bécsy, Laura Blecha, Alexander Bonilla, Adam Brazier, Paul R Brook, Sarah Burke-Spolaor, et al. The nanograv 15-year data set: Constraints on supermassive black hole binaries from the gravitational wave background. *arXiv preprint arXiv:2306.16220*, 2023.

[6] Bruce Allen and Adrian C. Ottewill. Detection of anisotropies in the gravitational-wave stochastic background. *Phys. Rev. D*, 56:545–563, Jul 1997.

[7] Bruce Allen and Joseph D. Romano. Detecting a stochastic background of gravitational radiation: Signal processing strategies and sensitivities. *Physical Review D*, 59(10), mar 1999.

[8] Pau Amaro-Seoane, Heather Audley, Stanislav Babak, John Baker, Enrico Barausse, Peter Bender, Emanuele Berti, Pierre Binetruy, Michael Born, Daniele Bortoluzzi, Jordan Camp, Chiara Caprini, Vitor Cardoso, Monica Colpi, John Conklin, Neil Cornish, Curt Cutler, Karsten Danzmann, Rita Dolesi, Luigi Ferraioli, Valerio Ferroni, Ewan Fitzsimons, Jonathan Gair, Lluis Gesa Bote, Domenico Giardini, Ferran Gibert, Catia Grimani, Hubert Halloin, Gerhard Heinzel, Thomas Hertog, Martin Hewitson, Kelly Holley-Bockelmann, Daniel Hollington, Mauro Hueller, Henri Inchauspe, Philippe Jetzer, Nikos Karnesis, Christian Killow, Antoine Klein, Bill Klipstein, Natalia Korsakova, Shane L Larson, Jeffrey Livas, Ivan Lloro, Nary Man, Davor Mance, Joseph Martino, Ignacio Mateos, Kirk McKenzie, Sean T McWilliams, Cole Miller, Guido Mueller, Germano Nardini, Gijs Nelemans, Miquel Nofrarias, Antoine Petiteau, Paolo Pivato, Eric Plagnol, Ed Porter, Jens Reiche, David Robertson, Norna Robertson, Elena Rossi, Giuliana Russano, Bernard Schutz, Alberto Sesana, David Shoemaker, Jacob Slutsky, Carlos F. Sopuerta, Tim Sumner, Nicola Tamanini, Ira Thorpe, Michael Troebs, Michele Vallisneri, Alberto Vecchio, Daniele Vetrugno, Stefano Vitale, Marta Volonteri, Gudrun Wanner, Harry Ward, Peter Wass, William Weber, John Ziemer, and Peter Zweifel. Laser interferometer space antenna, 2017.

[9] and J. Antoniadis, P. Arumugam, S. Arumugam, S. Babak, M. Bagchi, A.-S. Bak Nielsen, C. G. Bassa, A. Bathula, A. Berthereau, M. Bonetti, E. Bortolas, P. R. Brook, M. Burgay, R. N. Caballero, A. Chalumeau, D. J. Champion, S. Chanlaridis, S. Chen, I. Cognard, S. Dandapat, D. Deb, S. Desai, G. Desvignes, N. Dhanda-Batra, C. Dwivedi, M. Falxa, R. D. Ferdman, A. Franchini, J. R. Gair, B. Goncharov, A. Gopakumar, E. Graikou, J.-M. Grießmeier, L. Guillemot, Y. J. Guo, Y. Gupta, S. Hisano, H. Hu, F. Iraci, D. Izquierdo-Villalba, J. Jang, J. Jawor, G. H. Janssen, A. Jessner, B. C. Joshi, F. Kareem, R. Karuppusamy, E. F. Keane, M. J. Keith,

D. Kharbanda, T. Kikunaga, N. Kolhe, M. Kramer, M. A. Krishnakumar, K. Lackeos, K. J. Lee, K. Liu, Y. Liu, A. G. Lyne, J. W. McKee, Y. Maan, R. A. Main, M. B. Mickaliger, I. C. Niţ u, K. Nobleson, A. K. Paladi, A. Parthasarathy, B. B. P. Perera, D. Perrodin, A. Petiteau, N. K. Porayko, A. Possenti, T. Prabu, H. Quelquejay Leclere, P. Rana, A. Samajdar, S. A. Sanidas, A. Sesana, G. Shaifullah, J. Singha, L. Speri, R. Spiewak, A. Srivastava, B. W. Stappers, M. Surnis, S. C. Susarla, A. Susobhanan, K. Takahashi, P. Tarafdar, G. Theureau, C. Tiburzi, E. van der Wateren, A. Vecchio, V. Venkatraman Krishnan, J. P. W. Verbiest, J. Wang, L. Wang, and Z. Wu. The second data release from the european pulsar timing array. *Astronomy &amp Astrophysics*, 678:A50, oct 2023.

[10] J. Antoniadis, P. Arumugam, S. Arumugam, P. Auclair, S. Babak, M. Bagchi, A. S. Bak Nielsen, E. Barausse, C. G. Bassa, A. Bathula, A. Berthereau, M. Bonetti, E. Bortolas, P. R. Brook, M. Burgay, R. N. Caballero, C. Caprini, A. Chalumeau, D. J. Champion, S. Chanlaridis, S. Chen, I. Cognard, M. Crisostomi, S. Dandapat, D. Deb, S. Desai, G. Desvignes, N. Dhanda-Batra, C. Dwivedi, M. Falxa, F. Fastidio, R. D. Ferdman, A. Franchini, J. R. Gair, B. Goncharov, A. Gopakumar, E. Graikou, J. M. Grießmeier, A. Gualandris, L. Guillemot, Y. J. Guo, Y. Gupta, S. Hisano, H. Hu, F. Iraci, D. Izquierdo-Villalba, J. Jang, J. Jawor, G. H. Janssen, A. Jessner, B. C. Joshi, F. Kareem, R. Karuppusamy, E. F. Keane, M. J. Keith, D. Kharbanda, T. Khizriev, T. Kikunaga, N. Kolhe, M. Kramer, M. A. Krishnakumar, K. Lackeos, K. J. Lee, K. Liu, Y. Liu, A. G. Lyne, J. W. McKee, Y. Maan, R. A. Main, M. B. Mickaliger, H. Middleton, A. Neronov, I. C. Nitu, K. Nobleson, A. K. Paladi, A. Parthasarathy, B. B. P. Perera, D. Perrodin, A. Petiteau, N. K. Porayko, A. Possenti, T. Prabu, K. Postnov, H. Quelquejay Leclere, P. Rana, A. Roper Pol, A. Samajdar, S. A. Sanidas, D. Semikoz, A. Sesana, G. Shaifullah, J. Singha, C. Smarra, L. Speri, R. Spiewak, A. Srivastava, B. W. Stappers, D. A. Steer, M. Surnis, S. C. Susarla, A. Susobhanan, K. Takahashi, P. Tarafdar, G. Theureau, C. Tiburzi, R. J. Truant, E. van der Wateren, S. Valtolina, A. Vecchio, V. Venkatraman Krishnan, J. P. W. Verbiest, J. Wang, L. Wang, and Z. Wu. The second data release from the european pulsar timing array: V. implications for massive black holes, dark matter and the early universe, 2023.

[11] Y. Aoki, G. Endrődi, Z. Fodor, S. D. Katz, and K. K. Szabó. The order of the quantum chromodynamics transition predicted by the standard model of particle physics. *Nature*, 443(7112):675–678, oct 2006.

[12] M. Armano, H. Audley, G. Auger, J. T. Baird, M. Bassan, P. Binetruy, M. Born, D. Bortoluzzi, N. Brandt, M. Caleno, L. Carbone, A. Cavalleri, A. Cesarini, G. Ciani, G. Congedo, A. M. Cruise, K. Danzmann, M. de Deus Silva, R. De Rosa, M. Diaz-Aguiló, L. Di Fiore, I. Diepholz, G. Dixon, R. Dolesi, N. Dunbar, L. Ferraioli, V. Ferroni, W. Fichter, E. D. Fitzsimons, R. Flatscher, M. Freschi, A. F. García Marín, C. García Marirrodriga, R. Gerndt, L. Gesa, F. Gibert, D. Giardini, R. Giusteri, F. Guzmán, A. Grado, C. Grimani, A. Grynagier, J. Grzymisch, I. Harrison, G. Heinzel, M. Hewitson, D. Hollington, D. Hoyland, M. Hueller, H. Inchauspé, O. Jennrich, P. Jetzer, U. Johann, B. Johlander, N. Karnesis, B. Kaune, N. Korsakova, C. J. Killow, J. A. Lobo, I. Lloro, L. Liu, J. P. López-Zaragoza, R. Maarschalkerweerd, D. Mance, V. Martín, L. Martin-Polo, J. Martino, F. Martin-Porqueras, S. Madden, I. Mateos, P. W. McNamara, J. Mendes, L. Mendes, A. Monsky, D. Nicolodi, M. Nofrarias, S. Paczkowski, M. Perreur-Lloyd, A. Petiteau, P. Pivato, E. Plagnol, P. Prat, U. Ragnit, B. Raïs, J. Ramos-Castro, J. Reiche, D. I. Robertson, H. Rozemeijer, F. Rivas, G. Russano, J. Sanjuán, P. Sarra, A. Schleicher, D. Shaul, J. Slutsky, C. F. Sopuerta, R. Stanga, F. Steier, T. Sumner, D. Texier, J. I. Thorpe, C. Trenkel, M. Tröbs, H. B. Tu, D. Vetrugno, S. Vitale, V. Wand, G. Wanner, H. Ward, C. Warren, P. J. Wass, D. Wealthy, W. J. Weber, L. Wissel, A. Wittchen, A. Zambotti, C. Zanoni, T. Ziegler, and P. Zweifel. Sub-femto-g free fall for space-based gravitational wave observatories: Lisa pathfinder results. *Phys. Rev. Lett.*, 116:231101, Jun 2016.

[13] N. Bartolo, D. Bertacca, V. De Luca, G. Franciolini, S. Matarrese, M. Peloso, A. Ricciardone, A. Riotto, and G. Tasinato. Gravitational wave anisotropies from primordial black holes. *Journal of Cosmology and Astroparticle Physics*, 2020(02):028–028, feb 2020.

[14] N. Bartolo, D. Bertacca, S. Matarrese, M. Peloso, A. Ricciardone, A. Riotto, and G. Tasinato. Anisotropies and non-gaussianity of the cosmological gravitational wave background. *Physical Review D*, 100(12), dec 2019.

[15] N. Bartolo, E. Komatsu, S. Matarrese, and A. Riotto. Non-gaussianity from inflation: theory and observations. *Physics Reports*, 402(3-4):103–266, nov 2004.

[16] N. Bartolo, V. De Luca, G. Franciolini, A. Lewis, M. Peloso, and A. Riotto. Primordial black hole dark matter: LISA serendipity. *Physical Review Letters*, 122(21), may 2019.

[17] N. Bartolo, V. De Luca, G. Franciolini, M. Peloso, D. Racco, and A. Riotto. Testing primordial black holes as dark matter with LISA. *Physical Review D*, 99(10), may 2019.

[18] Nicola Bartolo, Daniele Bertacca, Robert Caldwell, Carlo R. Contaldi, Giulia Cusin, Valerio De Luca, Emanuela Dimastrogiovanni, Matteo Fasiello, Daniel G. Figueroa, Gabriele Franciolini, Alexander C. Jenkins, Marco Peloso, Mauro Pieroni, Arianna Renzini, Angelo Ricciardone, Antonio Riotto, Mairi Sakellariadou, Lorenzo Sorbo, Gianmassimo Tasinato, Jesú s Torrado, Sebastien Clesse, and Sachiko Kuroyanagi. Probing anisotropies of the stochastic gravitational wave background with LISA. *Journal of Cosmology and Astroparticle Physics*, 2022(11):009, nov 2022.

[19] Nicola Bartolo, Daniele Bertacca, Sabino Matarrese, Marco Peloso, Angelo Ricciardone, Antonio Riotto, and Gianmassimo Tasinato. Characterizing the cosmological gravitational wave background: Anisotropies and non-gaussianity. *Physical Review D*, 102(2), jul 2020.

[20] Nicola Bartolo, Chiara Caprini, Valerie Domcke, Daniel G. Figueroa, Juan Garcia-Bellido, Maria Chiara Guzzetti, Michele Liguori, Sabino Matarrese, Marco Peloso, Antoine Petiteau, Angelo Ricciardone, Mairi Sakellariadou, Lorenzo Sorbo, and Gianmassimo Tasinato. Science with the space-based interferometer LISA. IV: probing inflation with gravitational waves. *Journal of Cosmology and Astroparticle Physics*, 2016(12):026–026, dec 2016.

[21] Nicola Bartolo, Valerie Domcke, Daniel G. Figueroa, Juan Garcia-Bellido, Marco Peloso, Mauro Pieroni, Angelo Ricciardone, Mairi Sakellariadou, Lorenzo Sorbo, and Gianmassimo Tasinato. Probing non-gaussian stochastic gravitational wave backgrounds with LISA. *Journal of Cosmology and Astroparticle Physics*, 2018(11):034–034, nov 2018.

[22] Nicola Bartolo, Sabino Matarrese, and Antonio Riotto. CMB anisotropies at second-order II: analytical approach. *Journal of Cosmology and Astroparticle Physics*, 2007(01):019–019, jan 2007.

[23] D. Baumann. *Cosmology Part III Mathematical Tripos*. 2015.

[24] Daniel Baumann. Tasi lectures on inflation, 2012.

[25] Ido Ben-Dayan, Brian Keating, David Leon, and Ira Wolfson. Constraints on scalar and tensor spectra from in/isubeff/sub. *Journal of Cosmology and Astroparticle Physics*, 2019(06):007–007, jun 2019.

[26] Pierre Biné truy, Alejandro Bohé, Chiara Caprini, and Jean-François Dufaux. Cosmological backgrounds of gravitational waves and eLISA/NGO: phase transitions, cosmic strings and other sources. *Journal of Cosmology and Astroparticle Physics*, 2012(06):027–027, jun 2012.

[27] Latham A. Boyle and Alessandra Buonanno. Relating gravitational wave constraints from primordial nucleosynthesis, pulsar timing, laser interferometers, and the CMB: Implications for the early universe. *Physical Review D*, 78(4), aug 2008.

[28] Torsten Bringmann, Paul Frederik Depta, Thomas Konstandin, Kai Schmidt-Hoberg, and Carlo Tasillo. Does nanograv observe a dark sector phase transition?, 2023.

[29] T. S. Bunch and P. C. W. Davies. Quantum Field Theory in de Sitter Space: Renormalization by Point Splitting. *Proc. Roy. Soc. Lond. A*, 360:117–134, 1978.

[30] Chiara Caprini, Ruth Durrer, and Gé raldine Servant. The stochastic gravitational wave background from turbulence and magnetic fields generated by a first-order phase transition. *Journal of Cosmology and Astroparticle Physics*, 2009(12):024–024, dec 2009.

[31] Chiara Caprini and Daniel G Figueroa. Cosmological backgrounds of gravitational waves. *Classical and Quantum Gravity*, 35(16):163001, jul 2018.

[32] Chiara Caprini, Mark Hindmarsh, Stephan Huber, Thomas Konstandin, Jonathan Kozaczuk, Germano Nardini, Jose Miguel No, Antoine Petiteau, Pedro Schwaller, Gé raldine Servant, and David J. Weir. Science with the space-based interferometer eLISA. II: gravitational waves from cosmological phase transitions. *Journal of Cosmology and Astroparticle Physics*, 2016(04):001–001, apr 2016.

[33] P. Coles and F. Lucchin. *Cosmology: The Origin and Evolution of Cosmic Structure*. John Wiley & Sons, 2002.

[34] MAGIC Collaboration. A lower bound on intergalactic magnetic fields from time variability of 1es 0229+200 from MAGIC and Fermi/LAT observations. *Astronomy &amp Astrophysics*, 670:A145, feb 2023.

[35] Planck Collaboration. Planck 2015 results. *Astronomy &amp Astrophysics*, 594:A19, sep 2016.

[36] Planck Collaboration. Planck 2015 results. *Astronomy &amp Astrophysics*, 594:A13, sep 2016.

[37] Planck Collaboration. Planck 2018 results. ix. constraints on primordial non-gaussianity, 2019.

[38] Planck Collaboration. Planck 2018 results. VI. Cosmological parameters. , 641:A6, September 2020.

[39] Carlo R. Contaldi. Anisotropies of gravitational wave backgrounds: A line of sight approach. *Physics Letters B*, 771:9–12, aug 2017.

[40] Yanou Cui, Soubhik Kumar, Raman Sundrum, and Yuhsin Tsai. Unraveling cosmological anisotropies within stochastic gravitational wave backgrounds, 2023.

[41] Curt Cutler and Jan Harms. Big bang observer and the neutron-star-binary subtraction problem. *Physical Review D*, 73(4), feb 2006.

[42] Curt Cutler and Jan Harms. Big bang observer and the neutron-star-binary subtraction problem. *Phys. Rev. D*, 73, 02 2006.

[43] L. Valbusa Dall'Armi, A. Ricciardone, N. Bartolo, D. Bertacca, and S. Matarrese. Imprint of relativistic particles on the anisotropies of the stochastic gravitational-wave background. *Physical Review D*, 103(2), jan 2021.

[44] Lorenzo Valbusa Dall'Armi, Alina Mierna, Sabino Matarrese, and Angelo Ricciardone. Adiabatic or non-adiabatic? unraveling the nature of initial conditions in the cosmological gravitational wave background, 2023.

[45] Emanuela Dimastrogiovanni, Matteo Fasiello, and Gianmassimo Tasinato. Searching for fossil fields in the gravity sector. *Physical Review Letters*, 124(6), feb 2020.

[46] Scott Dodelson. *Modern Cosmology*. Academic Press, Elsevier Science, 2003.

[47] The eLISA Consortium. The gravitational universe, 2013.

[48] John Ellis, Malcolm Fairbairn, Gert Hütsi, Juhan Raidal, Juan Urrutia, Ville Vaskonen, and Hardi Veermäe. Gravitational waves from smbh binaries in light of the nanograv 15-year data, 2023.

[49] José R Espinosa, Thomas Konstandin, José M No, and Géraldine Servant. Energy budget of cosmological first-order phase transitions. *Journal of Cosmology and Astroparticle Physics*, 2010(06):028–028, jun 2010.

[50] Daniel G. Figueroa, Mauro Pieroni, Angelo Ricciardone, and Peera Simakachorn. Cosmological background interpretation of pulsar timing array data, 2023.

[51] Giacomo Galloni, Lorenzo Mai, and Leonardo Rebeschini. *Lecture Notes of Cosmology of the Early Universe*. 2020.

[52] Juan Garcí a-Bellido, Marco Peloso, and Caner Unal. Gravitational waves at interferometer scales and primordial black holes in axion inflation. *Journal of Cosmology and Astroparticle Physics*, 2016(12):031–031, dec 2016.

[53] Michael Geller, Anson Hook, Raman Sundrum, and Yuhsin Tsai. Primordial anisotropies in the gravitational wave background from cosmological phase transitions. *Physical Review Letters*, 121(20), nov 2018.

[54] Subhajit Ghosh, Soubhik Kumar, and Yuhsin Tsai. Free-streaming and coupled dark radiation isocurvature perturbations: constraints and application to the hubble tension. *Journal of Cosmology and Astroparticle Physics*, 2022(05):014, may 2022.

[55] John T. Giblin and James B. Mertens. Vacuum bubbles in the presence of a relativistic fluid. *Journal of High Energy Physics*, 2013(12), dec 2013.

[56] L. P. Grishchuk. Graviton Creation in the Early Universe. *Annals N. Y. Acad. Sci.*, 302:439, 1977.

[57] LP Grishchuk. Drift of particles in the field of a gravitational wave. *Zh. Eksp. Teor. Fiz*, 66:833–837, 1974.

[58] Christophe Grojean and Gé raldine Servant. Gravitational waves from phase transitions at the electroweak scale and beyond. *Physical Review D*, 75(4), feb 2007.

[59] Alan H. Guth. Inflationary universe: A possible solution to the horizon and flatness problems. *Phys. Rev. D*, 23:347–356, Jan 1981.

[60] Maria Chiara Guzzetti, Nicola Bartolo, Michele Liguori, and Sabino Matarrese. Gravitational waves from inflation. *La Rivista del Nuovo Cimento*, 39(9):399–495, Aug 2016.

[61] RW Hellings and GS Downs. Upper limits on the isotropic gravitational radiation background from pulsar timing analysis. *The Astrophysical Journal*, 265:L39–L42, 1983.

[62] Mark Hindmarsh, Stephan J. Huber, Kari Rummukainen, and David J. Weir. Gravitational waves from the sound of a first order phase transition. *Physical Review Letters*, 112(4), jan 2014.

[63] Mark Hindmarsh, Stephan J. Huber, Kari Rummukainen, and David J. Weir. Numerical simulations of acoustically generated gravitational waves at a first order phase transition. *Physical Review D*, 92(12), dec 2015.

[64] Stephan J Huber and Thomas Konstandin. Gravitational wave production by collisions: more bubbles. *Journal of Cosmology and Astroparticle Physics*, 2008(09):022, sep 2008.

[65] Stephan J. Huber and Miguel Sopena. An efficient approach to electroweak bubble velocities, 2013.

[66] Richard A. Isaacson. Gravitational radiation in the limit of high frequency. ii. nonlinear terms and the effective stress tensor. *Phys. Rev.*, 166:1272–1280, Feb 1968.

[67] Karsten Jedamzik and Andrey Saveliev. Stringent limit on primordial magnetic fields from the cosmic microwave background radiation. *Physical Review Letters*, 123(2), jul 2019.

[68] Fredrick A Jenet and Joseph D Romano. Understanding the gravitational-wave hellings and downs curve for pulsar timing arrays in terms of sound and electromagnetic waves. *American Journal of Physics*, 83(7):635–645, 2015.

[69] Alexander C. Jenkins and Mairi Sakellariadou. Shot noise in the astrophysical gravitational-wave background. *Physical Review D*, 100(6), sep 2019.

[70] Marc Kamionkowski and Ely D Kovetz. The quest for b modes from inflationary gravitational waves. *Annual Review of Astronomy and Astrophysics*, 54:227–269, 2016.

[71] Antoine Klein, Enrico Barausse, Alberto Sesana, Antoine Petiteau, Emanuele Berti, Stanislav Babak, Jonathan Gair, Sofiane Aoudia, Ian Hinder, Frank Ohme, and Barry Wardell. Science with the space-based interferometer elisa: Supermassive black hole binaries. *Phys. Rev. D*, 93:024003, Jan 2016.

[72] Edward W. Kolb and Michael S. Turner. *The Early Universe*, volume 69. 1990.

[73] Eiichiro Komatsu. The pursuit of non-gaussian fluctuations in the cosmic microwave background, 2002.

[74] Arthur Kosowsky, Michael S. Turner, and Richard Watkins. Gravitational radiation from colliding vacuum bubbles. *Phys. Rev. D*, 45:4514–4535, Jun 1992.

[75] Soubhik Kumar, Raman Sundrum, and Yuhsin Tsai. Non-gaussian stochastic gravitational waves from phase transitions. *Journal of High Energy Physics*, 2021(11), nov 2021.

[76] Sachiko Kuroyanagi, Tomo Takahashi, and Shuichiro Yokoyama. Blue-tilted tensor spectrum and thermal history of the universe. *Journal of Cosmology and Astroparticle Physics*, 2015(02):003–003, feb 2015.

[77] Mikko Laine and Aleksi Vuorinen. *Basics of Thermal Field Theory*. Springer International Publishing, 2016.

[78] Julien Lesgourgues. The cosmic linear anisotropy solving system (class) i: Overview, 2011.

[79] Andrew R. Liddle and David H. Lyth. *Cosmological Inflation and Large-Scale Structure*. Cambridge University Press, 2000.

[80] Chung-Pei Ma and Edmund Bertschinger. Cosmological perturbation theory in the synchronous and conformal newtonian gauges. *The Astrophysical Journal*, 455:7, dec 1995.

[81] Sabino Matarrese, Silvia Mollerach, and Marco Bruni. Relativistic second-order perturbations of the einstein–de sitter universe. *Physical Review D*, 58(4), jul 1998.

[82] Charles W. Misner, K. S. Thorne, and J. A. Wheeler. *Gravitation*. W. H. Freeman, San Francisco, 1973.

[83] Silvia Mollerach, Diego Harari, and Sabino Matarrese. Cmb polarization from secondary vector and tensor modes. *Phys. Rev. D*, 69:063002, Mar 2004.

[84] Silvia Mollerach and Sabino Matarrese. Cosmic microwave background anisotropies from second order gravitational perturbations. *Physical Review D*, 56(8):4494–4502, oct 1997.

[85] Andrii Neronov, Alberto Roper Pol, Chiara Caprini, and Dmitri Semikoz. NANOGrav signal from magnetohydrodynamic turbulence at the QCD phase transition in the early universe. *Physical Review D*, 103(4), feb 2021.

[86] Andrii Neronov, Dmitri Semikoz, and Oleg Kalashev. Limit on intergalactic magnetic field from ultra-high-energy cosmic ray hotspot in perseus-pisces region, 2021.

[87] Ue-Li Pen and Neil Turok. Shocks in the Early Universe. *Phys. Rev. Lett.*, 117(13):131301, 2016.

[88] Cari Powell and Gianmassimo Tasinato. Probing a stationary non-gaussian background of stochastic gravitational waves with pulsar timing arrays. *Journal of Cosmology and Astroparticle Physics*, 2020(01):017–017, jan 2020.

[89] Ted Pyne and Sean M. Carroll. Higher-order gravitational perturbations of the cosmic microwave background. *Physical Review D*, 53(6):2920–2929, mar 1996.

[90] Mariano Quiros. Finite temperature field theory and phase transitions, 1999.

[91] Daniel J. Reardon, Andrew Zic, Ryan M. Shannon, George B. Hobbs, Matthew Bailes, Valentina Di Marco, Agastya Kapur, Axl F. Rogers, Eric Thrane, Jacob Askew, N. D. Ramesh Bhat, Andrew Cameron, Małgorzata Curyło, William A. Coles, Shi Dai, Boris Goncharov, Matthew Kerr, Atharva Kulkarni, Yuri Levin, Marcus E. Lower, Richard N. Manchester, Rami Mandow, Matthew T. Miles, Rowina S. Nathan, Stefan Osłowski, Christopher J. Russell, René e Spiewak, Songbo Zhang, and Xing-Jiang Zhu. Search for an isotropic gravitational-wave background with the parkes pulsar timing array. *The Astrophysical Journal Letters*, 951(1):L6, jun 2023.

[92] A. Ricciardone, L. Valbusa Dall'Armi, N. Bartolo, D. Bertacca, M. Liguori, and S. Matarrese. Cross-correlating astrophysical and cosmological gravitational wave backgrounds with the cosmic microwave background. *Physical Review Letters*, 127(27), dec 2021.

[93] Antonio Riotto. Inflation and the Theory of Cosmological Perturbations, 2017.

[94] Barbara S. Ryden. Introduction to cosmology. 2002.

[95] R. K. Sachs and A. M. Wolfe. Perturbations of a cosmological model and angular variations of the microwave background. *Astrophys. J.*, 147:73–90, 1967.

[96] Florian Schulze, Lorenzo Valbusa Dall'Armi, Julien Lesgourgues, Angelo Ricciardone, Nicola Bartolo, Daniele Bertacca, Christian Fidler, and Sabino Matarrese. *GW CLASS: Cosmological Gravitational Wave Background in the Cosmic Linear Anisotropy Solving System.* 2023.

[97] Tristan L. Smith, Elena Pierpaoli, and Marc Kamionkowski. New cosmic microwave background constraint to primordial gravitational waves. *Physical Review Letters*, 97(2), jul 2006.

[98] Eric Thrane and Joseph D. Romano. Sensitivity curves for searches for gravitational-wave backgrounds. *Phys. Rev. D*, 88:124032, Dec 2013.

[99] M. Tristram, A. J. Banday, K. M. Górski, R. Keskitalo, C. R. Lawrence, K. J. Andersen, R. B. Barreiro, J. Borrill, L. P. L. Colombo, H. K. Eriksen, R. Fernandez-Cobos, T. S. Kisner, E. Martínez-González, B. Partridge, D. Scott, T. L. Svalheim, and I. K. Wehus. Improved limits on the tensor-to-scalar ratio using BICEP and Planck. *Physical Review D*, 105(8), apr 2022.

[100] Sunny Vagnozzi. Inflationary interpretation of the stochastic gravitational wave background signal detected by pulsar timing array experiments. *Journal of High Energy Astrophysics*, 39:81–98, aug 2023.

[101] Yuki Watanabe and Eiichiro Komatsu. Improved calculation of the primordial gravitational wave spectrum in the standard model. *Physical Review D*, 73(12), jun 2006.

[102] David J. Weir. Revisiting the envelope approximation: Gravitational waves from bubble collisions. *Physical Review D*, 93(12), jun 2016.

[103] Heng Xu, Siyuan Chen, Yanjun Guo, Jinchen Jiang, Bojun Wang, Jiangwei Xu, Zihan Xue, R. Nicolas Caballero, Jianping Yuan, Yonghua Xu, Jingbo Wang, Longfei Hao, Jingtao Luo, Kejia Lee, Jinlin Han, Peng Jiang, Zhiqiang Shen, Min Wang, Na Wang, Renxin Xu, Xiangping Wu, Richard Manchester, Lei Qian, Xin Guan, Menglin Huang, Chun Sun, and Yan Zhu. Searching for the nano-hertz stochastic gravitational wave background with the chinese pulsar timing array data release i. *Research in Astronomy and Astrophysics*, 23(7):075024, jun 2023.